INFORMATION TO USERS

This material was produced from a microfilm copy of the original document. While the most advanced technological means to photograph and reproduce this document have been used, the quality is heavily dependent upon the quality of the original submitted.

The following explanation of techniques is provided to help you understand markings or patterns which may appear on this reproduction.

1. The sign or "target" for pages apparently lacking from the document photographed is "Missing Page(s)". If it was possible to obtain the missing page(s) or section, they are spliced into the film along with adjacent pages. This may have necessitated cutting thru an image and duplicating adjacent pages to insure you complete continuity.

2. When an image on the film is obliterated with a large round black mark, it is an indication that the photographer suspected that the copy may have moved during exposure and thus cause a blurred image. You will find a good image of the page in the adjacent frame.

3. When a map, drawing or chart, etc., was part of the material being photographed the photographer followed a definite method in "sectioning" the material. It is customary to begin photoing at the upper left hand corner of a large sheet and to continue photoing from left to right in equal sections with a small overlap. If necessary, sectioning is continued again — beginning below the first row and continuing on until complete.

4. The majority of users indicate that the textual content is of greatest value, however, a somewhat higher quality reproduction could be made from "photographs" if essential to the understanding of the dissertation. Silver prints of "photographs" may be ordered at additional charge by writing the Order Department, giving the catalog number, title, author and specific pages you wish reproduced.

5. PLEASE NOTE: Some pages may have indistinct print. Filmed as received.

Xerox University Microfilms
300 North Zeeb Road
Ann Arbor, Michigan 48106

Electron tunneling and the proximity effect in Pb-Cd thin films

by

James R. Toplicar

A Dissertation Submitted to the
Graduate Faculty in Partial Fulfillment of
The Requirements for the Degree of
DOCTOR OF PHILOSOPHY

Department: Physics
Major: Solid State Physics

Approved:

Signature was redacted for privacy.

In Charge of Major Work

Signature was redacted for privacy.

For the Major Department

Signature was redacted for privacy.

For the Graduate College

Iowa State University
Ames, Iowa

1976

TABLE OF CONTENTS

LIST OF FIGURES

LIST OF TABLES

LIST OF SYMBOLS

ω	-	Electron energy parameter
$N(\omega)$	-	Electron density of states
Ω_N	-	Half-width of the gap in the density of states
Δ	-	BCS energy gap parameter
$\sigma(\omega)$	-	Normalized junction conductance
T_c	-	Junction critical temperature determined from $\sigma(0)$
$\xi_{N,S}$	-	The coherence length in the metal films
Δ_S^{Ph}	-	Phonon contribution to the pair potential (McMillan model)
$\Gamma_{S,N}$	-	Electron-lifetime parameters (McMillan model)
Δ_{fit}	-	Energy parameter used in the determination of μ^*
$\Delta_{.13}$	-	Value of Δfit that yields $\mu^* = 0.13$
$\Delta(\omega)$	-	Energy dependent pair potential
Δ_o	-	Magnitude of $\Delta(\omega)$ at the gap edge
E_p	-	Energy at which the peak occurs in $N(\omega)$
$Z(\omega)$	-	Electron renormalization function
μ^*	-	Coulomb pseudopotential
λ	-	Strength of the electron-phonon coupling

INTRODUCTION

Electron tunneling provides a powerful experimental method for an investigation of the superconducting state in metals. The tunneling technique is a very sensitive probe of the density of states in a superconducting material, and through the density of states a great deal can be learned about fundamental interactions in a superconductor. The early tunneling results of Giaever and Megerle[1] focused on a direct measurement of the density of states and gave strong experimental confirmation to the theory of superconductivity proposed by Bardeen, Cooper and Schrieffer (hereafter BCS)[2] in that they demonstrated the existence of a temperature-dependent gap in the excitation spectrum of the superconductor. Since these early experiments, electron tunneling techniques have been improved and applied to the investigation of a wide range of superconducting materials.[3]

In addition to the basic studies of the excitation spectrum of superconductors, the extreme sensitivity of the tunneling current to small changes in the electron density of states has made possible a critical examination of higher order interactions in superconductors and has stimulated theoretical work in these areas. Theoretical progress has been rapid and tunneling results confirm the present theory of superconductivity to be accurate to a few percent. Tunneling techniques have also been applied to the investigation of superconductors in a wide variety of circumstances. For example, anisotropy effects[4] have been studied and rather thorough studies of the tunneling phonon spectra have

been made for amorphous superconductors[5] and superconducting alloys[6]. The technique seems to be very generally applicable, and in this work, electron tunneling techniques have been used to study changes in the superconducting state due to the proximity effect in superimposed films of lead and cadmium. It has been known for some time that a composite structure of superimposed normal and superconducting thin films can exhibit properties far different from those of the original, isolated films. This is the so-called proximity effect. For example, the transition temperature of the superconductor can be considerably depressed; superconductivity can be induced in the otherwise normal metal; and the density of states in both metals is significantly altered. There has been theoretical interest[7,8,9] in all these subjects, but progress has been slow and adequate solutions for the superconducting-normal boundary problem are not yet available. Despite the experimental and theoretical interest, the problem of the superconducting-normal metal interface remains one of the poorly understood problems in the theory of superconductivity. To understand in detail how tunneling can be used to study the proximity effect, it is helpful to review the theoretical models for electron tunneling and to be familiar with the way the density of states influences the current-voltage characteristics of a junction. The theoretical results are essential in the interpretation of the tunneling data. We can then discuss the application of the tunneling technique to the proximity effect studies and review the experimental and theoretical approaches to the problem.

In this review we include a discussion of strong coupling effects in superconductors. Many investigators, including ourselves, have studied proximity sandwiches using lead thin films. Because of the strong coupling nature of lead, a consideration of strong coupling effects in these samples seems essential. These effects are well understood in uniform superconductors and considerable information can be obtained from analysis of tunneling results. We discuss how this analysis can be extended to non-uniform proximity sandwiches. By introducing the strong coupling analysis we are able to apply a very powerful experimental technique to probe the interactions near the superconductor-normal metal interface.

Electron Tunneling

Fisher and Giaever[10] first demonstrated that a current could be observed to flow between two metallic electrodes separated by a thin insulating layer and dramatic proof that the conduction mechanism through the insulator was indeed quantum mechanical tunneling of electrons came when a superconducting material was used as one of the electrodes. Changes in the current-voltage characteristics of the tunnel junction reflected the changes in the electron density of states associated with the onset of the superconducting transition. Using a simple model, Giaever and Megerle[1] were able to show that the tunneling current was controlled primarily by the density of states in the superconductor. At low temperatures, where the thermal smearing effects are small, the tunneling characteristics confirmed the BCS prediction of an energy gap and a square root singularity in the single particle density of states in the superconductor.

A calculation of the tunneling current can be carried out as an ordinary quantum mechanical barrier penetration problem. The barrier transmission probability P is determined by the energy of the incident electron E, the barrier height Vo, and the width of the barrier t.[11]

$$P \propto \exp\left[-2\sqrt{\frac{2m(Vo-E)}{\hbar^2}}\, t\right] \tag{1}$$

The strong energy dependence of the tunneling current arises from the fact that transitions across the barrier are restricted by the exclusion principle. The probability $T_{kk'}$ that an electron will leave a Bloch state k in metal 1 on one side of the barrier and tunnel to a state k' in metal 2 on the other side is given by Fermi's "golden rule".

$$T_{kk'} = \left(\frac{2\pi}{\hbar}\right) M^2 N_2(E)(1-f(E)) \tag{2}$$

Here $N_2(E)$ is the density of states in metal 2 and f(E) is the Fermi thermal occupation function[12]. The expression (1-f(E)) is the probability that the electron state at energy E is empty. M^2 is the squared matrix element for the transition. Bardeen[13] has argued that if the states k and k' lie near the Fermi surface, M^2 can be assumed independent of energy. If a voltage is applied across the barrier, the current that will flow can be calculated by summing the electron contributions from all initial states k and final states k'. Measuring all energies from the Fermi surface, we have

$$I(V) = C\int_{-\infty}^{\infty} N_1(E)N_2(E-V)[f(E)-f(E-V)]\, dE \tag{3}$$

The current is controlled by the density of states in the two metals and the temperature dependence is given by the Fermi functions.

Schrieffer[14] has used a more formal many body approach to the tunneling problem. He followed Cohen et al.[15] and presented the problem in terms of an effective tunneling Hamiltonian which perturbs the two metal system by destroying an electron in metal 1 and creating an electron in metal 2. Schrieffer has shown how coherence factors which define a non-thermal occupation of the electron Bloch states in the superconductor cancel out in the final expression for the tunneling current. These factors have been ignored in our derivation of the tunneling current. Amazingly, the more formal approach presented by Schrieffer predicts the same current-voltage behavior as given in Eq. (3). Higher order contributions to I(V)may occur due to multi-particle tunneling,[16] but these effects become vanishingly small for a barrier thickness of more than a few Angstroms.

The expression in Eq. (3) can be simplified by assuming that the form of the density of states in one of the metals is known. If metal 2 is a normal metal, the density of states $N_2(E)$ is a slowly varying function of energy near the Fermi surface. Because tunneling experiments involve energies within a few millielectronvolts of the Fermi energy, $N_2(E)$ can be considered constant. Then, Eq. (3) becomes

$$I(V) = C' \int_{-\infty}^{\infty} N_1(E)[f(E)-f(E-V)]\, dE \qquad (4)$$

a basic relation in our interpretation of the tunneling data.

An important experimental quantity is the voltage variation of the dynamic conductance dI/dV. Differentiating Eq. (4), we have

$$\frac{dI}{dV}(V) = C' \int_{-\infty}^{\infty} N_1(E) \left[\frac{1}{kT} \frac{\exp\left(\frac{E-V}{kT}\right)}{\left[\exp\left(\frac{E-V}{kT}\right)+1\right]^2} \right] dE \tag{5}$$

The term in brackets under the integral is the derivative of the Fermi function which we have written out explicitly. This derivative is a bell-shaped curve centered at E=V, and the width of the curve at half maximum is approximately 3.5kT. At T=0, the curve becomes a delta function, and Eq. (5) becomes

$$\frac{dI}{dV}(V) = C' N_1(V) \tag{6}$$

This important relation states that the dynamic conductance of the tunnel junction at T=0 is directly proportional to the electron density of states in metal 1. This equation is quite general and applies to any density of final states $N_1(V)$. The constant C' in Eq. (6) can be eliminated by suitably normalizing the conductance. For the case in which metal 1 is superconducting, the density of states is given by the BCS expression.[2]

$$N_{BCS}(E) = \begin{cases} \dfrac{N(0)|E|}{[E^2-\Delta^2]^{1/2}} & E \geq \Delta \\ 0 & E < \Delta \end{cases} \tag{7}$$

The constant C' in Eq. (6) is merely the conductance of the junction when both electrodes are normal. For the case of a BCS superconductor, the normalized conductance is given by

$$\sigma(V) = \frac{(dI/dV)_S}{(dI/dV)_N} = \frac{|V|}{[V^2-\Delta^2]^{1/2}} \tag{8}$$

A similar normalization applies for strong coupling or non-uniform superconductors. The general result is always given by

$$\sigma(V) = \frac{(dI/dV)_S}{(dI/dV)_N} = \frac{N(V)}{N(0)} \tag{9}$$

The normalized conductance for these cases is always equal to the electron density of states in the superconducting electrode.

The Proximity Effect

Electron tunneling techniques are particularly well suited for an investigation of the proximity effect in superimposed thin films because the tunneling electrons probe the properties of a metal within a few hundred Angstroms of the tunneling surface. The observed conductance corresponds to the density of states near this surface, and the presence of the normal metal in the sandwich appears in the tunneling characteristics through the non-local nature of the electron wave function. Part of the power of the electron tunneling technique is that it allows us to probe the proximity induced properties on a particular side of the proximity sandwich rather than an average bulk property of the sandwich.

Tunneling techniques were first applied to the study of the proximity effect by Smith *et al.*[17] They reported an induced gap in the excitation spectrum on the silver side of superimposed films of silver and lead. This was rather a preliminary study, and no detailed investigation of the electron density of states in the sandwich was made.

Somewhat later, Fulde and Maki[9] predicted that the presence of a normal metal contact has a pair breaking effect on the Cooper pairs in the superconductor. They were able to show that the presence of the normal metal cause a spatially dependent pair potential $\Delta(\omega)$ in the sample. This pair potential which acts on the Cooper pair,[2] is a result of the attractive electron-electron interaction in the superconductor. The strength of the pair potential is a function of the number of pairs condensed into the BCS ground state. This number of condensed pairs decreases near the normal-superconducting interface. We might imagine that Cooper pairs "leak" out of the superconductor into the normal metal where they tend to be broken. The pair potential, however, does not drop to zero at the interface because of the long range, non-local nature of the pairing phonon exchange in the superconductor. To understand this non-local character, it is helpful to remember that typical conduction electron velocities in the superconductor are on the order of 10^7cm/sec, and this implies that an electron can travel a considerable distance during a single period of a lattice vibration. An electron can therefore create a disturbance and move several thousand lattice spacings before the disturbance is absorbed by a paired partner electron. This pair, although physically separated, can exchange momentum and energy within the limits of the uncertainty principle.[18] In a sense, we can regard the Cooper pair as a large molecule extending over thousands of crystal lattice spacings. The spatial extent of the Cooper pair is called the coherence length ξ. At the superconducting-normal interface the Cooper pairs extend into the normal metal and the pairs are eventually broken because the net electron-electron interaction there is not conducive to the pairing process.

Under these conditions, the Cooper pairs have a finite lifetime and electron excitation spectrum displays lifetime broadening similar to that in superconductors containing magnetic impurities.[19]

Fulde and Maki made significant progress in the understanding of the proximity effect, but, unfortunately, their theoretical approach requires an approximation involving an expansion in powers of the pair potential. This approach is valid only near the transition temperature where the pair potential is small. A detailed comparison of theory and experiment is not possible in this regime because of the large thermal smearing effects. The theory, however, allows an exact solution at the transition temperature T_c of the proximity sandwich. The theory relates T_c to a pair breaking parameter Γ and the transition temperature of the pure superconductor.

$$\ell n(\frac{T_{cs}}{T_c}) = \psi(1/2 + \frac{\Gamma}{2\pi T_c}) - \psi(1/2) \qquad (10)$$

The parameter Γ is an energy width related to the life time of the Cooper pairs, and ψ is the digamma function.[20] An identical expression is obtained for Γ and T_c when one considers pair breaking due to magnetic impurities in a superconductor.[21] The theory for this case is well developed and predicts a density of states which is considerably more rounded than the BCS prediction. These smeared characteristics which extend into the gap in the excitation spectrum reflect lifetime broadening effects. The extent of this smearing is determined by the magnitude of the parameter Γ.

Several tunneling studies of the various aspects of the proximity effect have been attempted. Claeson and Gygax[22] made tunneling measurements

of the electron density of states of lead-silver proximity sandwiches and obtained tunneling curves in general qualitative agreement with pair breaking theory and reported a depression in the transition temperature and a reduction in the width of the gap in the density of states. The proximity sandwiches used in their work, however, showed large non-tunneling currents which complicated interpretation of the data. Hauser[23] has studied the tunneling characteristics of several different types of proximity sandwiches prepared by getter-sputtering at liquid nitrogen temperatures. Hauser's work was primarily concerned with the temperature dependence of the conductance of the proximity sandwiches at zero bias near T_c. He reported temperature dependences in general agreement with the prediction of the Fulde and Maki theory.[9] Guyon et al.[24] reported tunneling results on proximity sandwiches of a "dirty" superconductor InBi and normal Zn. The mean free path of these materials was on the order of a few hundred Angstroms, and the interactions between the metals was analyzed in terms of diffusion equations for normal electrons. Again the experimental effort was concentrated at the temperature region near T_c. Guyon et al. reported a smeared density of states in agreement with the prediction of Fulde and Maki.[9] They also observed that the temperature dependence of $\sigma(0)$, the zero bias conductance was quite different for tunneling into the normal N side of a proximity sandwich than that for the superconducting S side. While the S side results showed essential BCS behavior with $1-\sigma(0) \propto 1-T/T_c$, the N side display the empirical determined relationship $1-\sigma(0) \propto (1-T/T_c)^n$. Guyon et al. obtained n values between 2 and 3 for their samples.

Quite different techniques and materials were used in the above experiments,[17,22,23,24] but some common results were found. The density of states observed in the superimposed films does not agree with the BCS prediction inasmuch as the BCS singularity at the gap edge is considerably rounded in the proximity sandwiches. The transition temperature of the proximity sandwich is depressed, and the width of the gap in the density of states is reduced from that of the pure metal. All of these features are consistent with a pair breaking due to the spatial variation of the order parameter.

As yet there is no complete theory of all of the aspects of the proximity effect, but McMillan[25] developed a simple tunneling model which applies for a wide range of circumstances. He introduced a model for the proximity effect in which the metals in the sandwich perturb one another by the tunneling of the electrons across the interface between the two metals. A potential barrier is assumed to be formed at the normal (N)-superconducting (S) boundary, and the tunneling through this barrier is treated using the tunneling Hamiltonian method.[15] In addition, the films are assumed to be thin enough so that the thickness d is on the order of a coherence length, ξ, and the superconducting properties are uniform across the film. McMillan uses the self-energy equations of Nambu[26] and a self-consistent perturbation approach to solve for the pair potential on the two sides of the potential barrier. Because of the interaction between the films, the equations for the pair potential are coupled,

$$\Delta_S(\omega) = Z_S^{-1}(\omega)\left\{\Delta_S^{Ph} + \frac{i\Gamma_S\Delta_N(\omega)}{[\omega^2-\Delta_N^2(\omega)]^{1/2}}\right\} \tag{11}$$

$$\Delta_N(\omega) = Z_N^{-1}(\omega)\left\{\Delta_N^{Ph} + \frac{i\Gamma_N\Delta_S(\omega)}{[\omega^2-\Delta_S^2(\omega)]^{1/2}}\right\} \tag{12}$$

The renormalization function $Z_S(\omega)$ is given by

$$Z_S(\omega) = 1 + i\Gamma_S/[\omega^2-\Delta_N^2(\omega)]^{1/2} \tag{13}$$

The value of Δ_S^{Ph} is determined from the self-consistency condition

$$\Delta_S^{Ph} = \lambda_S\int_o^\infty \mathrm{Re}\{\Delta_S(\omega)/[\omega^2-\Delta_S^2(\omega)]^{1/2}\}\,d\omega \tag{14}$$

A pair of equations identical to Eqs. (13) and (14) is obtained for the parameters on the normal side with the N and S subscripts interchanged. The tunneling effects are introduced through Γ_S and Γ_N which are related to the time T_S that the electron spends in the superconductor.

$$\Gamma_S = \hbar/T_S = \frac{\hbar v_f \alpha}{2Bd_S} \tag{15}$$

Here v_f is the Fermi velocity, d_S is the thickness of the film, α is the barrier penetration probability at the interface, and B is a function of the ratio of the mean free path to the thickness of the film.

An iterative procedure is used to numerically solve for the pair potentials $\Delta_N(E)$ and $\Delta_S(E)$ from Eqs. (11) and (12). Once the energy dependent pair potentials are known, the tunneling density of states can be computed

$$N_{S,N}(\omega) = \mathrm{Re}\{\omega/[\omega^2 - \Delta_{S,N}^2(\omega)]\} \tag{16}$$

At the transition temperature T_c of the sandwich, the equations are linear and the self-consistency condition yields

$$\ell n\left(\frac{T_{cs}}{T_c}\right) = \frac{\Gamma_S}{\Gamma}\left[\psi(1/2+\Gamma/2\pi T_c) + \psi(1/2)\right] \qquad (17)$$

Where $\Gamma = \Gamma_S + \Gamma_N$ and T_{cs} is the transition temperature of the pure material. For the case of a thick normal metal film $\Gamma_N \simeq 0$ and Eq. (17) reduces to the pair-breaking expression of Eq. (10). The variation of the transition temperature of the sample as a function of the electron lifetime Γ_S for several values of Γ_N is shown in Figure 1. The variation of the pair potential for energies near the energy gap is shown in Figure 2. The pair potential was calculated from Eqs. (11) and (12) using parameters appropriate for our proximity sandwiches. In the low energy region, the pair potential has an imaginary component reflecting the finite lifetime of the Cooper pairs in the superconductor. At higher energies, the imaginary part approaches zero and the real part goes to Δ_S^{Ph}. The presence of the normal metal effects the pair potential in the superconductor primarily in the region where the electron energy is on the order of Γ_S. The electron density of states calculated from the pair potential is shown in Figure 3. On the S side, the density of states has a broadened peak at an energy near Δ_S^{Ph} and is BCS-like at higher energies where the proximity induced effects are small. The N side curve displays a similar peak just above Ω_N, the gap in the density of states. The theory predicts that the same energy gap will be measured on either side of the proximity sandwich. In an isolated superconductor, the

tunneling density of states is zero for all energies less than Δ_S^{Ph}. In the proximity sandwich, however, an electron injected into the superconductor at these energies is able to occupy an energy state in the "normal" metal. Such states are available for energies greater than Ω_N, the induced energy gap on the N side of the sandwich. The sampling depth for a tunneling electron is inversely proportional to the energy of the electron[27] times the $\mathrm{Im}\, Z_N$ and in a sufficiently clean metal this sampling depth can be large for low energy electrons. Therefore, one might expect to see structure due to the normal metal at low energies in the S density of states. In the actual experimental case, we might expect somewhat more smeared structure than the tunneling model predicts. In any case, the strong interaction between the superimposed films should be apparent primarily in the low-energy region. The McMillan theory is powerful in that it allows a complete solution for all of the measured quantities within the assumptions of the model. The results should be valid and subject to experimental tests at low temperatures where results are not clouded by thermal smearing effects.

Adkins and Kington[28] have applied this model to the analysis of their tunneling data on silver-lead and copper-lead proximity sandwiches. They report a variation of the gap in the density of states with sample thickness which is in good agreement with the McMillan model. Adkins and Kington assumed that the energy gap in their samples could be determined by fitting the measured value of $\sigma(0)$ to a BCS density of states, an assumption that may not be entirely justified. A comparison of the observed density of state to the predictions of the McMillan model was made using

the barrier penetration probability as an adjustable fitting parameter. It was found that the general shape of the experimental curves is similar to the McMillan prediction. Some discrepancies between theory and experiment might be expected, however, because relatively thick films were used in this study. The model is not strictly valid in this limit. Freake and Adkins[29] obtained somewhat better agreement to the McMillan model density of states in their tunneling work with Pb-Cu proximity sandwiches. Their results, especially for tunneling into the superconducting side of the sandwich displayed the major structure predicted by the McMillan theory. Vrba and Woods[30] performed electron tunneling experiments into Al-Sn proximity sandwiches. Care was taken to meet the conditions of the McMillan theory in that the Sn and Al films used in their samples were kept thin, and an oxide layer was intentionally formed between the films to decouple them. The magnitude of the barrier penetration probability could be adjusted by controlling the thickness of the barrier. The mean lifetime of the electron Γ_S was used as an adjustable parameter, and the experimental results were fitted to the results of the McMillan theory. The positions of the major structures in the experimental density of states is in good agreement with McMillan's theory. Exact agreements cannot be expected unless the barrier separating the thin films in the proximity sandwich were perfectly uniform. In the case of a non-uniform barrier, the transmission coefficient of the barrier would not be constant over the area of the junction, and the resulting density of states would be a combination of different McMillan curves.

The McMillan model is attractive because it lends itself well to interpretation of experimental data. The model offers a description of the density of states that is valid over a wide temperature range. The various experiments described above[28,29,30] tend to give evidence for the general applicability of the model for a variety of experimental cases.

Strong Coupling Effects

The tunneling model for the proximity effect predicts a strong energy dependence of the pair potential at low energies. An isolated pure superconductor such as Pb also shows an energy-dependent pair potential at energies near the Debye energy of the material where the electrons are strongly coupled to the phonons of the superconductor. These so-called strong coupling effects have been throughly studied in Pb, and there is a well developed theory accounting for the observed effects.

Strong coupling effects are apparent in a number of experiments. In their early tunneling work, Giaever and Megerle[1] found that the measured density of states of lead showed small but distinct deviations from the BCS predictions at energies comparable with the Debye energy in lead. Critical field curves of soft metals such as lead and mercury[31] also showed deviations from the predicted BCS parabolic dependence. Rowell and Kopf[32] made a detailed study of these effects in the tunneling characteristics of lead tunnel juctions and found the deviations were associated with the peaks in the lead phonon spectrum. Bermon and Ginsberg[33] reported similar deviations in the density of states in mercury. The observed energy gap and size of the specific heat jump at the transition temperature in lead

and mercury significantly differ from the BCS prediction. Anderson[34] suggested that these effects might arise from an unusually strong electron-phonon interaction in these materials. In the BCS model for superconductivity, the effective, attractive interaction between electrons which gives rise to a new ground state for the system was thought to arise from the electron-phonon interaction in the metal. For simplicity of calculations, this attractive interaction was assumed to be constant up to some cut off frequency usually taken to be the Debye frequency, but it was known that the interaction must have a more complicated energy dependence determined by the phonon density of states. To see how the phonons enter into the electron tunneling characteristics, it is helpful to recall that the BCS ground state is an ordered state in which the occupation of the single particle Bloch states occurs in pairs. When the net electron-electron interaction, which includes the attractive exchange of virtual phonons as well as the repulsive screened Coulomb interaction, is attractive, the electron sea condenses into this state of bound Cooper pairs. The phase space for the exchange of virtual phonons is greatest if the electron Bloch states are occupied or unoccupied in pairs of opposite momentum $(k,-k)$. As was shown by BCS, the configuration which maximizes the attractive interaction is the ground state where there is an exact occupation in pairs with zero center-of-mass momentum. Excitations from this ground state occur when an unpaired electron is added to the system or an electron is removed from an existing pair. Either of these events increases the free energy of the system as the phase space for virtual

phonon exchange is reduced for the remaining pairs. A minimum energy Δ is therefore required to create such an excitation. These electrons excited out of the gound state are called quasiparticles and are assumed to be long lived in the BCS model. However, in strongly coupled superconductors such as lead and mercury, the quasiparticle energy can be on the order of the Debye energy of the metal. When there is a high probability that the quasiparticle can loose energy by creating real phonons in the metal, their lifetimes are short and the quasiparticle energy is not well defined. One therefore expects to see deviations from the BCS behavior in metals in which the excitation energy $\Delta(\omega)$ is on the order of the Debye energy of the metal.

A formal field theoretical treatment of these strong coupling effects was formulated by Eliashberg[35] which takes into account the lifetime effects without resorting to the quasiparticle approximation. He used the method of Nambu[26] and Migdal[36] to define a system of equations relating a complex renormalization factor $Z_S(\omega)$ and the pair potential $\Delta(\omega)$ through the electron pairing self energy $\Sigma(\omega)$.

$$\omega Z_S(\omega) = \omega + \Sigma(\omega) \tag{18}$$

$$\Delta(\omega) = \Sigma(\omega)/Z_S(\omega) \tag{19}$$

Both $\Delta(\omega)$ and $Z_S(\omega)$ have imaginary parts reflecting the finite lifetimes of the excited electrons. Eliashberg derived the form of the Eqs. (18) and (19) appropriate for strongly coupled superconductors. These equations are coupled, non-linear, integral equations involving the phonon spectrum of the superconductor.

Morel and Anderson[37] obtained solutions to the Eliashberg equations assuming an Einstein model for the phonon spectrum. They introduced Coulomb interactions into the equations through a parameter μ^*, the effective Coulomb repulsion. In the pairing process, the Coulomb repulsion is propagated much faster than the phonon exchange. Because the paired electrons need never be near one another, the effective Coulomb interaction is thus reduced. McMillan[38] has written an expression for μ^* involving $N(0)V_c$, the instantaneous Coulomb repulsion; ω_o, the Debye cut off frequency; and ω_B, the characteristic electron frequency.

$$\mu^* = \frac{N(0)V_c}{1+N(0)V_c \ell n(\omega_B/\omega_o)} \tag{20}$$

Culler et al.[39] derived numerical methods to solve the Eliashberg equations using a Debye phonon spectrum and calculated an energy dependent pair potential displaying structure at energies near θ_D. This work established numerical techniques widely used by other investigators. Further numerical solutions were developed by Schrieffer et al.[40] using a realistic phonon spectrum based on neutron diffraction data for lead. In addition, they derived an expression relating the tunneling density of states to the complex pair potential $\Lambda(\omega)$.

$$N_T(\omega) = \frac{(dI/dV)_S}{(dI/dV)_N} = Re\{\frac{|\omega|}{[\omega^2-\Delta^2(\omega)]^{1/2}}\} \tag{21}$$

Here the pair potential is complex, $\Delta(\omega) = \Delta_1(\omega) + i\Delta_2(\omega)$. For a real $\Delta(\omega)$, the above expression reduces to the BCS result, Eq. (8).

Using this expression, Schrieffer and his co-workers were able to compare the predictions of the Eliashberg equations to the tunneling results of Rowell et al.[41] The phonon spectrum used in the calculation consisted of two Lorentzian peaks located at energies corresponding to the transverse and longitudinal peaks obtained from the neutron diffraction analysis of Brockhouse et al.[42] The electron density of states for lead calculated from the Eliashberg equations was in good agreement with the tunneling results. The major structures in the experimental density of states were reproduced despite the rather simple model used for the phonon spectrum in the numerical calculation.

A heuristic explanation of the origin of the phonon-induced structure in the density of states was presented by Scalapino.[43] He pointed out that the imaginary part of the pair potential, $\Delta_2(\omega)$, reflects energy loss processes while the real part, $\Delta_1(\omega)$, is a measure of the strength of the electron-phonon interaction. To see this more clearly, consider what happens for a simple peak in the phonon spectrum at energy ω_o. Because of the high density of phonon states at ω_o, an electron injected into the superconductor at energy ω_o has a high probability of emitting a real phonon and decaying to the gap edge. Because of this energy loss mechanism, we expect to find an increase in $\Delta_2(\omega)$ near ω_o. The response of the lattice to an electron injected with an energy near ω_o is similar to that of a harmonic oscillator driven near the resonance frequency. For electron energies less than ω_o, most of the ion cores are being driven at a frequency below their natural frequency and over-respond to the presence

of the injected electron. This over-response of the lattice is fundamental to the formation of an attractive electron-electron interaction. A region of net positive charge is formed by this over-response, and it is through the creation of this locally positive region that the Cooper pairs can maintain an attractive interaction. Therefore, we expect an increase in the effective, attractive electron-electron interaction for energies just below ω_o. In this energy range $\Delta_1(\omega)$ should rise sharply. For energies slightly above ω_o, the ion cores are driven above their natural frequency and respond out of phase to the injected electron. This causes an increased repulsive interaction in addition to the "quiet lattice" Coulomb repulsion between electrons. $\Delta_1(\omega)$ becomes negative in this energy range. At higher energies, weak structure occurs in $\Delta(\omega)$ associated with multi-phonon processes.

The energy variation of $\Delta(\omega)$ in lead is shown in Figure 4. The phonon density of states for lead is inserted at the appropriate energies. Notice that the variation of $\Delta(\omega)$ is considerably more complicated for the actual lead phonon spectrum than in our single phonon peak discussion. At low energies where the density of phonon states becomes vanishingly small, the complex function, $\Delta(\omega)$, reduces to the real constant, Δ, as in the BCS theory.

The numerically calculated pair potential of Schrieffer et al.[40] accounted for the structure in the experimental density of states and demonstrated the applicability of the Eliashberg equations to the analysis of tunneling results for strong-coupling superconductors. With a suitable choice of parameters, the tunneling results could be reproduced to a

few percent. McMillan and Rowell[44] showed that this procedure could be inverted and that one could actually extract the parameters for the Eliashberg equation from the tunneling data. These parameters are the phonon density of states times an average electron-phonon matrix element $\alpha^2F(\omega)$ and the Coulomb pseudo-potential μ^*.

For the case of a strong-coupling superconductor, the Eliashberg self-energy expression, Eqs. (18), (19), can be written:

$$\Delta(\omega)Z_o(\omega) = \int_{\Delta_o}^{\omega_c} d\omega' \, \mathrm{Re}\{\Delta(\omega')[\omega'^2-\Delta^2(\omega)]^{-1/2}\} \{K_+(\omega,\omega')-\mu^*\} \quad (22)$$

$$\omega[1-Z_o(\omega)] = \int_{\Delta_o}^{\infty} d\omega' \, \mathrm{Re}\{\omega'[\omega'^2-\Delta^2(\omega')]^{-1/2}\} \; K_-(\omega,\omega') \quad (23)$$

where the kernel $K_\pm(\omega,\omega')$ is given by

$$K_\pm(\omega,\omega') = \int_o^\infty d\omega_q \, \alpha^2F(\omega_q)[(\omega'+\omega+\omega_q + i\delta)^{-1} \pm (\omega'-\omega+\omega_q - i\delta)^{-1}] \quad (24)$$

The electron density of states is related to $\Delta(\omega)$ through Eq. (21).

An iteration process is used to find a solution to these equations and determine a value of μ^* and $\alpha^2F(\omega)$ that best fit the experimental density of states. The procedure starts with a zeroth order guess for μ^*, $\alpha^2F(\omega)$ and $\Delta(\omega)$. The initial value of μ^* is usually set to 0.13, the theoretical value for lead.[37] The first guess for $\alpha^2F(\omega)$ can be an arbitrary function over the range of the phonon energies, and the initial $\Delta(\omega)$ is usually set to Δ, the BCS value for the pair potential at the gap edge.

The initial values are inserted into the right hand side of Eqs. (22), (23) and (24), and the integral equation is solved iteratively until the expression for $\Delta(\omega)$ converges. The density of states can then be calculated

from Eq. (21). Changes are made in $\alpha^2F(\omega)$ based on the difference between the calculated and experimental density of states. The value of μ^* is adjusted so that $\Delta(\omega)$ gives the pair potential at the gap edge: $\Delta(\omega) = \Delta_0$ at $\omega=\Delta_0$. These new values are again inserted into the gap equation and the procedure is repeated until the calculated density of states is arbitrarily close to the experimental density of states. A flow chart diagram of the "unfolding" program is shown in Figure 5. This program has been used to analyze tunneling data on a number of superconductors[27, 45, 46] as well as intermetallic compounds[47] and alloys.[48] The calculated values of μ^* and $\alpha^2F(\omega)$ for these metals are in good agreement with the theoretical predictions for these values.[38] The structure in $\alpha^2F(\omega)$ mirrors the structure found in the phonon spectra for these materials using neutron diffraction techniques.

The reasonableness of the various calculated parameters demonstrates the accuracy of the unfolding procedure. A further test can be made on the validity of the program. The fitting procedure uses data from the tunneling density of states in the region of the phonon spectrum. The calculated density of states not only reproduces the phonon region but also faithfully reproduces the multiphonon structure which occurs at higher energies (12-30 meV). The fact that the calculated and experimental density of states agree in this high energy region provides strong experimental support for both the Eliashberg equations and the unfolding procedure.

EXPERIMENTAL SYSTEM AND PROCEDURE

Vacuum Evaporator

All of the thin film Pb-Cd proximity sandwiches for this study were prepared by evaporation in an oil-diffusion pumped high vacuum system capable of obtaining pressures of 10^{-6} Torr. The evaporations were carried out in an 8" X 10" bell jar evacuated by a 3" Cenco oil diffusion pump. A liquid nitrogen cold trap was used to prevent the backstreaming of pump oil into the bell jar. Because of the small volume of the bell jar relative to the size of the diffusion pump, the system was able to maintain a vacuum of better than 5×10^{-6} Torr during the deposition of the various thin films. The vacuum evaporator is shown in Figure 6. The high vacuum portion of the system includes a rotating substrate holder and masks, two evaporation sources, a quartz crystal thickness monitor and an aluminum cathode for the glow discharge anodization system.

Five separate evaporations were required in the fabrication of a single tunnel junction. The rotating substrate support allowed two of these evaporations to be carried out without breaking the vacuum. Use of the rotating system resulted in a considerable saving of time in the preparation of the junction. Such a system is essential in the fabrication of proximity sandwiches. It is important that the two metal films in the sandwich be in intimate contact. To accomplish this, the films must be deposited in rapid succession to avoid the absorption of a gaseous impurity layer between the films. Even at pressures of 10^{-6} Torr, the time for the absorption of a monolayer of gas on a freshly deposited film is no more than a few tens of seconds.[49] The rotating system allowed the

two films to be evaporated within 30 seconds of one another. The substrate was mounted on a brass substrate holder which was free to rotate on a rigidly supported brass disk which contained the masks. Alignment pins positioned the substrate directly above the masks for the deposition of the thin films. The evaporation sources were located directly under these masks at a distance of 20 cm. The distance between the mask and substrate was about 3 mm., therefore the edges of the deposited thin films were sharp. Using this system the various film overlays could be positioned on the substrate to ± 0.2 mm. Such minor misalignments of the mask or substrate did not affect the preparation of the junctions.

The evaporation sources used in the thin film deposition varied with the materials being deposited. For the Al and Pb evaporations, the evaporation source was a 0.5 mm. diameter tungsten wire wound into a conical basket about 7 mm. high. The baskets were supported by copper high current feedthroughs and heated by passing a current from a Kepco KS30-60 power supply. The temperature of such a basket as a function of the current flowing through it was determined by Delfs[50] using an optical pyrometer. The baskets could be heated to a temperature of 2000°C before breaking. This temperature is much higher than those encountered in the fabrication of the junctions in this experiment.

The SiO and Cd were evaporated from enclosed sources. Both of these materials have high vapor pressure at relatively moderate temperatures. SiO melts at 1702°C and has a vapor pressure of 10^{-4} Torr at 850°C. Cadmium melts at 320°C and has a vapor pressure of 10^{-4} Torr at 180°C.[49]

Because of their high vapor pressure, both of these materials were evaporated from baffled sources. The sources were made of tantalum with internal baffles and a small orifice open toward the substrate. The use of such evaporation sources for the highly volatile materials allowed adequate control of the film deposition rate despite the high vapor pressures.

The thickness of the various film deposits were determined during the deposition using a Sloan DTM-3 quartz crystal microbalance. The thickness of a film was determined by observing the change in resonant frequency of a quartz crystal as the thin film is deposited on it. To a good approximation, the frequency shift is proportional to the mass of the deposited material. The thickness monitoring system was calibrated for aluminum against a Varian Model 980-400 interference microscope. This calibration can be used for the other materials used in this experiment by adjusting for the density difference between the material and aluminum. Bulk densities were used in this adjustment. Spurious thermal drifts limited the accuracy of this system to about ± 15%. An alternate measurement of the thickness of the films on the completed junction was always made using the interference microscope. These measurements were limited by the 40Å resolution of the instrument. The two methods of determining thickness were generally in good agreement for all materials deposited in this experiment.

He-3 Cryostat

The current-voltage characteristics of the proximity sandwiches were measured over a temperature range from 10.0K to 0.3K using a conventional ^{3}He refrigerator.[51] The low temperature tail of the cryostat is shown in Figure 7. A detailed discussion of the principles of operation of such a system are available elsewhere.[52] Moreover, Haskell[53] has discussed the operating efficiencies and wiring scheme for the particular system we used. Therefore, only a discussion of the details pertaining to this experiment will be given here.

The quartz substrate containing two tunnel junctions was secured with Apiezon N grease to a copper block which was in good thermal contact with the liquid ^{3}He chamber. Directly behind the substrate, a germanium resistance thermometer was mounted in a close fitting hole in the copper block. The thermometer and associated electrical leads were thermally anchored to the copper with Apiezon N grease. Temperature control was accomplished by using two resistors, one as a thermometer and one as a heater, located in the same copper block. Because of the intimate thermal contact between the various systems and the observed response times, we are assured that the thermometer readings are indicative of the temperature of the substrate. The various electrical leads were thermally anchored with GE7031 varnish at the ^{3}He chamber and again at the ^{4}He chamber. This procedure reduces thermal gradients in the leads and, therefore, reduces the heat leak to the sample.

The germanium resistor GR1592 was the primary thermometer for this work. The thermometer was calibrated between 4.2 and 0.3K by Finnemore[54] using paramagnetic salt thermometry and He vapor pressure. In the range 4.2K and 20K, the thermometer was calibrated against a previously calibrated germanium thermometer GR65. The calibration points were fit to $\ell n\ T = \sum_{n=1}^{q} A_n (\ell nR)^{n-1}$ with a rms deviation of less than 0.002K over the entire range of temperatures. The constants determined from this fitting procedure are available elsewhere.[53] The temperature was determined from the resistance of the thermometer using a table generated from the polynomial fit. The resistance of the germanium thermometer was measured using a Leeds and Northrup K-3 potentiometer in a four terminal arrangement. The potentiometer null was determined using a Fluke 845A Null Detector. A measuring current of 10μA was used for temperatures above 1K and 1μA was used for low temperature work. No self heating effects were observed in the thermometer. These measurements were accurate to $\pm$ .025% giving rise to an uncertainty in temperature of about $\pm$ 0.003K.

Temperature control was maintained using a 3 wire, lead compensated Wheatstone bridge. The resistance of the control thermometer, a 470 Ω Speer carbon resistor, was balanced against a decade resistance. The off balance signal from the bridge was used to trigger a microswitch which controlled the incremental current to a 50Ω carbon resistor used as a heater. The ambient heater current is adjusted so that the Joule heating in the resistor nearly balanced the cooling power of the cryostat. The Wheatstone bridge was balanced at this point. If the sample cooled, the

off-balance signal from the bridge would supply an additional current to the heater to return the sample to the balance temperature. The system was able to maintain a constant temperature at the sample to ± 0.002K for several hours.

For temperatures between 4.2K and 1K temperature control could be achieved by controlling the vapor pressure above the liquid in the ^{4}He pot with a diaphram manostat.[55] More critical control was achieved by using the control bridge in conjunction with the manostat. Below 1K, the temperature of the sample was adjusted by varying the vapor pressure of the liquid ^{3}He by pumping on the ^{3}He chamber through a series of throttle valves. Control of temperature was achieved by use of the bridge and heater. The most critical temperature control was achieved at these low temperatures where the sensitivities of both the germanium and carbon thermometers were greatest.

Conductance Bridge Electronics

Much of the information derived from electron tunneling techniques is directly related to the normalized conductance of the tunnel junction. The data obtained in this work consisted of a series of dI/dV vs. V plots from an X-Y recorder. Here, I is the current flowing through the junction due to the applied bias voltage V. These measurements were made by applying a small ac signal to the junction and using harmonic detection techniques to measure dI/dV which was plotted as a function of applied dc bias voltage.

Above the transition temperature of the superconductor, the current-voltage characteristics of a tunnel junction are nearly ohmic, that is, the resistance of the junction is nearly independent of the applied voltage. Below the transition temperature a strong non-linearity developes in the I-V characteristics near zero bias due to the gap in the electron density of states in the superconductor. At higher bias voltages, far weaker deviations from linearity at voltages corresponding to the transverse and longitudinal peaks in the phonon spectrum are observed. The conductance bridge used in this experiment exploits this non-linearity. A schematic diagram of a simplified conductance bridge is shown in Figure 8. The bridge is in balance when $R_s = R_j$ and $C_s = C_j$ with a sinusoidal voltage $v_o e^{i\omega t}$ appearing across both R_s and R_j. Here R_j and C_j represent the resistance and capacitance of the tunnel junction. At this balance condition, no potential difference developed between points 1 and 2. These are the input terminals of the operational amplifier A. Under these conditions, the voltage output of the amplifier is zero.

Suppose that the resistance of the tunnel junction was made to change slightly by the application of a small dc voltage V. The balance condition is no longer met, and a potential difference will appear between points 1 and 2. The amplifier will respond to this input voltage by supplying a current δI through the feedback resistor R_f which returns the voltage drop across the junction to $v_o e^{i\omega t}$. Any resistive or capacitive mismatch between the junction and the reference elements R_s and C_s will be compensated by the additional current δI supplied by the operational amplifier, restoring the bridge balance. Under these conditions, the current I will

flow across the reference elements R_s and C_s. Since the voltage drop across the elements is $v_o e^{i\omega t}$.

$$I = v_o e^{i\omega t}(1/R_S + i\omega C_S) \tag{25}$$

The current-voltage characteristics of the junction are non-linear. Therefore, the current flowing through the junction must have a harmonic content if the voltage across the junction is to be the purely sinusoidal $v_o e^{i\omega t}$. Rogers[56] writes a Taylor series expansion for the current in this situation.

$$I + \delta I = (dI/dv + i\omega C_J) v_o e^{i\omega t} + 1/4 \frac{d^2 I}{dv^2} v_o^2 e^{i2\omega t} \ldots \tag{26}$$

Here the dynamic conductance $dI/dv = 1/R_j$ since the resistance of the junction is voltage dependent. If the amplitude v_o is small, the series converges rapidly. The voltage output of the operational amplifier is given by

$$\delta V = v_o e^{i\omega t} + R_f \, \delta I \tag{27}$$

Using Eqs. (25), (26) and (27) we can solve for δv

$$\delta v = R_f[dI/dv - \frac{1}{R_S} + \frac{1}{R_f} + i\omega(C_X - C_S)] v_o e^{i\omega t} + 1/4 \, R_f \frac{d^2 I}{dv^2} v_o^2 e^{i2\omega t} \tag{28}$$

The "in phase" component of the first harmonic term in this expression is a linear function of dI/dv, the conductance of the junction. The voltage δv is measured at frequency ω using PAR HR-8 lock-in amplifier. For the component at frequency ω, the null condition is

$$dI/dv = 1/R_s - 1/R_f \tag{29}$$

The feedback resistor is effectively in a parallel combination with the junction.

Since δv at frequency ω is a linear function of dI/dv, only two points are necessary to calibrate the conductance bridge. One point, $dI/dv = 0$ is obtained by switching the junction out of the circuit. The other point was taken at the null condition where dI/dv is given by Eq. (29). A simplified version of the entire conductance bridge and bias supply is shown in Figure 9. The PAR HR-8 lock-in amplifier with a Type B pre-amplifier was used as the detector for the system. The output of the lock-in was displayed on the Y axis of a Hewlett-Packard 7001 X-Y Recorder. The dc bias voltage was measured directly across the junction using a Hewlett-Packard 419A Microvoltmeter. It is necessary that this voltmeter have a high input impedance to both ac and dc signals because of its position in the circuit. The output of the voltmeter was displayed on the X axis of the X-Y recorder.

The dc bias was supplied by a ramp generator shown in Figure 9. This circuitry allows the dc voltage across the junction to be varied at a rate nearly independent of the junction resistance. The bias voltage could also be varied manually to set the initial voltage for the sweep or to locate structure in the conductance curves.

The ac modulation voltage across the junction was measured with an oscilloscope. At low temperatures, it is desirable to keep the peak value of the modulation voltage less than kT to avoid smearing sharp structure in the conductance. The kT smearing amounts to $86\mu eV$ per K. This restriction limits the modulation to about $25\mu eV$ at 0.3K. Modulation voltages of

from 30 to 50 μeV were used in this study. These voltages resulted in good signal to noise ratio at the detector. The 1600Hz noise level detected at the junction depends on the resistance of the junction and the bandwidth and time constant of the detector. Typically, this noise was on the order of 20 nanovolts for all our measurements.

Operating at 50μeV modulation, the bridge was able to detect changes in conductance of a 500Ω sample on the order of a few parts in 10^4. The performance is somewhat degraded for higher resistance samples. The system could accept junctions with resistances from 10Ω to 10KΩ with no changes in the circuitry.

The conductance bridge was calibrated for each sample while a dc bias voltage was applied to the junction. This bias voltage is chosen so that the sample conductance at the bias voltage does not change when the junction undergoes a superconducting transition. This means biasing the junction at voltages well away from the energy gap or phonon structure. For samples with a phonon spectrum similar to Pb, 30meV is a reasonable bias voltage. At this voltage, the X-Y recorder is adjusted so that the balance point occurs at mid-scale on the Y axis. The junction is then switched out of the circuit. The Y axis of the recorder then indicates the zero conductance position. This zero level can be adjusted to a suitable location on the recorder (usually the zero of the Y axis) by slightly increasing or decreasing the ac modulation to the bridge. The calibrated conductance is then displayed linearly on the Y axis. The sensitivity of the calibration can be increased or decreased by changing the sensitivity of the lock-in amplifier.

This calibration procedure was checked using a decade resistor as a "dummy" junction. The calibration procedure was found to be correct to better than 1%. The bridge is linear in conductance to better than 1%, and the output is stable to better than 1 part in 10^4 per hour.

The bridge circuitry is based on a design discussed by Rogers et al.[57] which permits a four terminal measurement of the sample. The system is, therefore, insensitive to small changes in the lead resistance to the sample. The apparent change in conductance being less than 5×10^{-4} per 1 ohm change in lead resistance. Such insensitivity to lead resistance changes is important when dealing with thin film tunnel junctions. Since part of the lead resistance is due to the thin film superconductor, substantial changes in lead resistance can occur at the superconducting transition. The effect of such abrupt changes of resistance is minimized in this bridge.

Sample Preparation

The thin film tunnel junctions described in this study were of two geometries, $Al/Al_2O_3/Pb\text{-}Cd$ and $Al/Al_2O_3/Cd\text{-}Pb$. Aluminum was used as a base electrode in these films because high quality aluminum films can be prepared using standard evaporation techniques. These films form clean, uniform surface oxides which make reliable tunnel barriers.

The choice of materials for the proximity sandwich is somewhat restricted because of the possibility of interdiffusion and solubility of the metals. Clearly such effects are to be avoided, and one is limited to materials which show little mutual solubilities. The solid solubility

of Pb in Cd is less than 2 wt.% at room temperature,[58] and no known intermetallic compounds exist. Furthermore, certain proximity sandwiches of these materials were kept at room temperature for up to two days without any measurable change in their transition temperatures. This indicates that there is little diffusion after the preparation of the junction.

The thin films of these materials were vacuum deposited onto a 1" X 1/2" X 1/16" fused quartz substrate. The substrate was cleaned sequentially in acetone, NaOH and aqua regia. The substrate was then boiled in Decontam detergent and given a final rinse in isopropanol. A stream of nitrogen gas was used to dry the substrate and to remove any dust particles.

When the substrate had dried, it was examined under a microscope and then mounted in a general purpose diffusion pumped vacuum system for the evaporation of the gold electrical contacts. This vacuum system was capable of achieving pressures of 10^{-5} Torr and is described in detail by Haskell.[53] A gold thin film was deposited onto the substrate through a stainless steel mask with six holes. The gold film was approximately 1000Å thick. The positioning of these gold electrodes on the substrate is shown in Figure 10.

The substrate was removed from the evaporator once the electrical leads were deposited and 99.99% pure indium was soldered onto the edges of the gold contacts. This solder would eventually be used to attach lead wires to the tunnel junction. The substrate was mounted in the rotating

substrate support and a section of #40 copper wire was attached from the support to one of the gold contacts on the substrate. This wire served to ground that electrode. This procedure was needed to keep the aluminum film at ground potential during the glow discharge oxidation. The rotating substrate support was mounted into the high vacuum system which contained the Al and SiO evaporation sources. The bell jar was flushed with oxygen prior to being evacuated to 10^{-6} Torr.

The materials used in the preparation of the proximity sandwiches were nominally 99.999% pure Al obtained from Cominco (Lot EM 438), nominally 99.999% pure Pb from Cominco (Lot EM 2287), and nominally 99.999% pure Cadmium from Cominco (Lot HPM 2437). A small section of each of the metals (about 250 mg) was cut from the parent ingot, cleaned and loaded into the appropriate evaporation source.

The aluminum was cleaned in a dilute solution of sodium hydroxide, the lead was etched in a 3:1 solution of 30% hydrogen peroxide and acetic acid, and the cadmium was cleaned in a dilute solution of nitric acid. The samples were rinsed sequentially in deionized water and methanol, then blown dry with a stream of nitrogen. After this cleaning procedure, care was taken when handling the samples and tweezers and gloves were used to mount the metal sample in the evaporation sources.

About 45 minutes were required for the vacuum system to achieve a vacuum of 10^{-6} Torr at which time the evaporation sources were outgassed. For the aluminum sample, this was accomplished by passing 10 amperes of current through the tungsten basket. At this current, the temperature of the basket is about 1000° C, considerably above the melting point of aluminum (660° C). There is an abrupt pressure rise as dissolved and

absorbed gasses leave the aluminum and basket. After a minute, the current was slowly decreased, and the pressure in the vacuum system returned to 10^{-6} Torr. A similar procedure was followed for the other evaporation sources. The SiO source has a much lower resistance than the tungsten wire baskets and, therefore, required a current of 250A to obtain a temperature of 900° C. The Cd source was outgassed at 250° C requiring a current of 50A. Throughout the outgassing procedure, the substrate was rotated away from the masks and was thus shielded from direct contact with any impurities.

Approximately 30 minutes after the outgassing, the aluminum film was deposited. The substrate was rotated over the stainless steel mask which defined the pattern of the Al thin film on the substrate. This pattern consisted of a single strip 0.04 cm. wide and 2.5 cm. long running between two of the gold contacts. The aluminum was evaporated at 1400° C at a rate of about 200Å per minute to a thickness of approximately 1000Å as determined by the quartz thickness monitor. Aluminum has a tendency to embrittle the tungsten wire and higher evaporation rates caused the basket to break. The system was allowed to cool for a few minutes, and the substrate was rotated over the SiO mask. This mask was designed so that the SiO film covered the entire substrate except in the region of the gold contacts and two 0.04 cm. X 0.04 cm. strips at right angles to the Al film. This arrangement is shown in Figure 10. The SiO film was evaporated at a rate of approximately 10Å per second to a thickness of about 700Å. This film is used to electrically insulate the Al film except

in the two 0.04 cm. X 0.04 cm. areas which serve as the junction sites. These are the only areas where direct electrical contact with the Al film is possible.

The next step in the procedure was the oxidation of the Al film to form the tunnel barrier. In his early experiments, Giaever[59] accomplished this oxidation by simply exposing the Al film to room air for a short time. Because the thermal oxidation rate for Al depends critically on the temperature and the presence of the water vapor in the air, this method is difficult to control and reproducibility is poor. In addition, one runs the risk of impurity contamination in the oxide. Both the reproducibility and contamination problems can be avoided using a glow discharge oxidation technique. Miles and Smith[60] have demonstrated that clean, uniform oxides can be grown on many metals by exposing them to an oxygen plasma. Jaklevic and Lambe[61] used this oxidation method in their study of interactions in the junction barrier so there is good evidence that this procedure yields uniform oxides. The ionized oxygen forms an oxide on aluminum very efficiently. The thickness of this oxide layer can be controlled by varying the exposure time or by applying a small positive voltage to the sample.

The glow discharge was initiated 20 minutes after the SiO evaporation. This time allowed the sample to return to room temperature. The diffusion pump was valved off from the bell jar, and 50μ of dry oxygen gas was introduced into the system. A glow discharge was initiated by applying 600 volts negative potential to a pure Al ring which served as the

discharge cathode shown in Figure 6. In this study, the Al film was kept at ground potential with respect to the cathode. The time the sample is exposed to the glow discharge determines the thickness of the oxide. For an aluminum film unmasked by SiO, an exposure time of ten minutes resulted in a tunnel junction with a resistance of about 500Ω and an estimated oxide thickness of 20Å. When the film was masked with SiO, an oxidation time of only three minutes produced a similar junction.

At first, it was thought that the SiO layer extended into the junction area, but an examination with the interference microscope proved this not to be the case. No adequate explanation for this apparent increase in oxidation rate for the SiO masked samples was determined.

Once the oxidation had been completed, the glow discharge was stopped and the system was brought to atmospheric pressure. The masks and evaporation sources for the Pb and Cd depositions were placed in the evaporator. This procedure usually took about three minutes. The system was then again pumped down and the final evaporations were performed to complete the junction. For junctions of the type $Al|Al_2O_3|Pb\text{-}Cd$, the Pb was evaporated through a suitable mask forming two tunnel junctions on the substrate, one of which was immediately covered with a film of Cd. For junctions of the other geometry, the masks were interchanged and the Cd film was deposited first. Although Cd sticks quite readily to a deposited Pb film, it has a very low sticking coefficient to the quartz substrate. Therefore, junctions of the type $Al|Al_2O_3|Cd\text{-}Pb$ were difficult to prepare and required careful control of the Cd evaporation rate. It was found

that passing a current of 50A through the Cd evaporation source produced a suitable evaporation rate for the Cd. At this current, the temperature of the Cd source was approximately 250° C. Even at this temperature, the Cd tended to re-evaporate from the walls of the vacuum system. A series of baffles were used to collimate the vapor stream and to prevent the re-evaporated Cd from striking the substrate. Even with these precautions, the percentage of good Al|Al_2O_3|Cd-Pb junctions was about 20%. However, those that were used in this study had Cd films displaying mirror-like surfaces and excellent electrical properties.

The evaporation of the Pb and Cd metals completed the junctions. A typical sample is shown in Figure 10. The sample consists of two tunnel junctions. One is a proximity sandwich with a Pb-Cd or Cd-Pb electrode, the other is a reference junction with a pure Pb or Cd electrode. This reference junction serves as a quality control for the proximity sandwich. The current-voltage characteristics of the reference should agree with the BCS predictions. If anomalies appear in the reference junction, the proximity sandwich should be treated as suspect. The reference junction also played another role. The current-voltage characteristics of the proximity sandwiches are somewhat smeared due to pair-breaking effects. These characteristics in the corresponding reference junctions are quite sharp and exhibit negative resistance characteristics. The reference junction was used to accurately determine the energy gap and transition temperature of the Al electrode. Since both the reference junction and the proximity sandwich share the same Al electrode, this measured gap and transition temperature was used in the analysis of the conductance data from the proximity sandwich.

Conductance Measurements

Immediately after the final evaporation, the completed sample was mounted in the ^3He cryostat. It is difficult to predict whether a given junction will display usable low temperature characteristics solely from the room temperature behavior. It was necessary to nonetheless develop certain room temperature criteria for the evaluation of the tunnel junctions. In this study, only junctions with room temperature resistances between 10Ω and 5KΩ were considered. Of these junctions, only those displaying non-linear conductance versus bias voltage characteristics were selected for low temperature study. A good junction, therefore, should have a room temperature resistance on the order of 100Ω and slightly parabolic conductance-voltage characteristics. When a junction which met these criteria was found, it was sealed in the vacuum can and cooled to liquid nitrogen temperature. The junction usually reached 77K in three or four hours. The conductance of the junction was monitored during this period. If electron tunneling is the major contribution to the conductance across the barrier, the conductance should be temperature independent or at best increase slightly. Any decrease in conductance as the temperature is lowered is a sign of metallic shorts in the barrier. Junctions which showed these characteristics were rejected. The more reliable junctions were cooled to 4.2K.

When the junctions had reached 4.2K, the bridge was balanced and the Y axis of the X-Y recorder was calibrated to display sample conductance as previously described. The zero conductance level was positioned at the

bottom of the graph paper and the conductance sensitivity was set at 20% per inch by adjusting the ac modulation voltage to the bridge and the sensitivity of the lock-in amplifier. The sample was then cooled to 1K, and the conductance at zero dc bias was recorded. As a final test of the junction quality, we demanded that this conductance be less than 1% of the normal state conductance. Because of the gap in the density of states in the superconductor, no zero bias tunneling current can flow through the barrier at reduced temperatures. Therefore, any measured zero bias conductance at these temperatures comes from a non-tunneling mechanism. Here we are making the demand that these non-tunneling "leakage" currents be less than 1% of the tunneling current. Other investigators have reported large non-tunneling currents when dealing with proximity sandwiches.[22] All of the junctions discussed here displayed "leakage" conductances of less than 1% of the normal state conductances. The zero bias and normal state resistance of the junctions discussed here are listed in Table 1.

The data for this study consisted of a series of dI/dV vs. V traces obtained from the X-Y recorder. Typically, 15 such traces were made for each junction at temperatures from the transition temperature of the junction to 0.3K. These traces were made at a sensitivity such that the entire density of states could be displayed conveniently on the graph paper. These traces were usually made at a sensitivity at which one inch on the graph paper corresponded to a conductance change of 20%. The lowest temperature data always included traces of the phonon induced structure

Table I. Summary of tunnel junction characteristics

Sample	d_S(Å)	d_N(Å)	R_N(Ω)	R_o(kΩ)	T_c(K)	Ω_N(meV)	E_p	Ω/kT_c
39-2	670	--	1240	307	7.22	1.38	1.38	2.22
23-1	950	471	2250	585	6.61	0.93	1.27	1.63
39-1	670	460	1050	378	6.27	0.72	1.22	1.33
80-1	500	458	172	265	5.85	0.57	1.07	1.13
93-2	330	510	253	236	4.86	0.43	0.73	1.03
109-2	650	1200	231	148	4.46	0.33	0.68	0.86
123-2	880	830	48	172	5.88	0.38	0.59	0.751
123-1	--	830	52	168	0.56	0.075	0.075	1.58

in the density of states made at a higher sensitivity. These traces were made at sensitivities of 1% or 2% per inch depending on the size of the phonon induced structure. In addition, conductance traces were made at temperatures slightly above T_c of the sample for normalization of the data. The normal state traces were taken at the same sensitivity as the corresponding superconducting state measurements.

The conductance data points measured from the X-Y plots were transferred to computer cards for normalization and analysis. Approximately 60 points at equal energy (bias voltage) intervals were taken in the gap region. Conductance measurements at these same 60 points were taken from the normal state data for normalization of the conductance. Normally, 180 points were taken in the phonon region from the 0.3K high sensitivity traces. Again, normal state points were also taken for data normalization.

The data in the gap region were normalized numerically using a computer. The transition temperature and the energy gap of the junction were determined from the normalized conductance. The temperature dependence of the zero bias conductance was used to determine the transition temperature of the junction. Hauser[23] has shown that the normalized zero bias conductance, $\sigma(0)$, linearly approaches unity as T approaches T_c. The transition temperature of a sample is found by plotting $\sigma(0)$ vs. T for temperatures near T_c and extrapolating to $\sigma(0) = 1$. This procedure is illustrated in Figure 11. The method gives a transition temperature for the junction which is very close (<.01K) to that found by resistance measurements on the same film.[46]

The determination of the energy gap in the BCS-like reference junctions was quite direct. At temperatures below the transition temperature of Al, peaks occur in the conductance at voltages corresponding to the sum and difference of the energy gaps of the two superconductors. In the reference junctions, these peaks are quite sharp and allowed an unambiguous determination of two energy gaps. At higher temperatures, the value of the energy gap was obtained by fitting the $\sigma(0)$, the zero bias conductance of the sample, to the BCS theoretical curves using the numerical methods described by Bermon.[62] For the reference junctions, the two methods of measuring the energy gap agreed to 2%. The determination of the gap in the density of states is considerably more difficult because the structure in the electron density of states in the proximity sandwiches is smeared due to lifetime effects. In fact, if the superconducting film in the sandwich is sufficiently thin, there will be no gap in the density of states.[9] None of our samples, however, exhibited this gapless behavior. At low temperatures where thermal smearing can be ignored, tunneling theory predicts a gap in the density of states for $V \leq |\Omega_N + \Delta_{Al}|$ where Ω_N is the gap in the density of states in the proximity sandwich and Δ_{Al} is the gap in the Al electrode. At 0.3K, the width of the zero conductance region is approximately $2(\Omega_N + \Delta_{Al})$.

The analysis of the data in the region of the phonon induced structure was done numerically in three stages. The phonon induced structure (strong coupling effects) appear in the tunneling characteristics as small deviations from the predicted BCS density of states. To display these effects

more clearly, the usual procedure is to calculate the ratio of the experimental density of states to an appropriate BCS density of states. The normalization is straightforward for an ideal superconductor with the fiducial BCS density of states chosen to have the same energy gap as experimental density of states. Many superconductors exhibit non-ideal behavior including multi-energy gaps as in the case of Nb_3Sn,[47] leakage conductances as in the case of La,[45] and lifetime broadening associated with the spatial variation of the pair potential as in the case of proximity sandwiches. In these cases, the choice of the fiducial BCS density of states is less obvious. We have normalized our tunneling results by dividing the experimental data by a fiducial BCS density of states. This BCS density of states was chosen so that peak in the fudicial curve occurs at the same energy as the peak in the experimental data. Since the data were taken at temperatures below the transition temperatures of the Al electrode, the peak in the density of states occurs at a voltage $V = \Delta_{Al} + E_p$ where Δ_{Al} is the energy gap in the Al electrode and E_p locates the maximum in the density of states in the proximity sandwich. The fiducial BCS density of states used in this analysis is, therefore, given by the convolution integral Eq. (3). By adopting this normalization procedure, we proceed as if the proximity sandwich were an ideal superconductor with an energy gap E_p. We do not mean to imply by this procedure that the proximity sandwich is BCS-like. We are merely extending the standard procedures to include non-ideal superconductors. The value of E_p is an unambiguously defined characteristic energy used to parameterize the tunneling results for the proximity sandwiches.

Stage one of the data analysis performs two numerical operations. First, the raw dynamic conductance data for the sample in the superconducting state is divided by the normal state conductance data to yield the electron density of states for the sample. This experimental density of states is then reduced by dividing by the fiducial BCS curve appropriate for the particular proximity sandwich. In the phonon region, we are primarily interested in the deviations from the BCS model predictions. Reducing the experimental density of states in this manner, these small deviations are enhanced, and the data are conveniently handled in this manner. The conductance data is recorded as a function of electron energy as measured from the Fermi energy of the proximity sandwich. The energy is recorded as eV where e is the electron charge and V is the dc bias applied to the junction. When discussing the phonon induced structure, it is convenient to shift the zero of energy to the gap edge. At T=0, this energy corresponds to the lowest energy state in the quasi-particle spectrum. Therefore, it is convenient to shift the energy zero in the output of stage one to correspond to E_p.

The second stage of data analysis is designed to remove the influence of the Al electrode from the tunneling characteristics. Because the phonon data are taken below T=0.3K, the measured conductance contains contributions from the density of states in the superconducting aluminum. The second stage of analysis removes this contribution assuming a BCS density of states in the aluminum electrode using the energy gap measured in that electrode. This procedure requires the deconvolution of the current integral given in Eq. (4). The output of this stage is the reduced density of states for the proximity sandwich.

Stage three of the data analysis consists of a modified version of the McMillan program[44] which numerically inverts the Eliashberg gap equations to give the phonon spectrum $\alpha^2F(\omega)$, the energy gap parameter $\Delta(\omega)$ and the Coulomb pseudopotential μ^* appropriate for the proximity sandwich. The details of the modifications of the McMillan program will be discussed at length in the following sections.

RESULTS AND DISCUSSION

Superconducting Transition Temperature

Many investigators[22,23,29] have reported that the superconducting properties of superimposed normal and superconducting thin films can be quite different from the original isolated metals. The transition temperature and energy gap of the superconducting film is depressed, and superconductivity is induced into the normal film. All of these effects were observed in our Pb-Cd proximity sandwiches. A summary of the results derived from tunneling experiments for the eight junctions discussed in this work is given in Table 1. The data for five of the junctions were obtained by tunneling into the superconducting (Pb) side of the proximity sandwich, and the remaining three junctions were investigated on the normal (Cd) side. The parameter, R_N in Table 1., is the normal state resistance of the tunnel junction measured at 77K, and R_o is the zero bias resistance measured with the junction in the superconducting state at 0.3K. In all of the proximity sandwiches discussed here, the ratio of R_N to R_o is less than 0.01, indicating that leakage currents are negligible in our samples. Tunneling electrons are the major contribution to the current through the junction which means the measured conductance dI/dV is proportional to the electron density of states in the sample.

The superconducting transition temperatures were determined by linearly extrapolating the temperature dependence of $\sigma(0)$ near the critical temperature as described earlier. The transition temperature decreases with decreasing lead thickness, the Cd thickness being approximately constant

at 500Å in the Pb-Cd samples. The variation of the measured T_c of the sandwich with the thickness of the lead film is shown in Figure 12. On the same graph we have plotted the results of Hauser et al.[23] for lead-platinum proximity sandwiches deposited by getter-sputtering at 77K along with the results of Claeson and Gygax[22] for evaporated sandwiches of lead and silver. Also shown are the T_c vs. d_S predictions of the de Gennes - Werthamer[7,8] theory of the proximity effect. The theory calculates the form of the spatial variation of the order parameter in terms of the coherence length ξ. We have calculated the theoretical results for a family of T_c vs. d_S curves for a variety of ξ_S and ξ_N. As shown in the figure, a rather good fit to the data is obtained for ξ_n = 500Å and ξ_S = 150Å, so there is qualitatively good agreement with the theory. There is some uncertainty in the determination of the coherence length in these samples, but it is probably true that the coherence lengths involved are on the order of the thickness of the films. If we assign these more realistic values for ξ in the films, the resulting theoretical curve lies below the experimental data. The tunneling results for the previously published Pb-Pt and Pb-Ag data show a T_c vs. d_S behavior similar to our Pb-Cd results. This is somewhat surprising since the normal metal films were of different materials in the various studies. As it turns out, the de Gennes - Werthamer theoretical results are also insensitive to the properties of the normal metal in the proximity sandwich. The calculated sandwich transition temperatures shows only a weak dependence on the transition temperature of the "normal" film and is strongly dependent on the thickness of the superconducting films involved.

Because of the uncertainty that exists in the determination of the coherence lengths in our films, we are unable to critically test the de Gennes - Werthamer theory. However, the general agreement of experiment and theory underline the fact that the observed depression of transition temperatures are indeed proximity effects induced by finite electron lifetimes and not the result of spurious interdiffusion of the metals comprising the sandwich.

Electron Density of States

The proximity effect also manifests itself in characteristic changes in the electron density of states in the sandwich. We have applied electron tunneling techniques to investigate these changes on both the superconducting (Pb) and normal (Cd) sides of our proximity sandwiches. The normalized conductance curves for all of the sandwiches investigated display lifetime broadening effects and an energy gap in the excitation spectrum that is reduced from that of bulk lead. These effects are illustrated in Figure 13 in which we have plotted the normalized conductance at 2.5K for a 670Å Pb reference junction along with that for our 670Å and 330Å Pb-Cd proximity sandwiches. As the Pb is made thinner, the lifetime broadening is markedly increased and the gap in the excitation spectrum is reduced. The normalized conductance curves obtained from the reference junction agree with the BCS density of states calculated with the Bermon[62] program to within 2% for $\omega<2\Delta$. The small differences that do occur can be attributed to strong coupling effects in the Pb. However, the conductance measured at low temperatures for the proximity sandwiches cannot be fitted

to a BCS density of states with reasonable accuracy. This fact is illustrated in Figure 14 in which we have plotted the normalized conductance at 1.36K for our 670Å Pb-Cd proximity sandwich along with the BCS conductance for a superconductor with the same transition temperature, T_c = 6.28K. The structure in the BCS curve is considerably sharper than that in the proximity sandwich. The experimental curve is definitely not BCS-like. The fit cannot be substantially improved by adjusting the energy gap parameter used in calculating the BCS curve. Decreasing the magnitude of Δ will decrease the height of the calculated peak at a given temperature but also decreases the width of the gap in the excitation spectrum. At very low temperatures, the BCS density of states becomes singular for all values of Δ, while rounded peaks, characteristic of lifetime broadening, persist in the proximity sandwiches.

All of the proximity sandwiches investigated in this study showed a definite energy gap in the experimental density of states at 0.3K. In this work we use the term energy gap in the strict sense to mean the energy range, measured from zero bias voltage, over which the density of states is zero. The magnitudes of the energy gaps for our samples measured at 0.3K, Ω_N, are listed in Table 1. Also listed is the parameter E_p which is the energy at which the peak occurs in the density of states. In the BCS theory $\Omega_N = E_p$ at T = 0.0K since the density of states is singular at the gap edge. In the proximity effect regime, however, the quasiparticle energy states are broadened due to the spatial variation of the pair potential, and these broadened states extend to destroy the sharp structure at the gap edge. Evidence for such a gap is observed on the Cd

side of the proximity sandwich at temperatures as high as 5.8K and thicknesses of the Cd film as large as 830Å and 1200Å. Measurements made on a 1200Å Cd reference junction resulted in T_c = 0.56K and Δ= 0.075meV. The data for the Cd-Pb proximity sandwiches listed in Table 1. show that the gap and transition temperature on the Cd side of the sandwich are enhanced by the presence of the lead even for relatively thick Cd films. These findings are in agreement with the experimental work of Guyon et al.[24] and Adkins and Kington[28] who also report a well-defined gap in the density of states measured from the normal metal side of the proximity sandwich. In addition, these observations are in accord with the McMillan[25] theory of the proximity effect which predicts a gap in the excitation spectrum over a wide range of thicknesses of the normal metal film.

One might argue that the observed energy gaps on the Cd side of our junctions may be due to pinholes in the Cd film or some sort of alloying of the normal and superconducting films. If such effects were present, the observed energy gap in the Cd would behave essentially as that in the superconducting (Pb) film. The temperature variation of the energy gap is reflected in the temperature dependence of $\sigma(0)$, the zero bias conductance. Guyon et al.[24] has shown that $1-\sigma(0)$ is essentially proportional to $|\Delta|^2$ (the square of the pair potential) for T near T_c. In Figure 15 we have plotted $1-\sigma(0)$ vs. $1-T/T_c$ measured on the superconducting side of four proximity sandwiches. The data lie very close to the BCS prediction being linear in $(1-T/T_c)$ near T_c and implying that on the superconducting side Δ varies as $(1-T/T_c)^{1/2}$. In Figure 16 we have

plotted the same parameters measured on the normal side of two proximity sandwiches. When these data are fitted to the empirical relationship $1-\sigma(0) \propto (1-T/T_c)^n$, we obtain values for n of 1.5 for the 900Å film and 1.8 for the 1200Å film. Guyon et al.[24] have obtained n values between 2.3 and 3.0 for their zinc-lead-bismuth proximity sandwiches. Vrba and Woods[30] have obtained values of n ranging from 1 to 6 in their study of aluminum-tin proximity sandwiches with the value of n increasing with increasing coupling between the films. The McMillan theory of the proximity effect allows values of n ranging from n = 1 (BCS behavior) for very strongly coupled films to $n > 2$ for weakly coupled films. Our values are consistent with moderate coupling between the Pb and Cd films in our samples. The shape of the curves in Figures 15 and 16 clearly show the difference between intrinsic and induced superconductivity in our proximity sandwiches. The superconducting properties observed on the Cd side of the sandwich are indeed proximity induced effects and are not the results of pinholes or alloying which would exhibit BCS behavior.

The density of states measured on the Cd side of the proximity sandwich is also quite different from the BCS predictions. These differences are brought out clearly in Figure 17 in which we compare the normalized conductance, measured at 2.24K for a 830Å Cd-900Pb proximity sandwich with a BCS curve with the same energy gap, Ω_N. There is no structure in the experimental curve which can be attributed to tunneling directly into the Pb film through pinholes in the Cd. The experimental density of states is larger than the BCS prediction at energies just

above the gap and drops lower than the BCS curve at slightly higher energies. Since the spatially dependent pair potential is smallest near the surface of the Cd film, we expect the density of excited states to be larger on the Cd side at low energies. On the other hand, the density of excited states on the Pb side of the junction is greatest at higher energies. The lowest energy excited state available to a tunneling electron lies just above Ω_N, and the same energy gap should be measured by tunneling from either side of the sandwich. Figure 18 shows the normalized conductance curves for two proximity sandwiches, one measured on the Pb side, the other on the Cd side of the sandwiches. The two sandwiches have approximately the same transition temperature. The enhanced density of states just above Ω_N in the Cd and the gradual rise in the Pb are apparent. The available density of states in the Cd rise sharply at low energies and drop off faster than the BCS prediction at higher energies.

The only theory of the proximity effect which allows a calculation of the excitation spectrum in a proximity sandwich for temperatures well below T_c is that of McMillan.[25]

The McMillan tunneling model of the proximity effect considers the interaction between superimposed normal metal (N) and superconducting (S) thin films by assuming that the films are coupled by electrons tunneling through the potential barrier at the interface. McMillan treats this interaction between the films using a second order self-consistent perturbation approach in which the superconducting properties of the films

are assumed to be uniform across the film thickness. The theoretical predictions of the theory are therefore strictly valid only for relatively thin films which are weakly coupled to one another through a barrier at the interface. Several tunneling experiments[28,29,30] have shown qualitative agreement with the predictions of the theory, and the model seems applicable in a number of cases. We have applied this model in the analysis of our tunneling data. The results of this analysis are shown in Table 2. The basic parameters of the McMillan theory Γ_S, Γ_N, Δ_S^{Ph} and Δ_N^{Ph} are derived from the experimental data. The magnitude of Γ_S and Γ_N were calculated from the measured transition temperature of the proximity sandwiches using Eqs. (15) and (17). As the (S) film in the sandwich is made thinner, Γ_S increases and the transition temperature of the sandwich, T_c, is depressed. In this study we have found that T_c varies nearly linearly with Γ_S and is nearly independent of Γ_N. Vrba and Woods[30] report a similar T_c dependence in their work with Al-Sn proximity sandwiches. The theoretical variation of the sandwich transition temperature with the parameters Γ_S and Γ_N is shown in Figure 1. The values of Γ_S were used to calculate the effective barrier transmission coefficient, α, at the lead-cadmium interface using Eq. (15). This coefficient is on the order of 0.1 for all sandwiches investigated by tunneling into the (S) side. This value of the transmission coefficient seemed somewhat small because care was taken to avoid contamination between the films composing the proximity sandwich. This value of $\alpha = 0.1$ is to be compared with a value of $\alpha = 0.4$ found by Rowell and McMillan[63] in tunneling

Table 2. Parameters derived from the McMillan model for the proximity effect

Sample	T_c(K)	Γ_S(meV)	Γ_N(meV)	Δ_S^{Ph}(meV)	Δ_N^{Ph}(meV)	Ω_N(meV)
39-2	7.22	0	--	--	--	1.38
23-1	6.61	0.08	0.42	1.23	0.18	0.93
39-1	6.27	0.13	0.49	1.15	0.29	0.72
80-1	5.85	0.18	0.52	1.04	0.40	0.57
93-2	4.86	0.18	0.54	0.72	0.56	0.43
109-2	4.46	0.38	0.53	0.93	0.77	0.33
123-2	5.88	0.16	0.25	1.08	0.40	0.38
123-1	0.56	0	--	--	--	0.75

experiments measuring resonance effects in superimposed films of silver and lead. It seems that the formation of a contamination barrier between the films of the sandwich is possible even when the evaporation procedure is carried out in very high vacuum. In a vacuum of 3×10^{-6} Torr, a monolayer of gas strikes a clean surface every second, and therefore, a layer of absorbed gas between the films is unavoidable. The barrier formation process is further complicated since this absorbed layer is likely penetrated by the second metal evaporated to complete the proximity sandwich. Whether an actual oxide layer is formed between the two films depends on the metals involved and probably on other factors such as evaporation rates and substrate temperature. Furthermore, one must realize that the barrier between the films in the McMillan model need not be an actual oxide layer. The differing electronic and atomic structures of the two metals would contribute to a potential barrier reflecting electrons at the interface.

We were able to calculate the energy variation of the pair potential predicted by the McMillan theory from the experimental values of Γ_S and Γ_N using Eqs. (11) and (12) and the iterative numerical procedure described earlier. Once the energy dependence of the pair potential is known, a theoretical electron density of states can then be calculated from Eq. (16). The parameter Δ_S^{Ph} which enters into Eq. (11) and (12) is difficult to calculate within the framework of the model since it involves iterative solutions of the self-consistency integral Eq. (14). In the analysis, we have used Δ_S^{Ph} as an adjustable parameter in a fitting procedure in which

Δ_S^{Ph} was adjusted so that the peak in the calculated density of states would occur at the same energy as the experimental peak (E_p) at low temperatures. The calculated density of states has one adjustable parameter, Δ_S^{Ph}, which fixes the position of the peak in the density of states. The other necessary parameters can be calculated within the model from the measured transition temperature of the proximity sandwich. A typical energy dependent pair potential and density of states calculated from the model are shown in Figures 2 and 3. These results were obtained with values of Γ_S, Γ_N and Δ_S^{Ph} appropriate for our 670Å proximity sandwich. A detailed comparison between the predictions of the model and the experimental results for the 670Å and 330Å proximity sandwiches are shown in Figures 19 and 20. The agreement with the McMillan theory is quite good. In the thicker film, the theoretical density of states displays a small peak at energies just above Ω_N. This structure is not observed in any of our proximity sandwiches. The experimental results of several other investigators[28] have failed to show this low energy structure. At temperatures above the transition temperature of the Al electrode, the tunneling conductance can be calculated from Eq. (5) using the density of states derived from the McMillan theory. At these temperatures, thermal smearing effects begin to become important, and the low energy structure is not observable. The results of such a calculation along with the experimental conductance are shown in Figures 21, 22, 23, and 24. The agreement between theory and experiment is quite good, and similar agreement is obtained at other temperatures above the transition temperature of the Al.

Vrba and Woods[30] have performed tunneling experiments into tin-aluminum proximity sandwiches taking care to meet the conditions imposed by the McMillan theory in that metal films used were very thin, and the interaction between the films was decoupled by the intentional formation of an oxide at the films' interface. Under these rigorous conditions, the experimental density of states for many of their proximity sandwiches exhibited the double-peak structure at low energy predicted by the McMillan model. This structure was reportedly very dependent on the barrier transmission probability α and the film thickness. The fact that the low energy structure is not observed in our samples is not surprising. The low energy structure is due to excitations in the Cd region of the proximity sandwich. In our thicker samples, the tunneling electrons may not be able to sample these excitations due to a short mean free path. More fundamentally, the McMillan theory does not take into account the true space dependence of the order parameter in the sandwiches. In thicker sandwiches, this spatial variation may become important and affect the structure in the observed density of states. Our experimental data for the thicker samples look like McMillan curves for much larger values of Γ_S and α than are calculated from the measured transition temperature. As α increases, electrons are transferred rapidly across the interface, and the films are strongly coupled and the peaks in the electron density of states move together. In a sense, the structure in the measured density of states is what one might expect from a clean interface, although the transition temperature and energy gap are in agreement with $\alpha \simeq 0.1$.

As an alternative explanation, lack of agreement might be the result of a non-uniform barrier between the films in the proximity sandwich. The observed density of states may be a combination of McMillan curves with different decoupling barriers. Whatever the source, the discrepancies are small, and the McMillan model describes the tunneling density of states quite well, especially in the region near the peak in the density of states. The predictions of the model are in good agreement with experiment if one operates within the restrictions of the theory. The model offers the most complete description of the proximity effect available. It would be very useful to have a model that is valid for thick films incorporating mean free path dependencies. Such a theory would require knowledge of the spatial dependence of the pair potential and a complete solution of the Gor'kov[64] equations. Until such a theory is available, only semiquantitative agreement with experimental results can be expected.

Phonon Spectrum

The reduced densities of states in the region of the phonon spectrum of the proximity sandwiches are shown in Figure 25. The curves shown are the output of stage two of the data analysis and represent the measured tunneling density of states divided by a fiducial BCS density of states. The energy scale is measured from E_p for all of the data shown. Because of the lifetime broadening due to the spatial variation of the pair potential in the proximity sandwiches, E_p does not represent the smallest

excitation energy in the proximity sandwiches. The density of states near E_p are considerably smeared with a non-zero density of states at energies below E_p. Nevertheless, there is a significant peak in $N(\omega)$ at $\omega = E_p$, and the energy of this peak in the density of states determines the energies at which the phonon induced structure appear. This fact is made clear by comparing the reduced density of states for the proximity sandwiches to the results for the 670Å Pb reference junction which exhibits essentially BCS behavior. For the Pb reference junction, the value of E_p is equal to the BCS energy gap parameter in the Pb. We, therefore, should expect to see strong coupling effects at energies above E_p corresponding to the transverse and longitudinal peaks in the Pb phonon spectrum. The reduced density of states for the 670Å lead reference junction drops off abruptly at 4.5 and 8.5 meV, the energies of the peaks in the phonon spectrum of lead. This same structure can likewise be seen in the reduced density of states in our proximity sandwiches. With the energy scale measured from E_p for each sample, the phonon induced structure for all of our samples appears at approximately 4.5 and 8.5 meV. This means, as might be expected, the phonon spectrum in the lead film dominates the strong coupling effects in the proximity sandwiches. The structure in the reduced density of states is somewhat less sharp in the proximity sandwiches than in the lead reference junction. This is most apparent in the thinner proximity sandwiches and reflects the lifetime broadening of the electronic states due to the spatial variation of the pair potential across the sample. The strength of the coupling, and therefore, the size of the deviations in the reduced density of states,

is approximately proportional to $(T_c/\theta_D)^{2.46}$ This variation of the coupling strength with T_c is clearly seen in our proximity sandwiches. The size of the deviation in the reduced density of states at 8.5meV is 5.5% of the normal conductance for the lead reference junction T_c = 7.22K and 22% of the normal conductance for the 330Å proximity sandwich T_c = 4.86K. The size of the phonon induced structure varies approximately as T_c^2.

The observed structure in all of the samples shown in Figure 25 is consistent with strong coupling effects in lead. The deviations in the reduced density of states at energies greater than the Debye cutoff frequency in lead (~10meV) can be associated with multiphonon processes. There is a finite pairing interaction in the cadmium and the presence of the lead film should induce an additional, stronger interaction in the cadmium film. We might, therefore, expect weak structure in the reduced density of states near the Debye energy of cadmium (~16meV).[38] No such structure, however, is observed in any of our samples.

The McMillan unfolding program[44] was used to numerically invert the Eliashberg gap equation to give the pair potential, $\Delta(\omega)$; the effective phonon spectrum, $\alpha^2F(\omega)$; and the Coulomb pseudopotential, μ^* that best fit the experimentally determined density of states. This program has been applied to a number of superconducting materials, and the results have been confirmed by neutron scattering experiments. The program has been widely accepted as a reliable source of information on the electron-phonon interaction in superconducting materials. For proximity sandwiches,

however, a modification of the McMillan procedure is required to account for the lifetime broadening effects introduced into the tunneling characteristics by the spatial variation of the pair potential in the samples. This spatial dependence alters the energy dependence of $\Delta(\omega)$ and, consequently, the density of states $N(\omega)$. These lifetime effects are most important near the gap edge but also influence the phonon induced structure as is apparent in the reduced density of states in Figure 25. A complete description of the tunneling results in Pb-Cd proximity sandwiches, therefore, should include interactions due to the spatial variation of the pair potential as well as strong coupling effects.

The effect of the lifetime broadening on the phonon induced structure can be studied by applying the standard McMillan program to analyze the tunneling data. This approach has been used for other non-ideal superconductors as, for example, Nb_3Sn. The results of the unfolding program using the standard McMillan procedure are given in Table 2. The parameter λ is the strength of the electron phonon coupling introduced by McMillan.

$$\lambda = 2\int_0^\infty \frac{\alpha^2 F(\omega)}{\omega}\, d\omega \tag{30}$$

In terms of the BCS theory, λ corresponds to $N(0)V$.

The average phonon frequency $\langle\omega\rangle$ is defined as follows

$$\langle\omega\rangle = \int_0^\infty \alpha^2 F(\omega)\, d\omega \Big/ \int_0^\infty \frac{\alpha^2 F(\omega)}{\omega}\, d\omega \tag{31}$$

The calculated parameters for our 670Å lead reference junction with no cadmium backing are in excellent agreement with the results of McMillan and Rowell.[46] This was the case with every pure lead reference junction

investigated, so we are confident in the general applicability and our interpretation of the standard unfolding program. The results for the proximity sandwiches, however, show considerable variation. The parameters λ and $\langle\omega\rangle$ show a slow increase as the lead thickness in the sandwich is decreased. The calculated value of μ^*, however, increases rapidly with decreasing lead thickness reaching 0.56 for the 330Å proximity sandwich. The theoretical estimates for μ^* are in the range of 0.1 to 0.2 for most metals, so these very high values are most likely an artifact caused by the failure to properly account for lifetime effects in the unfolding procedure.

Lou and Tomash[45] reported an anomalously small value (0.01) for μ^* in their tunneling work on La, and this low value of μ^* was attributed to impurity attenuation of the phonon induced structure in the tunneling electron density of states in the La at high energies near the Debye energy. They found that by arbitrarily enhancing the structure in the tunneling data, the value of μ^* could be brought into agreement with theory without drastically affecting the major features in the phonon spectrum calculated with the McMillan program.

This approach, however, does not seem to apply to the case of our data. We would have to attenuate rather than enhance the phonon induced structure, and the magnitudes of the attenuations are unreasonable. We have found that a 10% attenuation of the observed density of states lowers the calculated μ^* by roughly 10%. The large attenuations that would be needed to bring the calculated μ^* to the theoretical value is

unjustified for our samples. Also, an impurity induced change in μ^* seems unlikely for our samples because the reference junctions prepared at the same time as the proximity sandwiches show no such effects.

To understand how these anomalously high values of μ^* might arise, it is necessary to understand the role of λ and μ^* in the Eliashberg equations and to review the procedure by which these parameters are derived in the unfolding routine. The size of λ indicates the strength of the electron-phonon coupling in the material and, thus, is important in governing the amplitude of the phonon-induced structure in the electron density of states. A large λ is indicative of a strong electron-phonon interaction which favors the formation of Cooper pairs. The value of μ^*, on the other hand, is related to the strength of the screened Coulomb repulsion between electrons. This repulsion tends to interfere with the pairing process. The net electron-electron interaction includes both of these opposing interactions. The net interaction can be either repulsive as in the case of normal metals or attractive as in the case of superconducting materials. The competition between the interactions governed by μ^* and λ is evident in the form of the Eliashberg gap expression, $\Delta(\omega)$ Eq. (22). The expression for $\Delta(\omega)$ has two contributions; a phonon contribution, dependent on λ through the kernel $K(\omega,\omega')$, and a negative Coulomb contribution dependent on μ^*.

The McMillan unfolding program determines the value of μ^* from the value of $\Delta(\omega)$ at the gap edge $\omega = \Delta_o$. $\Delta(\omega)$ is calculated using a phonon spectrum $\alpha^2F(\omega)$ that best fits the experimental density of states.

The value of μ^* is adjusted so that $\Delta(\omega)$ has the proper value at the gap edge. For electron energies very near the gap edge, the density of available phonon states approaches zero, and, therefore, at these energies the Eliashberg strong-coupling theory reduces to the BCS weak coupling results. The value of $\Delta(\omega)$ should approach Δ_o for energies near the gap edge ($\omega=E_p$). The unfolding program determines the value of Coulomb pseudopotential by adjusting μ^* so that $\Delta(\omega) = \Delta_o$ for energy $\omega = E_p$. This adjustment is made at each stage of the iterative procedure. If the value of the phonon-induced structure is too small in comparison to the calculated magnitude of $\Delta(\omega)$ at the gap edge, the program will return a small value of μ^* as in the La case. On the other hand, if the induced structure is larger than the calculated magnitude of $\Delta(\omega)$ would warrant, a value of μ^* larger than the theoretical value would result.

We have already established that the presence of the cadmium in the proximity sandwich reduces both the transition temperature and the pair potential in the lead and broadens the density of states at low energies. It seems likely that the incorporation of these proximity-induced interactions into the Eliashberg equations and unfolding program might produce a value of μ^* in agreement with theory.

The Eliashberg theory predicts the pair potential to be strongly energy-dependent for energies near the peaks in the phonon spectrum. This variation of $\Delta(\omega)$ gives rise to the observed phonon-induced structure in the density of states. The McMillan tunneling model for the proximity effect predicts the pair potential will be energy-dependent at low energies.

It is reasonable that the proximity induced interactions could be introduced into the Eliashberg equations without interfering with the phonon induced variations of $\Delta(\omega)$. To this end, Liu[65] has suggested a new renormalization function that includes both strong coupling effects and lifetime effects due to pairbreaking.

$$Z'(\omega) = Z_{Ph}(\omega) + \frac{i\Gamma}{[\omega^2-\Delta^2(\omega)]^{1/2}} \tag{32}$$

Here, $Z_{Ph}(\omega)$ is the strong-coupling renormalization from the Eliashberg expression Eq. (22). Γ is a lifetime parameter due to the proximity effect. To avoid numerical difficulties associated with the singularity in this expression, we have used an approximate form of Eq. (32) derived from the McMillan model, Eq. (20), of the proximity sandwich

$$Z'(\omega) = Z_{Ph}(\omega) + \frac{i\Gamma_S}{[\omega^2-\Omega_N^2]^{1/2}} \tag{33}$$

Here, Γ_S is the lifetime parameter calculated from the transition temperature of the sample and Ω_N locates the break in the density of states of the proximity sandwich. For the small values of Γ_S appropriate for our proximity sandwiches, this additional term in the renormalization function has little effect on the variation of $\Delta(\omega)$ at high energies near the phonon-induced structure. At lower energies, this additional term reproduces the energy dependence of $\Delta(\omega)$ due to the proximity effects. There is at present no theory which incorporates both strong-coupling and proximity-induced effects. The modification of the renormalization function seems to be a satisfactory first approach to the problem.

Because of the energy dependence of the pair potential at low energies, it is not possible to experimentally determine the magnitude of $\Delta(\omega)$ for energies near $\omega = E_p$. The magnitude of $\Delta(\omega)$ at $\omega = E_p$ corresponds to the BCS parameter Δ_o only in the limit $\Gamma_s = 0$, since lifetime effects are important in $\Delta(\omega)$ at low energies. It is important to remember that the magnitude of the pair potential can be identified with the size of the gap in the density of states only in the BCS theory. Indeed, the pair potential is in general not a directly observable experimental quantity, and, therefore, one can calculate the magnitude of the pair potential only in the framework of a given theory. At the present time, there is no theory which adequately describes the density of states for the proximity sandwiches. Consequently, there is no unambiguous way to calculate the magnitude of the pair potential from an experimentally determined density of states. If we are to use the value of $\Delta(\omega)$ at $\omega = E_p$ as the criterion for the determination of μ^*, we must resort to fitting the experimental data to a theoretical model to determine the magnitude of $\Delta(\omega)$ at that energy. An obvious first guess is to associate the energy E_p with the magnitude of the pair potential evaluated at $\omega = E_p$. This choice is motivated by the equation for the density of states, Eq. (21).

The density of states is a maximum at an energy $\omega = E_p$. From the form of Eq. (21) we can conclude that this maximum occurs when $\Delta(\omega) = \omega$ which gives the condition $\Delta(\omega) = E_p$ at the peak in the density of states. This value seems to be a reasonable estimate of the magnitude of the pair

potential at low energies, and the determination of the value of μ^* from this estimate is analogous to the methods used for ideal superconductors.

Another estimate of the magnitude of the pair potential can be obtained by fitting the experimental electron density of states to the theoretical prediction of the McMillan[25] model for the proximity effect. This fitting procedure was discussed earlier, and the results are listed as Δ_S^{Ph} in Table 2. The magnitude of the pair potential determined from the McMillan theory, $\Delta_S(\omega)$, agrees with our earlier estimate of $\Delta(\omega) = E_p$ to within 6% for all of our samples. Such agreement is encouraging, but it must be pointed out that both of these values are merely estimates. The McMillan model does not provide an exact description of the observed density of states, so the pair potential calculated from this model serves only as a reasonable approximation to the experimental case. A more exact determination of $\Delta(\omega)$ would require a more complete theoretical description of the interactions at the normal-superconductor interface. No such theoretical model is available at present.

Since the exact magnitude of the pair potential cannot be determined experimentally, and the uncertainty in the value of the pair potential gives rise to an uncertainty in the value of μ^* calculated by the unfolding program, we have adopted a semi-empirical approach to the analysis of the data. The modified McMillan program was used to unfold the experimental data using $\Delta_{fit} = E_p$ at $\omega = E_p$ as the condition on the pair potential used to determine μ^*. Realizing that this condition is at best an approximate one, we have obtained solutions to the Eliashberg equations

for several other values of Δ_{fit} near E_p. The results of this study are given in Table 3. The value of μ^* decreases with increasing Δ_{fit} since a small Coulomb term is then needed to make the calculated $\Delta(\omega) = \Delta_{fit}$ at $\omega = E_p$ given the observed structure in the density of states. The magnitude of the phonon spectral function decreases with decreasing μ^* as Δ_{fit} is increased. The shape of the spectral function remains unchanged. In our 330Å proximity sandwich, in which the lifetime smearing is most severe, we have varied Δ_{fit} from 0.73 to 0.80 meV, the corresponding values of μ^* range from 0.52 to 0.13. The magnitude of the calculated spectral function decreases by 18% for the various solutions, and this is reflected in the changes in the magnitude of λ which is sensitive to changes in the phonon spectrum. The parameter Δ_{fit} governs both the magnitude (but not the shape) of $\alpha^2F(\omega)$ and the value of μ^* calculated by the program. This is true for all the proximity sandwiches investigated and is most apparent in the 330Å junction for which Δ_{fit} was varied over a considerable range to determine Δ_{fit} that results in $\mu^* = 0.13$ ($\Delta_{.13}$). Solutions were obtained for all samples with $\mu^* = 0.13$, the value calculated for our pure lead reference junction. The magnitude of the pair potential which results in $\mu^* = 0.13$ ($\Delta_{.13}$) lies very close to E_p for the samples. In fact, the values of E_p and $\Delta_{.13}$ agree to better than 5% for all of the proximity sandwiches with the exception of the 330Å sample in which these parameters differed by 8%. Table 4 lists a complete set of parameters calculated using the modified McMillan program and assuming $\mu^* = 0.13$, the theoretical value for Pb. Under this assumption,

Table 3. Results of the unfolding program

	E_p (meV)	Δ_{fit} (meV)	μ^*	λ	$\langle\omega\rangle$
39-2	1.38	1.38	.131	.151	5.34
23-1	1.27	1.27	0.23	1.90	4.94
		1.29	0.20	1.74	4.97
		1.31	0.15	1.57	5.04
		1.32*	0.13	1.49	5.08
39-1	1.22	1.16	0.38	2.34	5.15
		1.22	0.17	1.63	5.30
		1.24*	0.13	1.49	5.43
		1.26	0.08	1.35	5.51
80-1	1.07	1.07	0.15	1.50	5.72
		1.074*	0.13	1.40	5.84
		1.08	0.114	1.34	5.92
		1.085	0.110	1.33	5.93
93-2	0.73	0.73	0.52	2.08	5.31
		0.75	0.37	1.80	5.46
		0.77	0.26	1.57	5.61
		0.80*	0.13	1.34	5.88

*$\Delta_{fit} = \Delta_{.13}$

Table 4. Unfolding results assuming $\mu^* = 0.13$

Sample	E_p (meV)	Δ_S^{Ph} (meV)	Δ_{fit}	Γ_S (meV)	λ	$\langle\omega\rangle$
39-2	1.38	--	1.38	0	1.51	5.34
23-1	1.27	1.23	1.32	0.08	1.49	5.08
39-1	1.22	1.15	1.24	0.13	1.49	5.43
80-1	1.07	1.04	1.074	0.18	1.40	5.84
93-2	0.73	0.72	0.80	0.32	1.34	5.88

the calculated values of λ and $\langle\omega\rangle$ for our proximity sandwiches differ from those for the pure lead reference junction by less than 15%. This general agreement is also noticed when one examines the phonon spectral functions $\alpha^2F(\omega)$ calculated for the proximity sandwiches in Figure 26. While there are some small changes in $\alpha^2F(\omega)$ as the Pb thickness in the proximity sandwich is decreased, the overall features are those of pure lead. The positions of the transverse and longitudinal peaks in the phonon spectra are relatively unchanged throughout the series. The structure at 3.8meV associated with a Van Hove singularity in the phonon spectrum of lead appears (although considerably less sharp) in all but the thinnest proximity sandwich. In general, the energy resolution of the phonon spectrum for the proximity sandwiches is degraded from the case of the pure lead spectrum. Because of the lifetime broadening effects in the proximity sandwiches, all of the features display a minimum energy width Γ_S which tends to round off sharp features.

If the lifetime correction term in the renormalization function is omitted in the calculation of $\Delta(\omega)$ from the Eliashberg equations, a high energy tail at energies above the longitudinal peak appears in the calculated spectral function $\alpha^2F(\omega)$. The effect of the correction term is illustrated in Figure 26, where we have shown the spectral function for the 330Å proximity sandwich without the correction term. Because of the complex, non-linear, convolution integral involved in the Eliashberg equation for $\Delta(\omega)$, the effect of our modified renormalization on the calculated $\alpha^2F(\omega)$ is impossible to determine from first principles.

From Figure 27. we can see that the primary effect of the correction term is to eliminate most of the unphysical high energy tail. The lifetime correction term is necessary to properly account for the lifetime broadening in the electron density of states as well as the high energy region of the phonon spectral function.

The pair potential for our 500Å Pb-Cd proximity sandwich, calculated with the modified McMillan procedure assuming $\mu^* = 0.13$ is shown in Figure 28. These results can be compared with the pair potential calculated for pure lead shown in Figure 4. The overall magnitude of the pair potential for the proximity sandwich is reduced at all energies from the pure lead case. This reduction in the pair potential is responsible for the reduced gap in the electron density of states in the proximity sandwiches. The major structures in the Pb pair potential are reproduced in the results for the proximity sandwich. The important differences occur at low energies where $\mathrm{Im}\Delta(\omega)$ in the pure Pb goes to zero while $\mathrm{Im}\Delta(\omega)$ in the proximity sandwiches becomes negative as the electron energy approaches zero. This effect is important in determining the shape of the electron density of states at low energies. Since $\mathrm{Im}\Delta(\omega)$ is non-zero at low energies, there cannot be a singularity in the electron density of states. This fact can be seen from the form of the density of states expression, Eq. (21). The shape of $\Delta(\omega)$ in the low energy region (0-3 meV) where proximity induced effects are most important follows the prediction of the McMillan model for the proximity effect. The fact that $\Delta(\omega)$ is complex even near the gap edge accounts for the observed lifetime broadening in $N(\omega)$ at low energies.

The electron density of states calculated from the derived pair potentials, $N_c(\omega)$ can be directly compared to the experimental density of states, $N_{exp}(\omega)$, for the proximity sandwiches. For all of our samples $N_c(\omega)$ agrees with $N_{exp}(\omega)$ to better than 0.1% for the energy range (2-35 meV). This small deviation is reason for confidence in the calculated $\Delta(\omega)$ and in the operation of the unfolding procedure.

After obtaining unfolding results for a variety of input parameters, we feel that the strong-coupling parameters for our proximity sandwiches are known to about 15%. The uncertainty is related to our inability to determine the value of $\Delta(\omega)$ at the gap edge. To within this experimental uncertainty, our results show that the strong-coupling effects in our proximity sandwiches can be accounted for by the interactions in the lead film. The presence of the cadmium film effects the coupling primarily by depressing the pair potential in the lead at all energies and introducing lifetime effects which alter the form of the pair potential at low energies. The lifetime term in the renormalization, $Z(\omega)$, which follows from the McMillan model for the proximity effects seems to account for all proximity induced interactions in the samples. Although the transition temperatures of the thinnest samples have been depressed by 35%, and the width of the gap in the density of states has been reduced by more than 50% from the values for the bulk superconductor, the strong-coupling effects present in the sandwiches are essentially those of bulk lead.

SUMMARY

The tunneling characteristics of Pb-Cd proximity sandwiches in which the Pb thickness ranges from 950Å to 330Å are in qualitative agreement with the McMillan model of the proximity effect. There is some discrepancy in as much as certain low energy structure predicted by the model, which arise from interactions in the Cd film, are not observed in the density of states measured on the Pb side of the junction. The density of states measured on the Cd side displays a well defined gap even for relatively thick Cd films. For example, an energy gap of 0.33meV was measured in a 1200Å thick Cd film comprising a proximity sandwich. This energy gap is nearly 25% of that observed in bulk Pb, implying that superconductivity can be induced over a considerable distance in these samples.

Phonon-induced structure is observed in the measured density of states on the superconducting side of the proximity sandwiches. The magnitude of this structure scales as T_c^2 of the sandwich, but the position and shape of the structure are essentially unchanged as the Pb film thickness is decreased. The density of states in the phonon region was numerically unfolded using a modified McMillan-Eliashberg technique to obtain the phonon spectral function $\alpha^2F(\omega)$ for the proximity sandwiches. Lifetime effects were introduced into the Eliashberg equations through the complex renormalization function $Z(\omega)$. Due to the fact that the magnitude of $\Delta(\omega)$ at the gap edge cannot be reliably determined from the experimental data, the value of μ^* cannot be calculated with certainty for the proximity sandwiches. The phonon spectral functions calculated

assuming $\mu^* = 0.13$ agree with those of pure lead to $\pm$ 15%. The primary effect of the lifetime correction is the reduce a high-energy tail in the calculated spectrum and such corrections, though approximate, seem to be a reasonable first approach to the problem. A more exact treatment would require a more complete theoretical description of the space and energy dependence of the pair potential in the proximity effect regime.

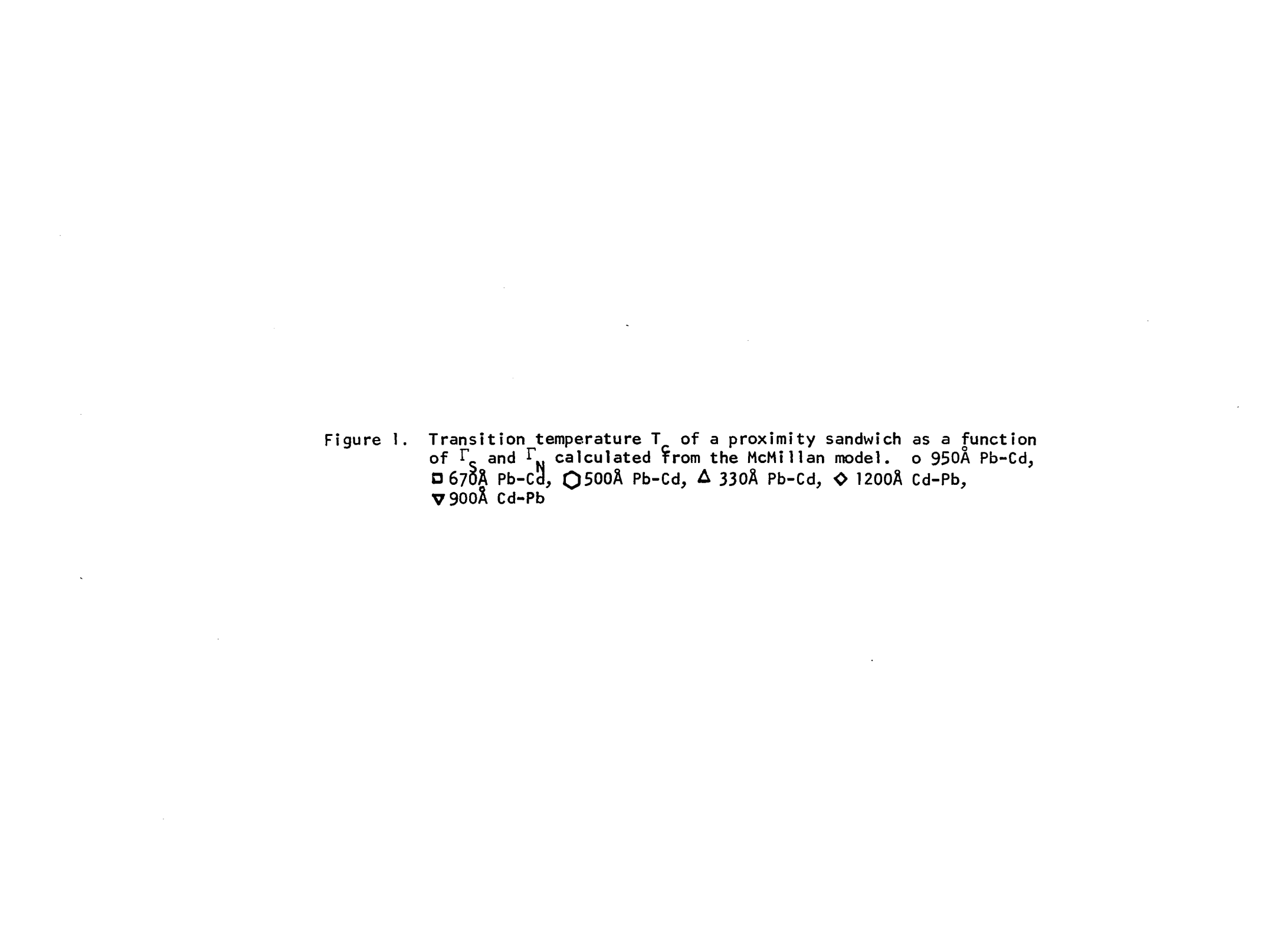

Figure 1. Transition temperature T_c of a proximity sandwich as a function of Γ_S and Γ_N calculated from the McMillan model. o 950Å Pb-Cd, □ 670Å Pb-Cd, ⬡ 500Å Pb-Cd, △ 330Å Pb-Cd, ◇ 1200Å Cd-Pb, ▽ 900Å Cd-Pb

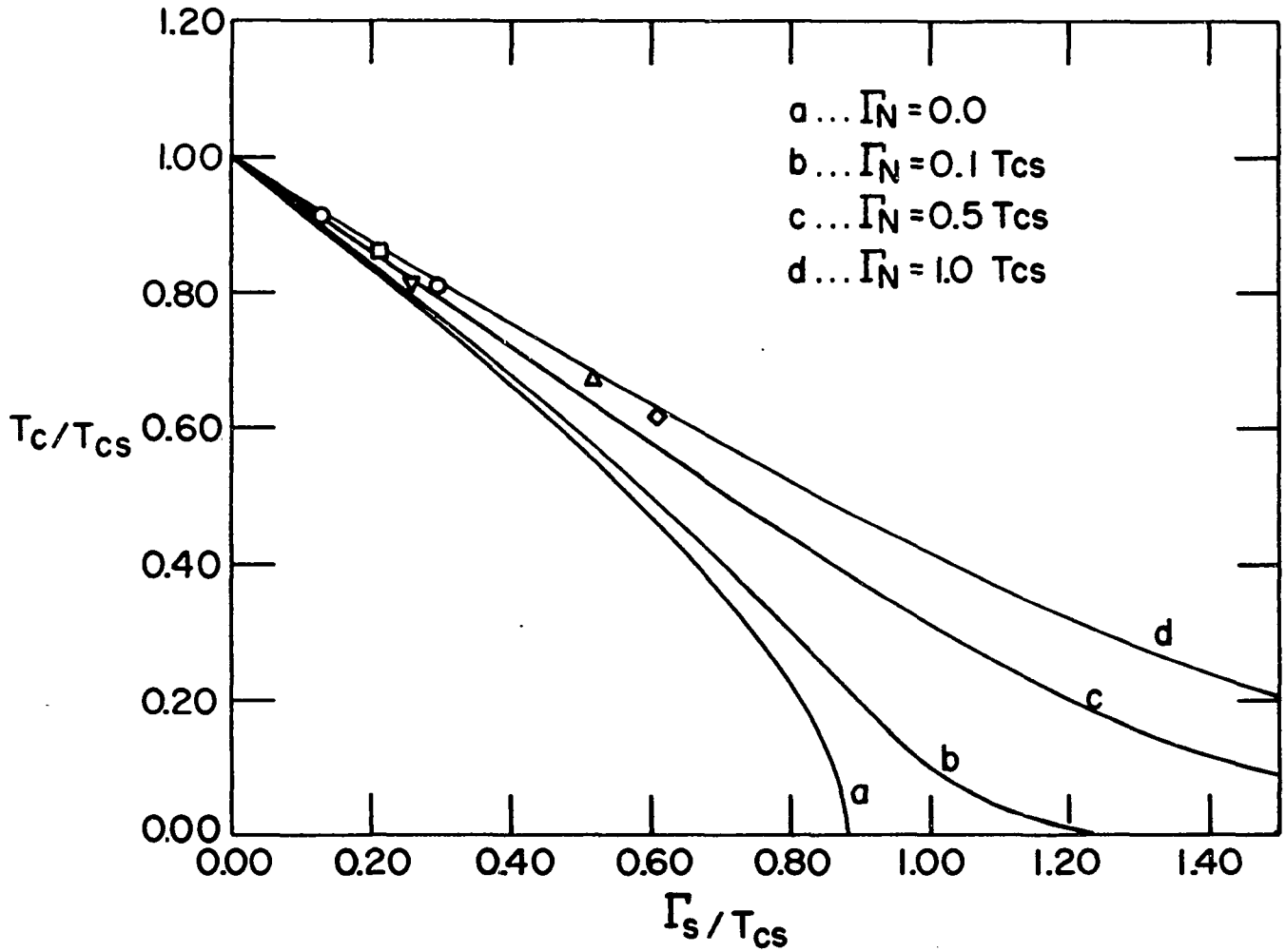
a ... Γ_N = 0.0
b ... Γ_N = 0.1 Tcs
c ... Γ_N = 0.5 Tcs
d ... Γ_N = 1.0 Tcs
T_c/T_{cs}
Γ_s/T_{cs}
1.20
1.00
0.80
0.60
0.40
0.20
0.00
0.00
0.20
0.40
0.60
0.80
1.00
1.20
1.40
a
b
c
d

Figure 2. The real and imaginary parts of the pair potential in the S side of a proximity sandwich calculated from the McMillan model with $\Gamma_S = 0.13\text{meV}$, $\Gamma_N = 0.42\text{meV}$, $\Delta_S^{Ph} = 1.15\text{meV}$, $\Delta_N^{Ph} = 0.181\text{meV}$, derived from the tunneling results for the 670Å proximity sandwich

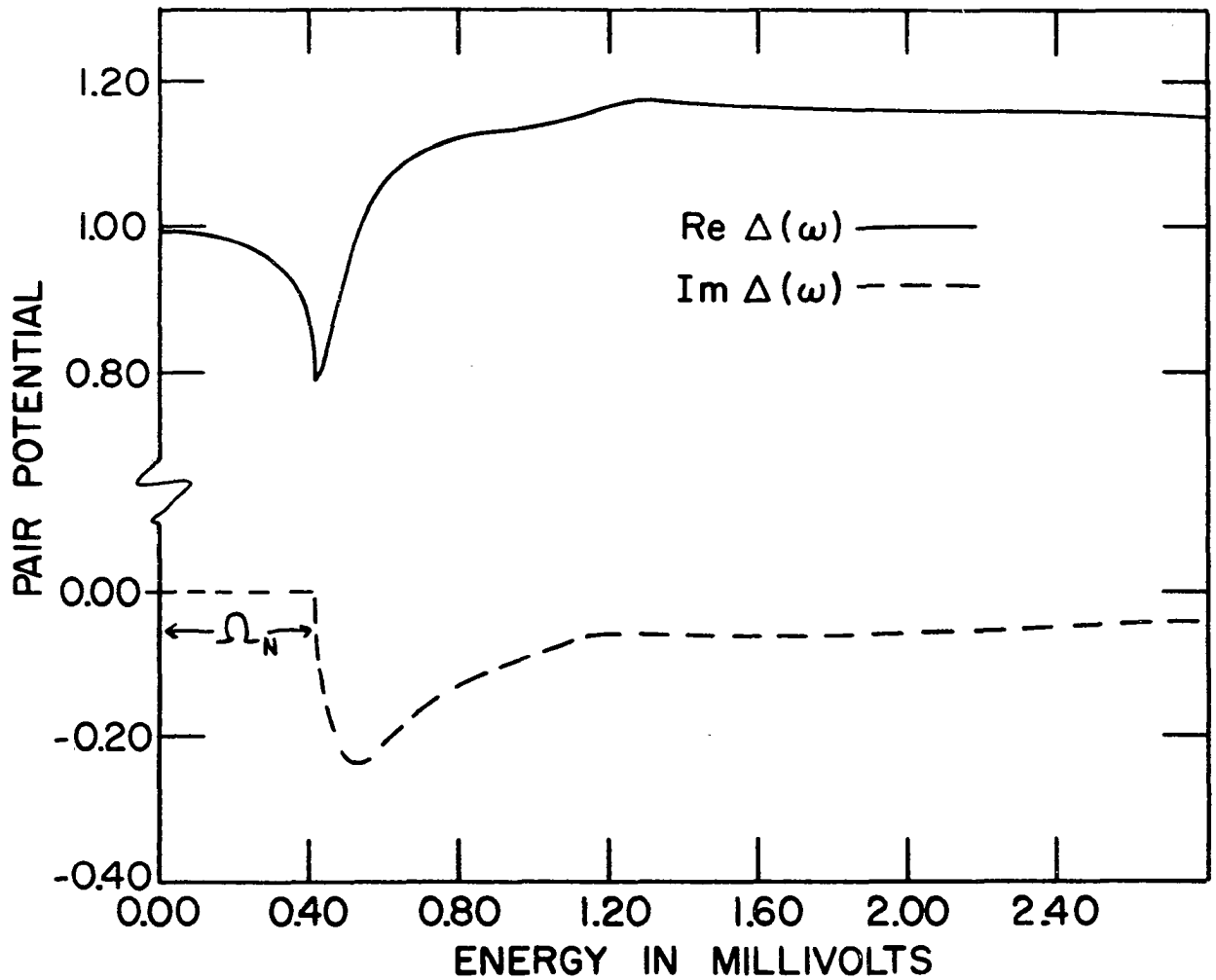
1.20
1.00
0.80
0.00
-0.20
-0.40
PAIR POTENTIAL
Re Δ(ω)
Im Δ(ω)
Ω_N
0.00
0.40
0.80
1.20
1.60
2.00
2.40
ENERGY IN MILLIVOLTS

Figure 3. The density of states calculated from the McMillan model with $\Gamma_S = 0.13\text{meV}$, $\Gamma_N = 0.42\text{meV}$, $\Delta_S^{Ph} = 1.15\text{meV}$, $\Delta_N^{Ph} = 0.181\text{meV}$ derived from the tunneling results for the 670Å proximity sandwich

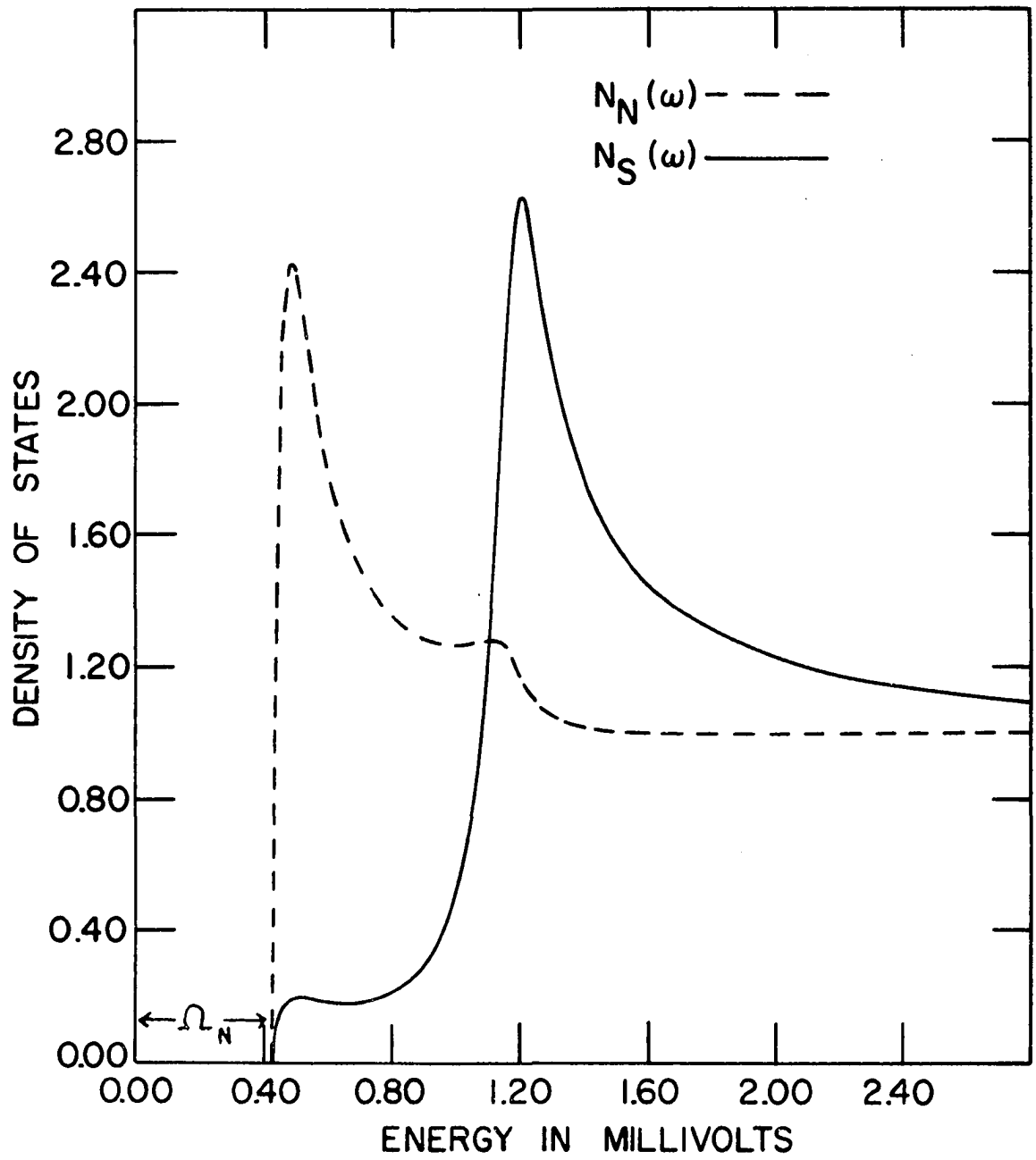
$N_N(\omega)$ - - -
$N_S(\omega)$ ———
2.80
2.40
2.00
1.60
1.20
0.80
0.40
0.00
DENSITY OF STATES
Ω_N
0.00
0.40
0.80
1.20
1.60
2.00
2.40
ENERGY IN MILLIVOLTS

Figure 4. The real and imaginary parts of the pair potential for Pb calculated from the Eliashberg equations and the phonon spectrum responsible for the structure

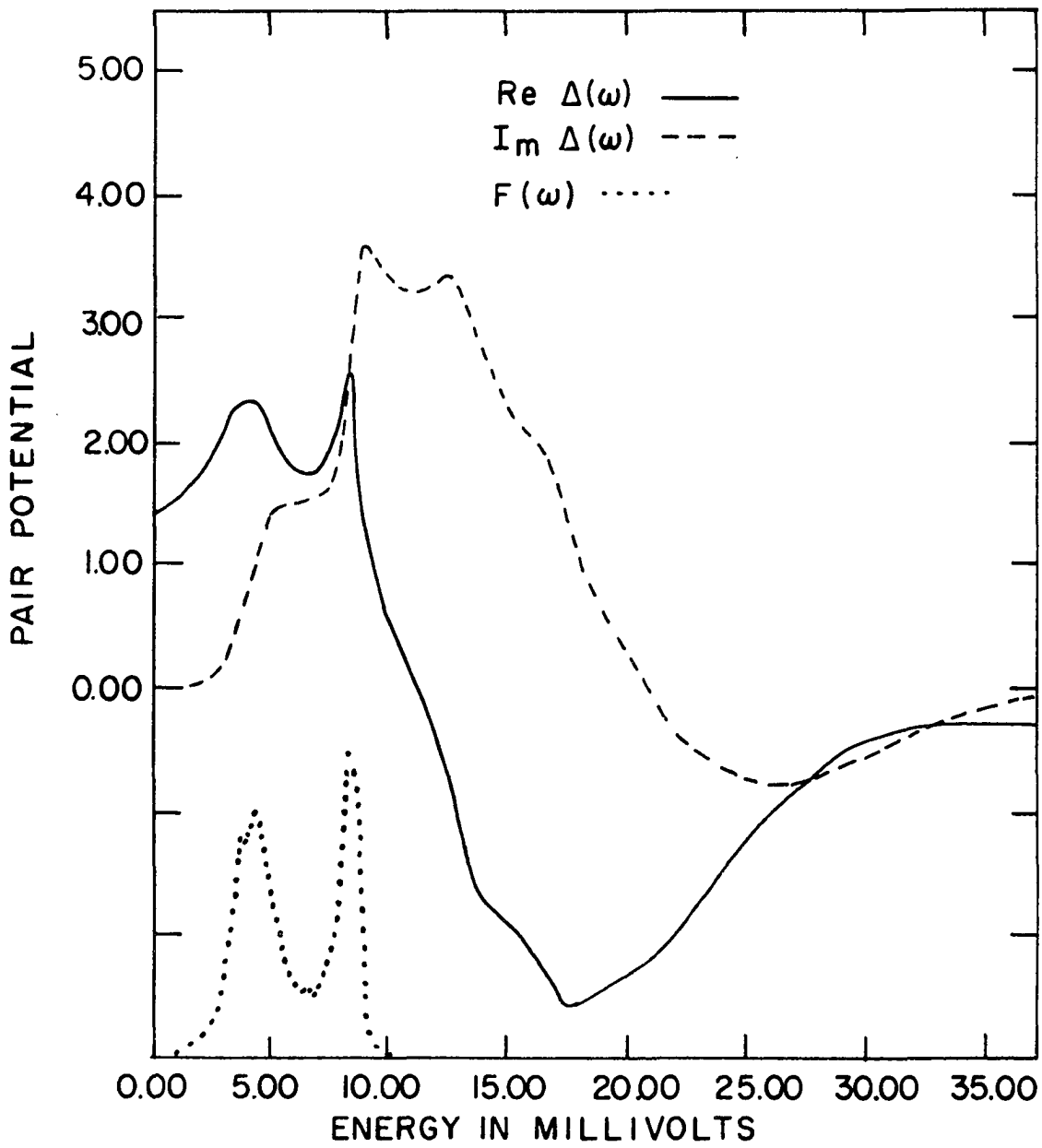
Re Δ(ω)
Im Δ(ω)
F(ω)
PAIR POTENTIAL
5.00
4.00
3.00
2.00
1.00
0.00
0.00
5.00
10.00
15.00
20.00
25.00
30.00
35.00
ENERGY IN MILLIVOLTS

Figure 5. Schematic diagram of the McMillan computer unfolding program

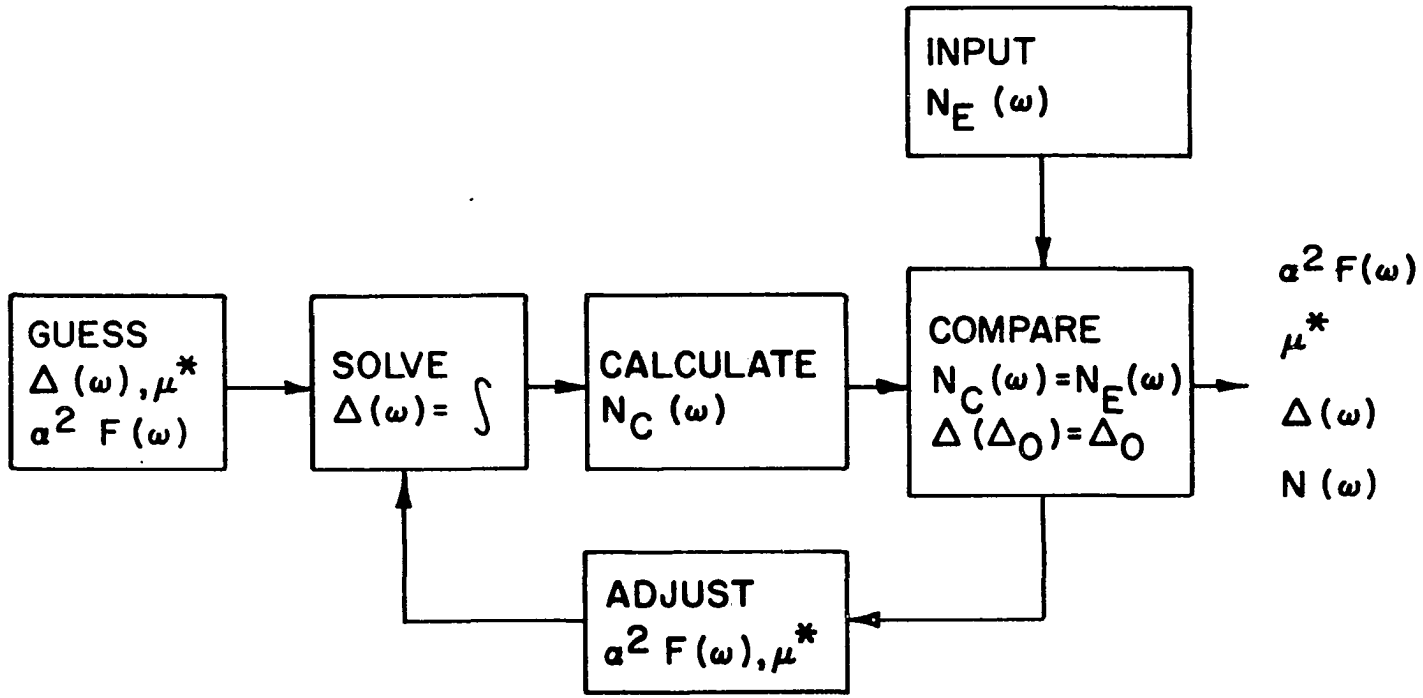
INPUT
$N_E(\omega)$
GUESS
$\Delta(\omega), \mu^*$
$\alpha^2 F(\omega)$
SOLVE
$\Delta(\omega) = \int$
CALCULATE
$N_C(\omega)$
COMPARE
$N_C(\omega) = N_E(\omega)$
$\Delta(\Delta_O) = \Delta_O$
$\alpha^2 F(\omega)$
μ^*
$\Delta(\omega)$
$N(\omega)$
ADJUST
$\alpha^2 F(\omega), \mu^*$

Figure 6. Vacuum evaporator

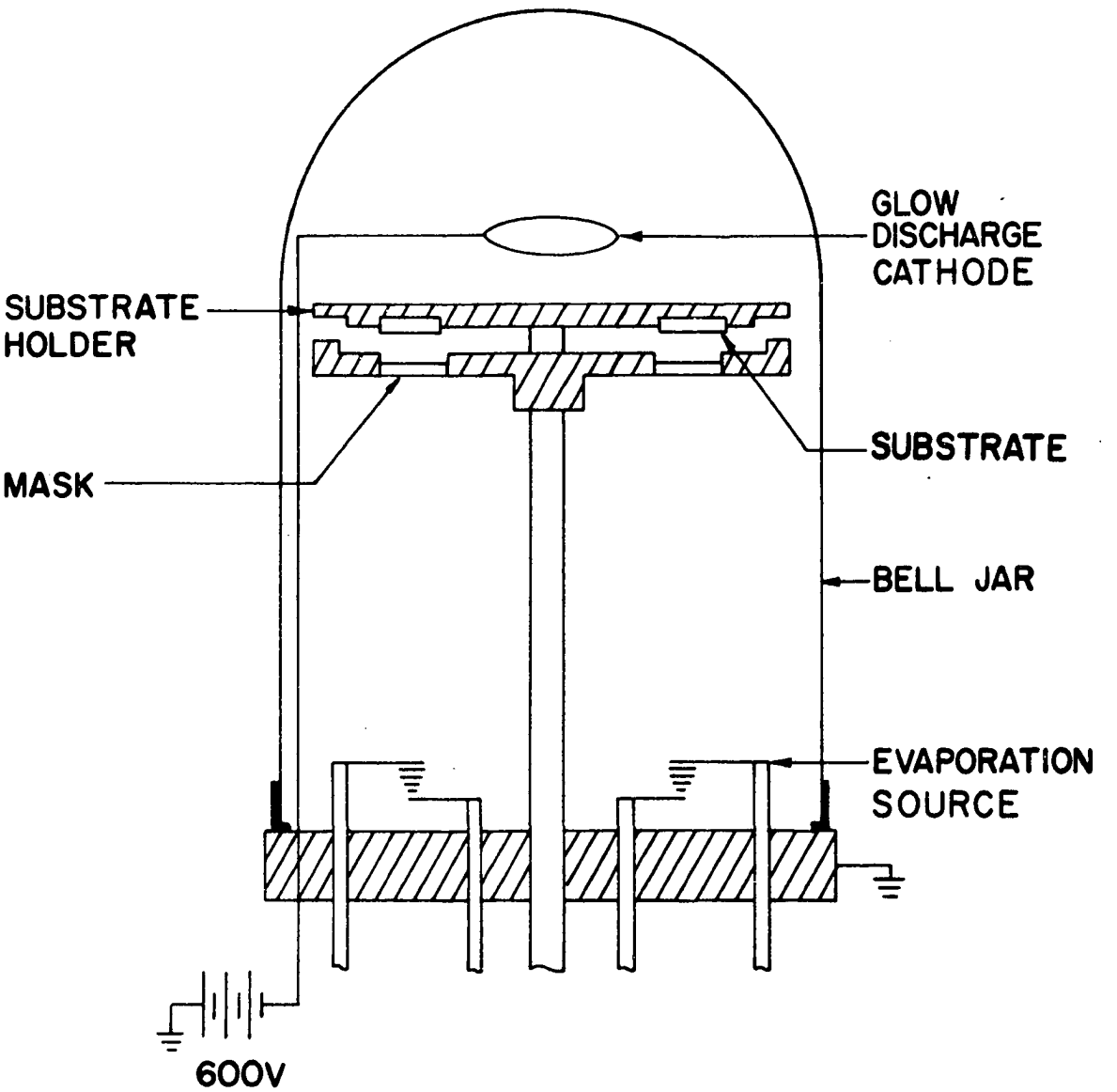
GLOW
DISCHARGE
CATHODE
SUBSTRATE
HOLDER
SUBSTRATE
MASK
BELL JAR
EVAPORATION
SOURCE
600V

Figure 7. Low temperature tail of the ^3He cryostat

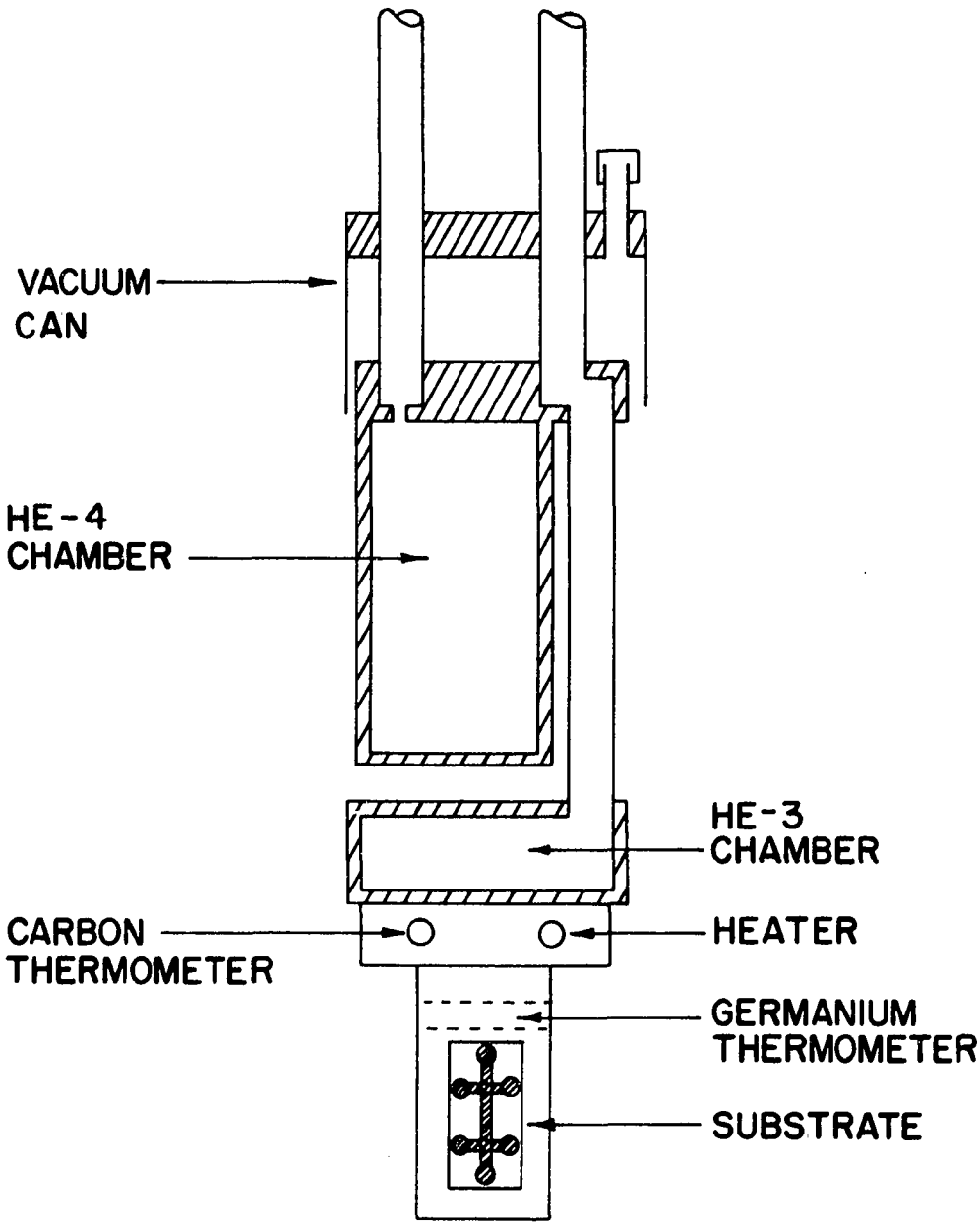
VACUUM
CAN
HE-4
CHAMBER
HE-3
CHAMBER
CARBON
THERMOMETER
HEATER
GERMANIUM
THERMOMETER
SUBSTRATE

Figure 8. Simplified schematic of the conductance bridge

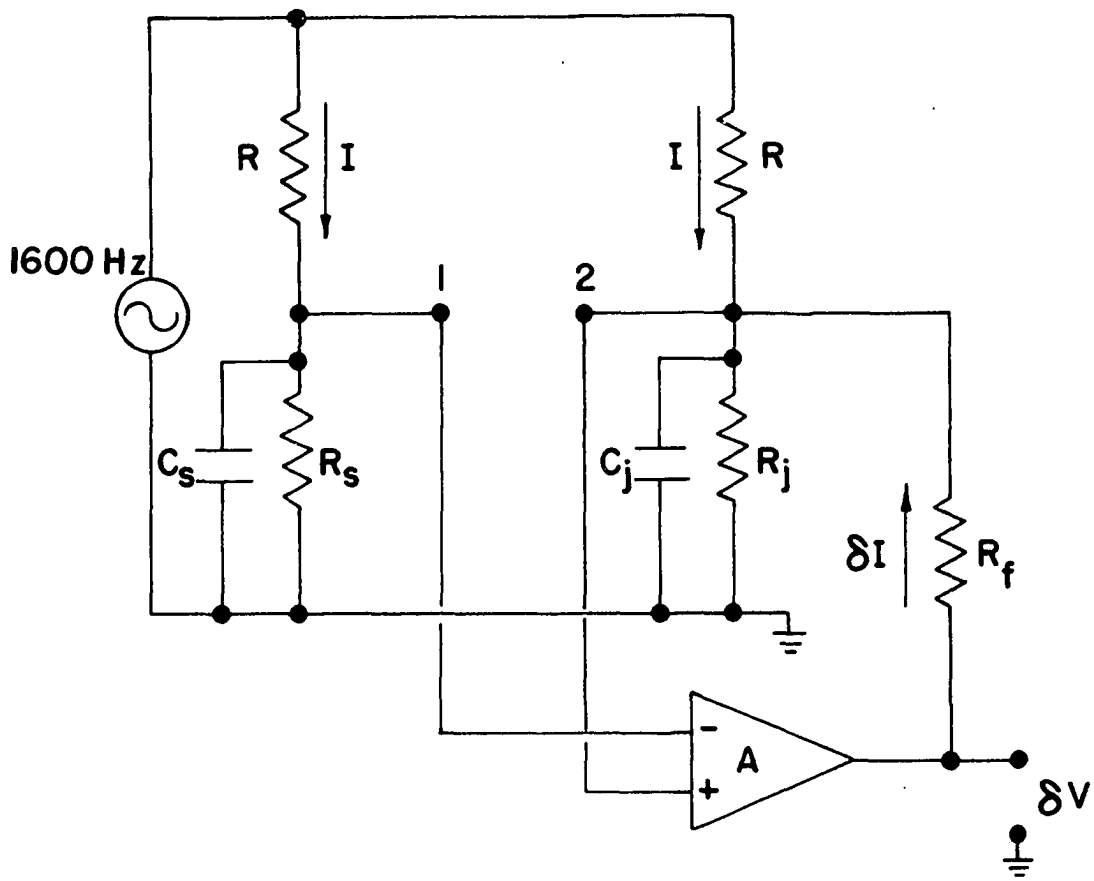
R
I
I
R
1600 Hz
1
2
C_s
R_s
C_j
R_j
δI
R_f
A
δV

Figure 9. Conductance bridge and bias supply

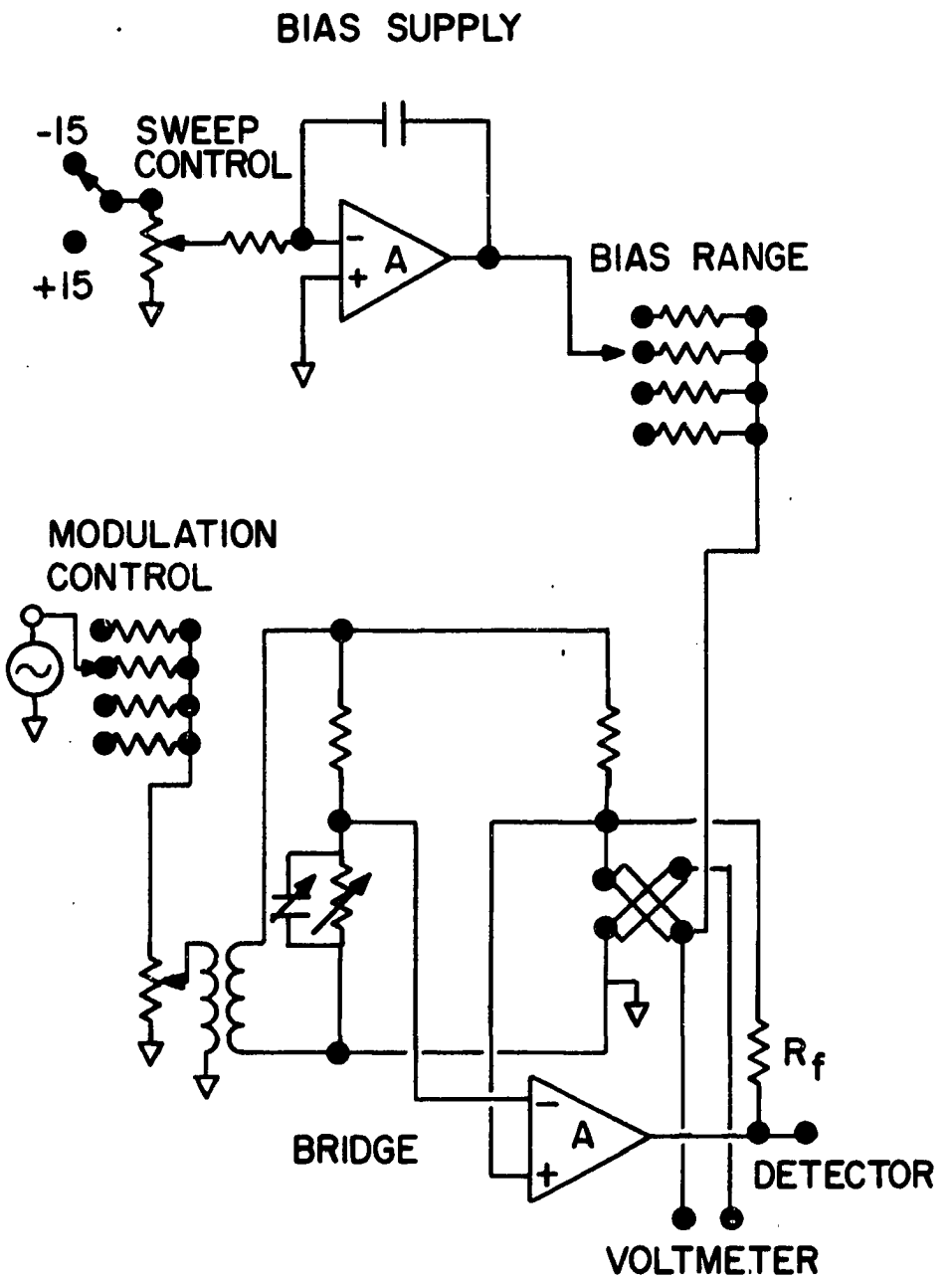
BIAS SUPPLY
-15
SWEEP
CONTROL
+15
A
BIAS RANGE
MODULATION
CONTROL
R_f
BRIDGE
A
DETECTOR
VOLTMETER

Figure 10. Tunnel junction geometry

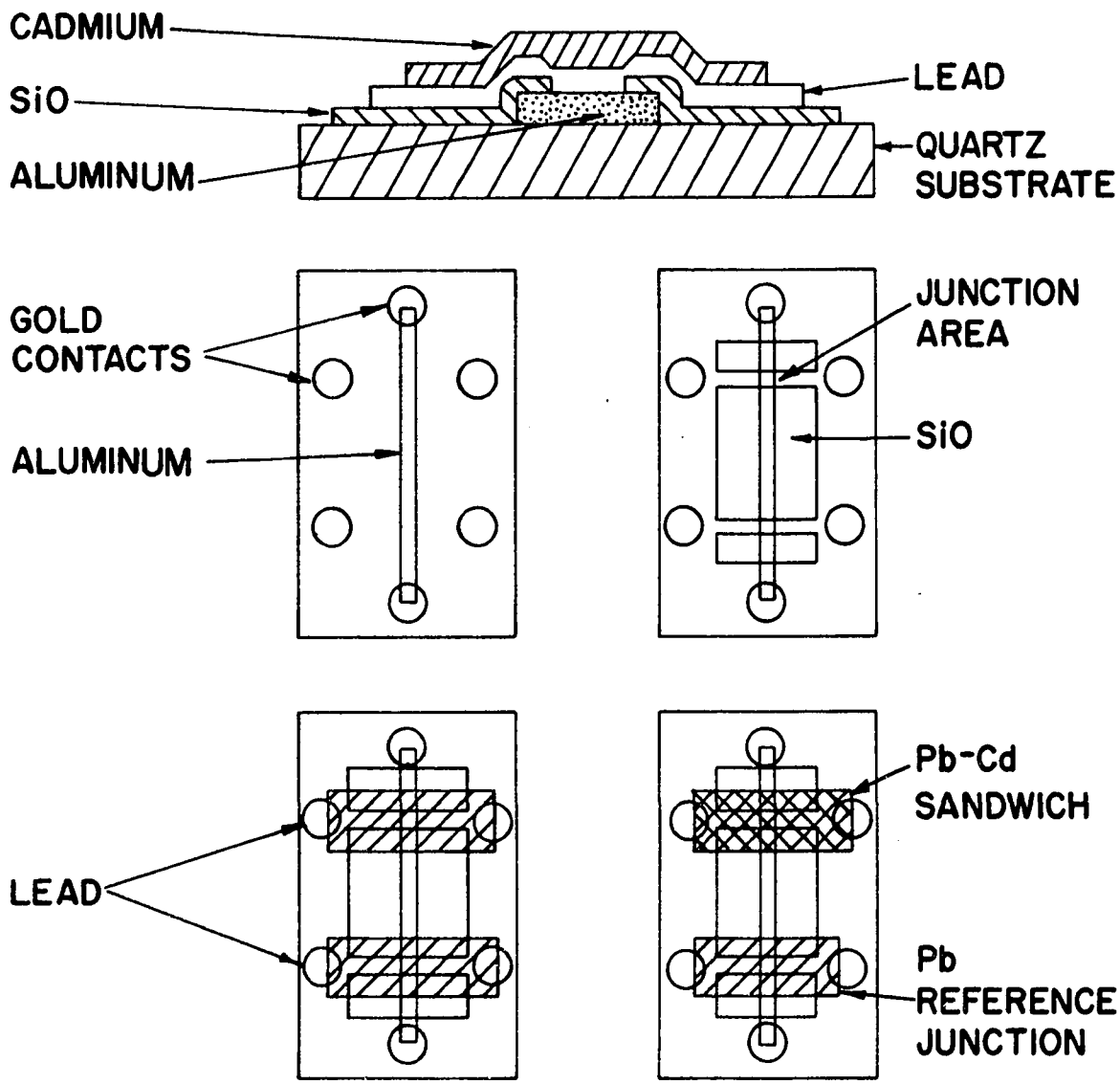
CADMIUM
SiO
ALUMINUM
LEAD
QUARTZ
SUBSTRATE
GOLD
CONTACTS
ALUMINUM
JUNCTION
AREA
SiO
LEAD
Pb-Cd
SANDWICH
Pb
REFERENCE
JUNCTION

Figure 11. Extrapolation procedure for determining T_c for the 670Å Pb-Cd proximity sandwich

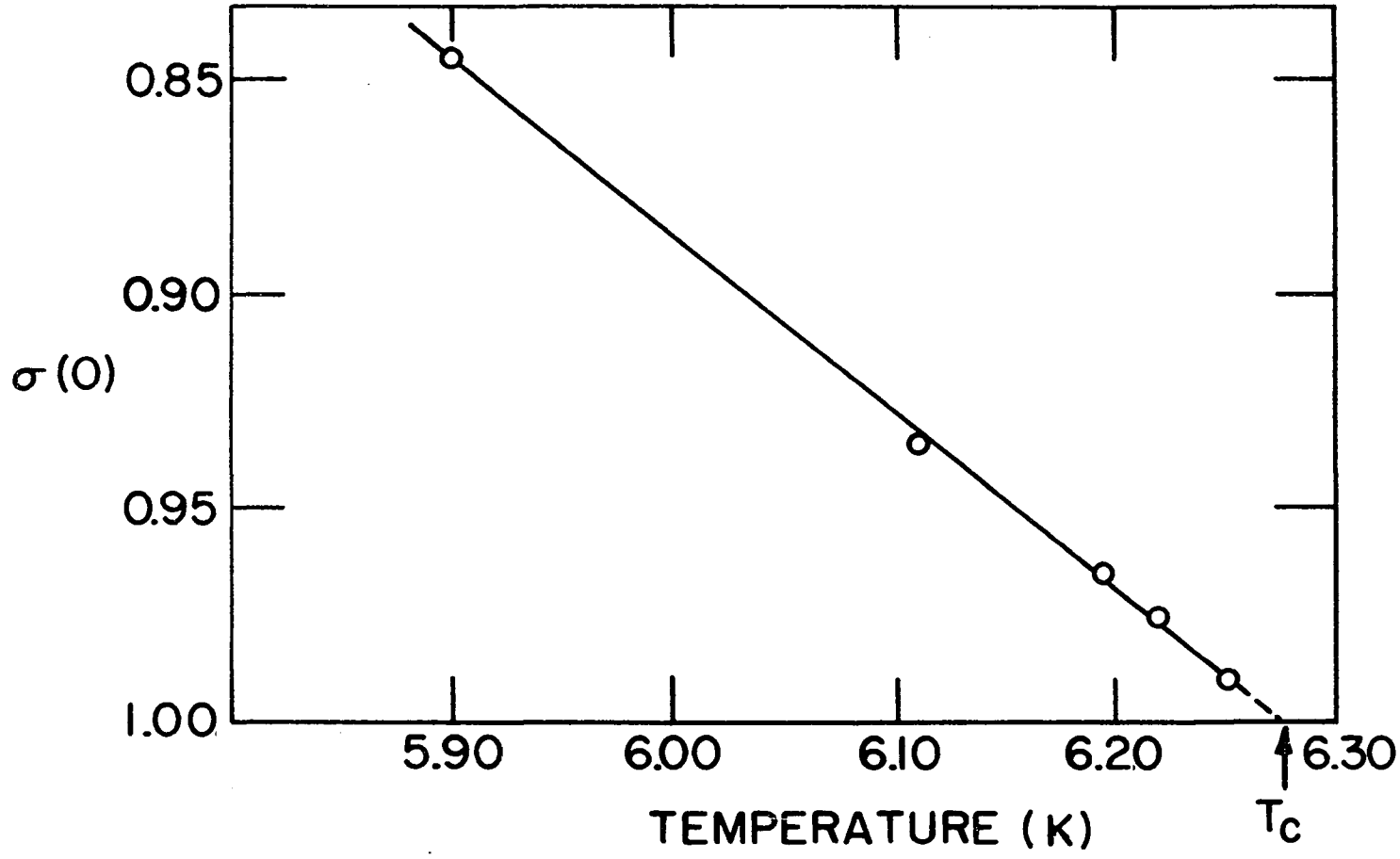
0.85
0.90
0.95
1.00
σ(0)
5.90
6.00
6.10
6.20
6.30
TEMPERATURE (K)
Tc

Figure 12. Variation of the transition temperature of the proximity sandwiches as a function of thickness of the superconducting film

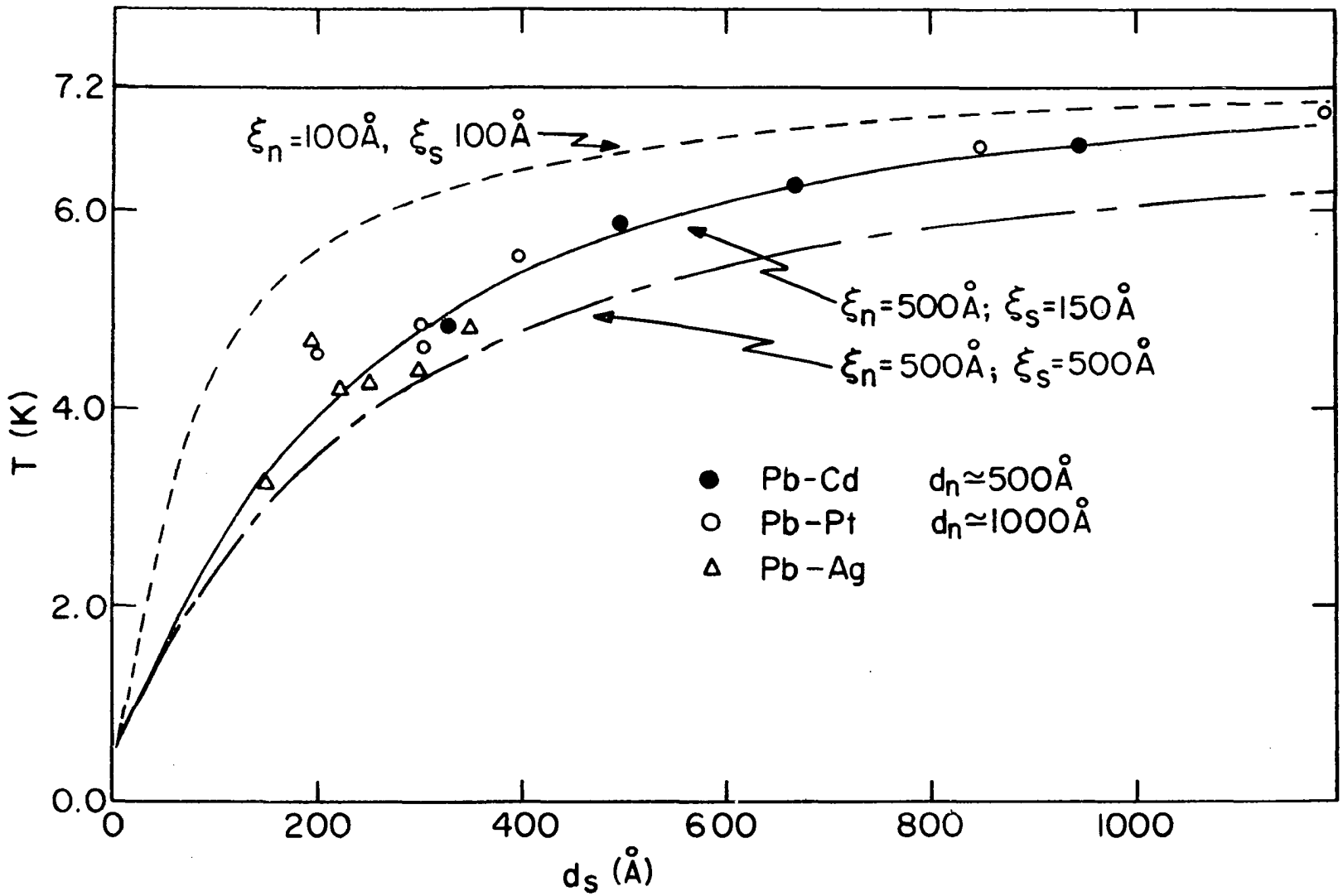
7.2
6.0
4.0
2.0
0.0
T (K)
0
200
400
600
800
1000
d_s (Å)
ξ_n=100Å, ξ_s 100Å
ξ_n=500Å; ξ_s=150Å
ξ_n=500Å; ξ_s=500Å
Pb-Cd $d_n \simeq 500$Å
Pb-Pt $d_n \simeq 1000$Å
Pb-Ag

Figure 13. Proximity induced changes in the density of states near the gap edge

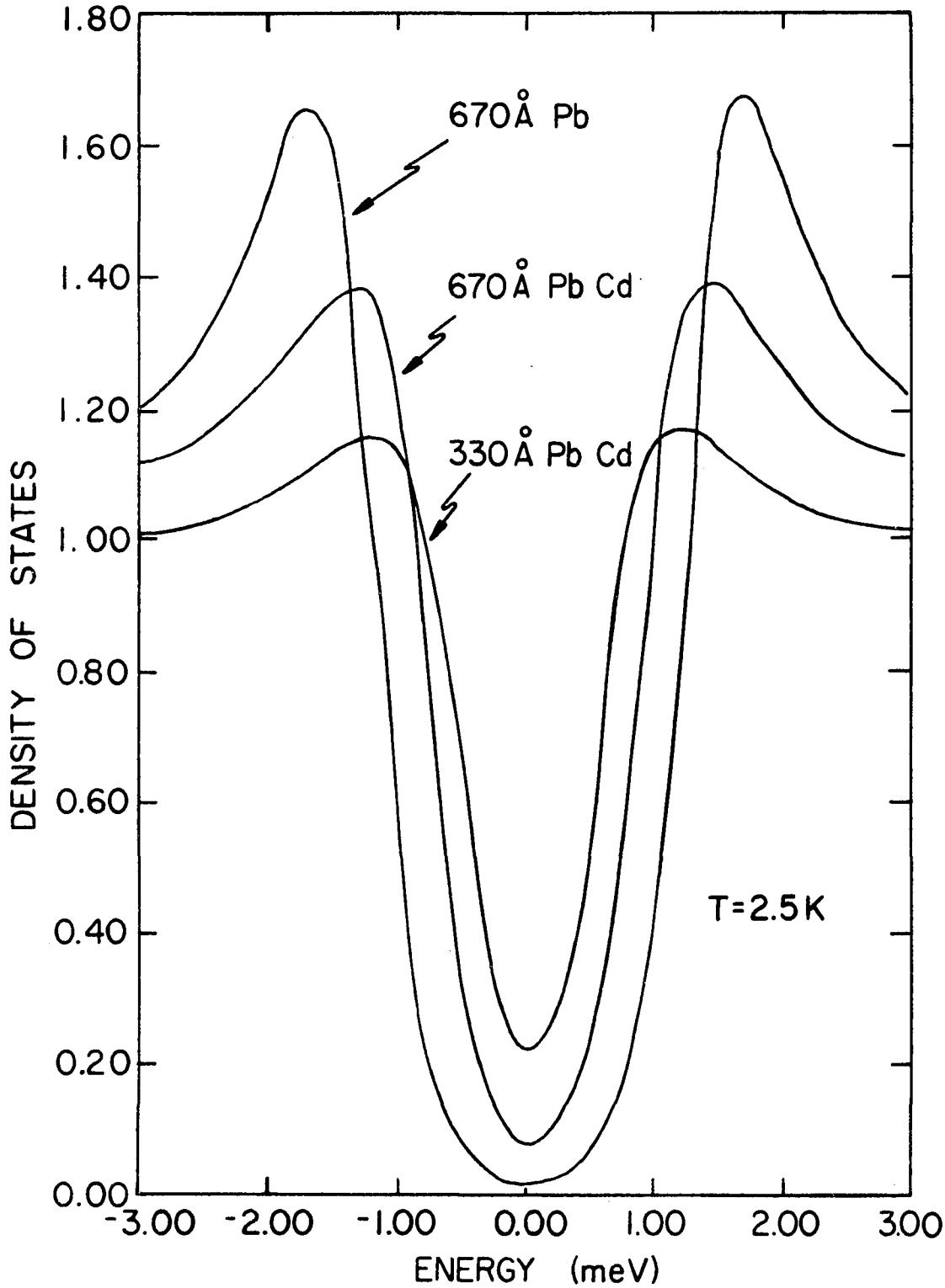
1.80
1.60
1.40
1.20
1.00
0.80
0.60
0.40
0.20
0.00
DENSITY OF STATES
670Å Pb
670Å Pb Cd
330Å Pb Cd
T=2.5K
-3.00
-2.00
-1.00
0.00
1.00
2.00
3.00
ENERGY (meV)

Figure 14. Electron density of states predicted by the BCS theory (solid line) and the experimental conductance (circles) for the 670Å Pb-Cd proximity sandwich

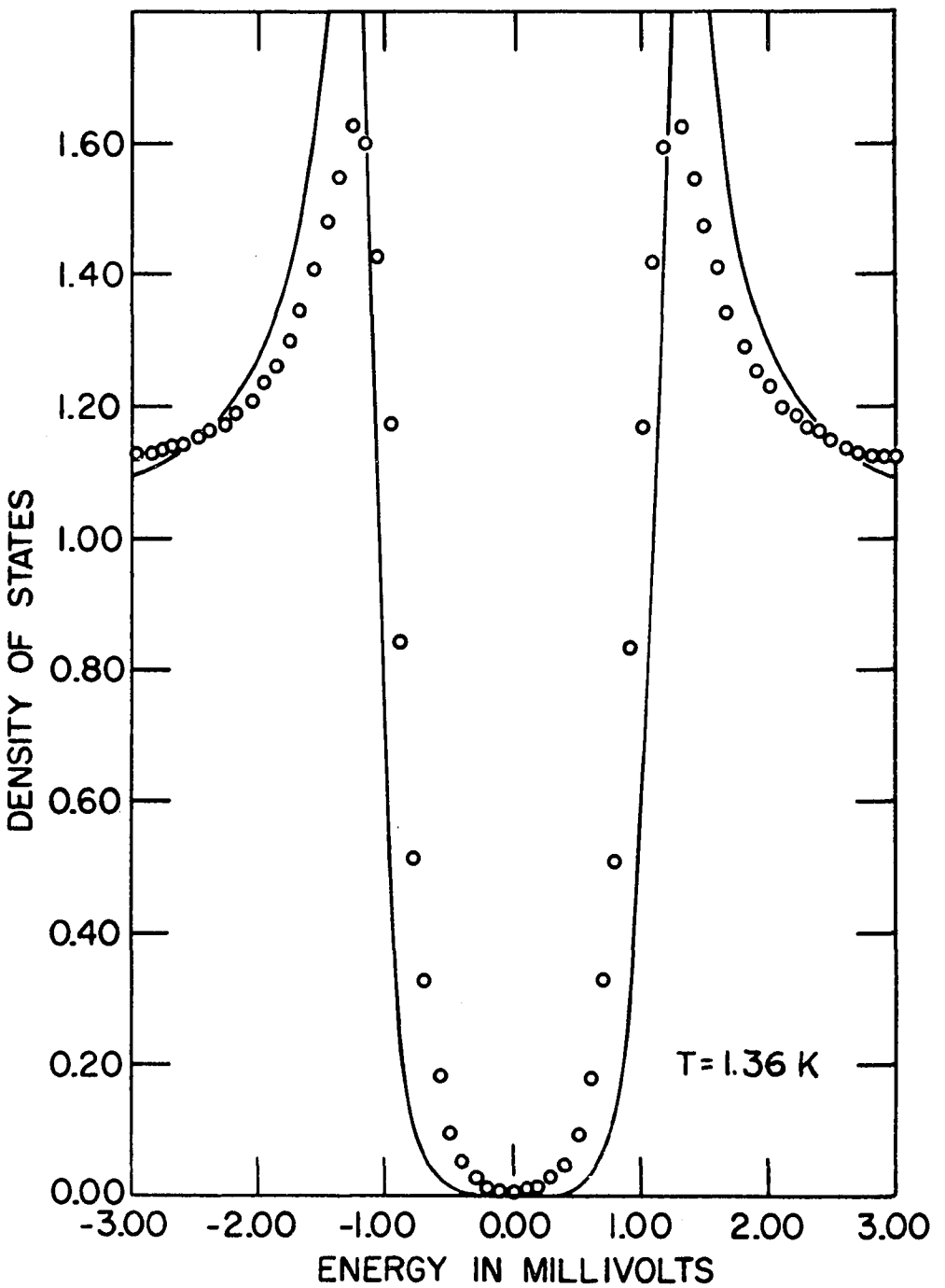
1.60
1.40
1.20
1.00
0.80
0.60
0.40
0.20
0.00
DENSITY OF STATES
T= 1.36 K
-3.00
-2.00
-1.00
0.00
1.00
2.00
3.00
ENERGY IN MILLIVOLTS

Figure 15. Variation of $\sigma(0)$ with temperature, measured from the superconducting side of the proximity sandwiches

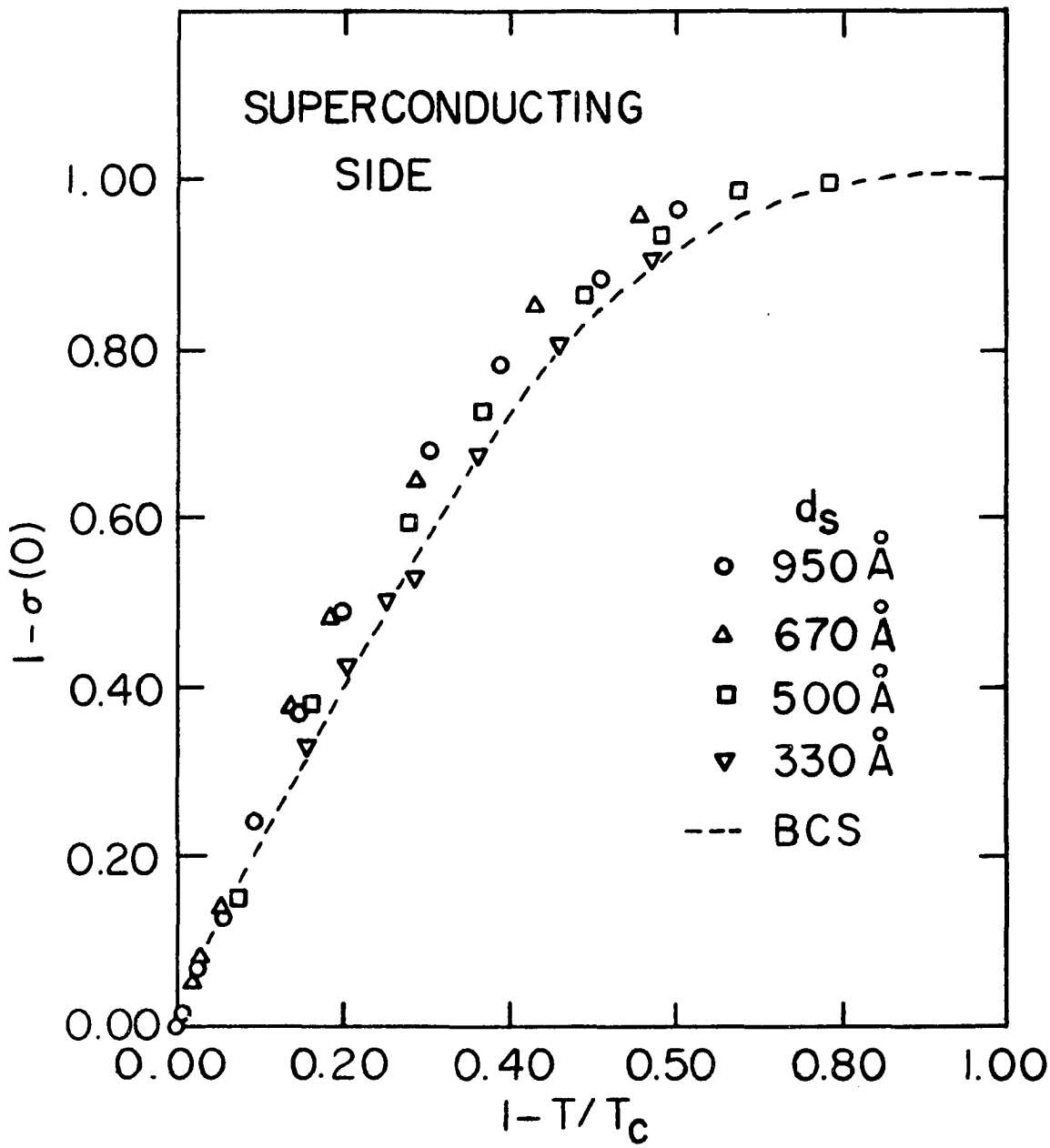
SUPERCONDUCTING
SIDE
1.00
0.80
0.60
0.40
0.20
0.00
1 - σ(0)
0.00
0.20
0.40
0.50
0.80
1.00
1 - T/ Tc
ds
950 Å
670 Å
500 Å
330 Å
BCS

Figure 16. Variation of $\sigma(0)$ with temperature, measured from the normal side of the proximity sandwiches

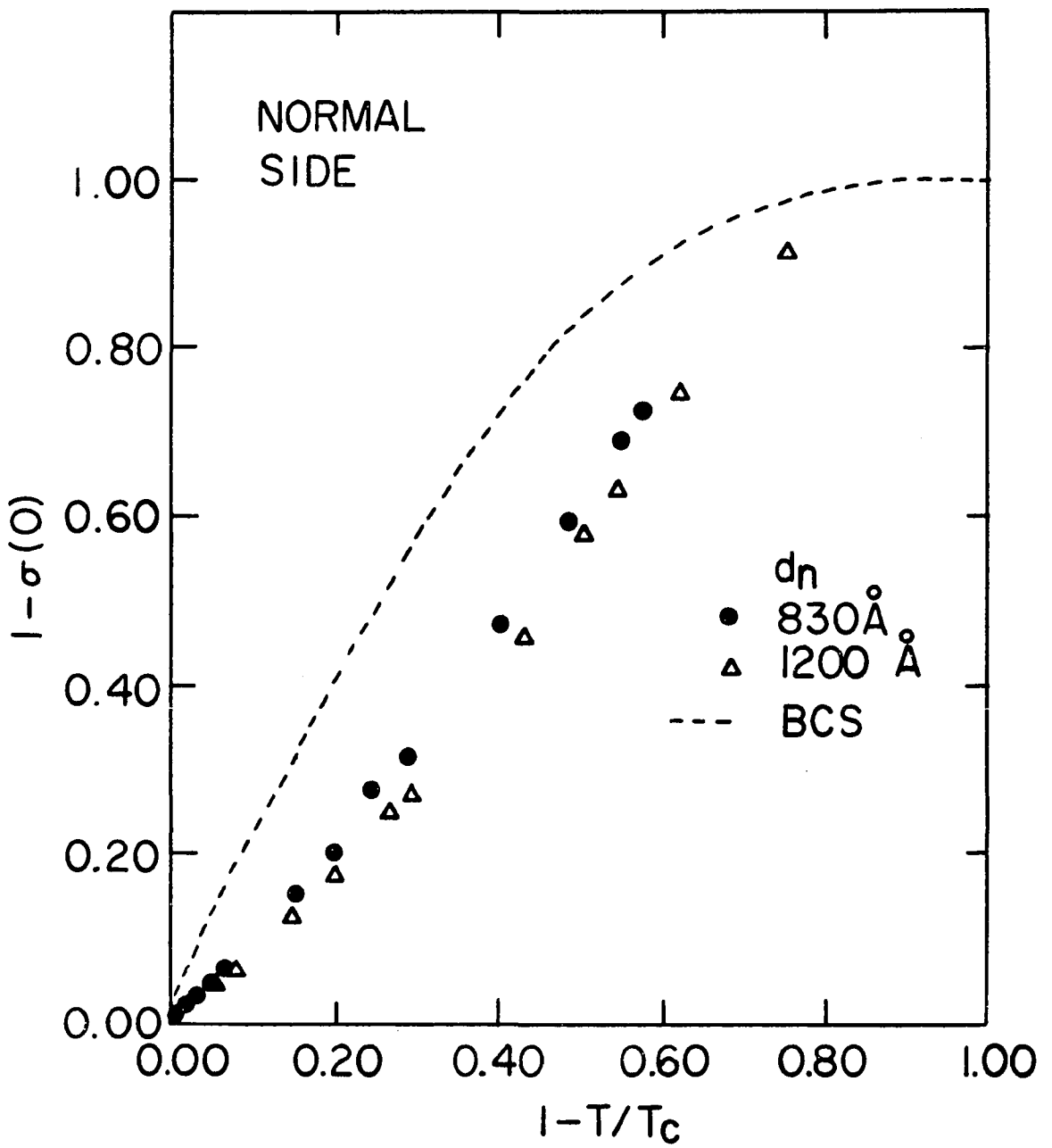
NORMAL
SIDE
1.00
0.80
0.60
0.40
0.20
0.00
0.00
0.20
0.40
0.60
0.80
1.00
1-σ(0)
1-T/Tc
dn
830Å
1200 Å
BCS

Figure 17. Electron density of states predicted by the BCS theory (solid line) and the experimental conductance (circles) for the 830Å Cd-Pb proximity sandwich

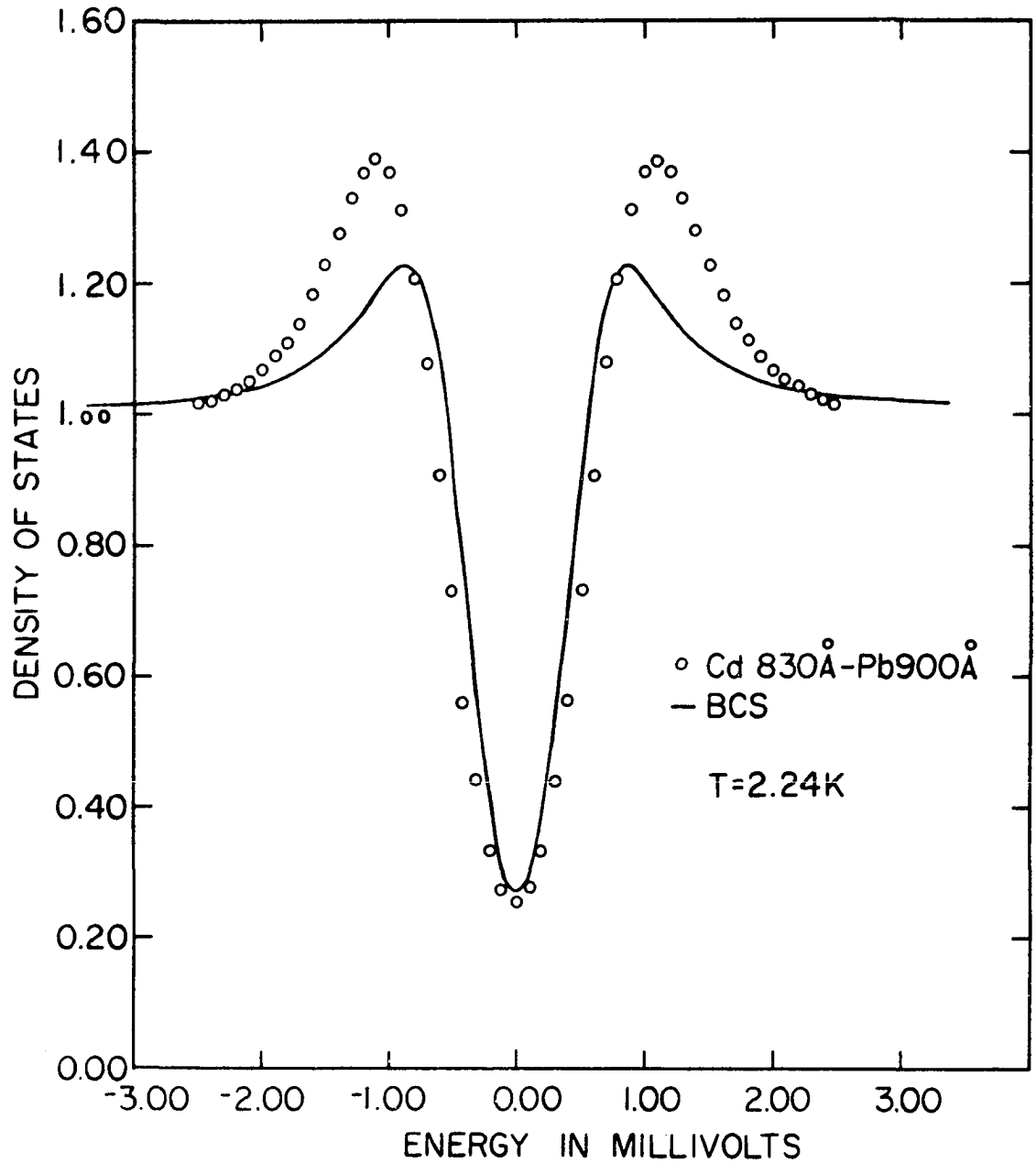
1.60
1.40
1.20
1.00
0.80
0.60
0.40
0.20
0.00
DENSITY OF STATES
-3.00
-2.00
-1.00
0.00
1.00
2.00
3.00
ENERGY IN MILLIVOLTS
o Cd 830Å-Pb900Å
— BCS
T=2.24K

Figure 18. Tunneling conductance near the gap edge measured on the normal and superconducting sides of two proximity sandwiches with similar T_c

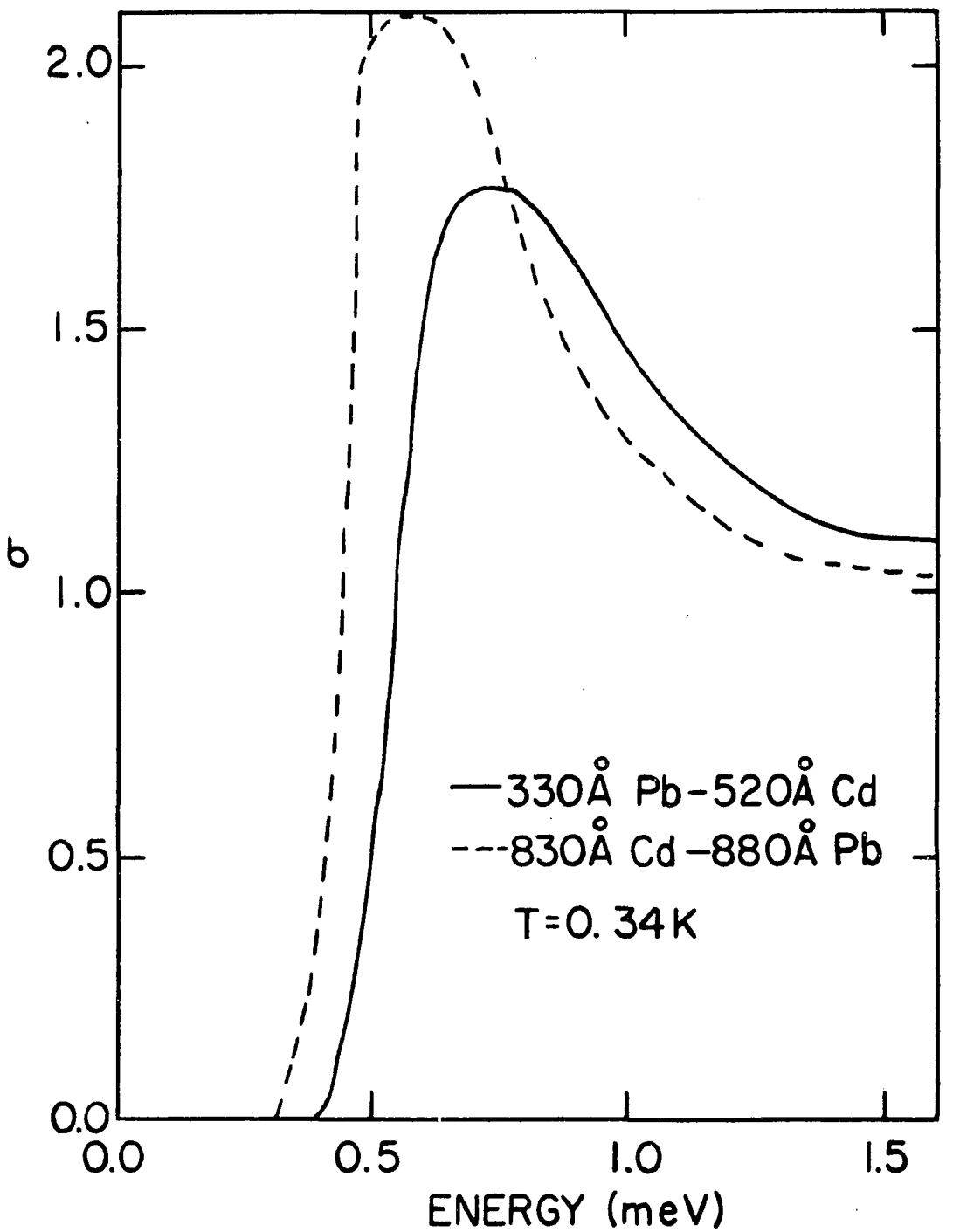
2.0
1.5
1.0
0.5
0.0
b
0.0
0.5
1.0
1.5
ENERGY (meV)
—330Å Pb-520Å Cd
---830Å Cd-880Å Pb
T=0.34K

Figure 19. Tunneling conductance near the gap edge and the prediction of the McMillan model for the 670Å Pb-Cd proximity sandwich

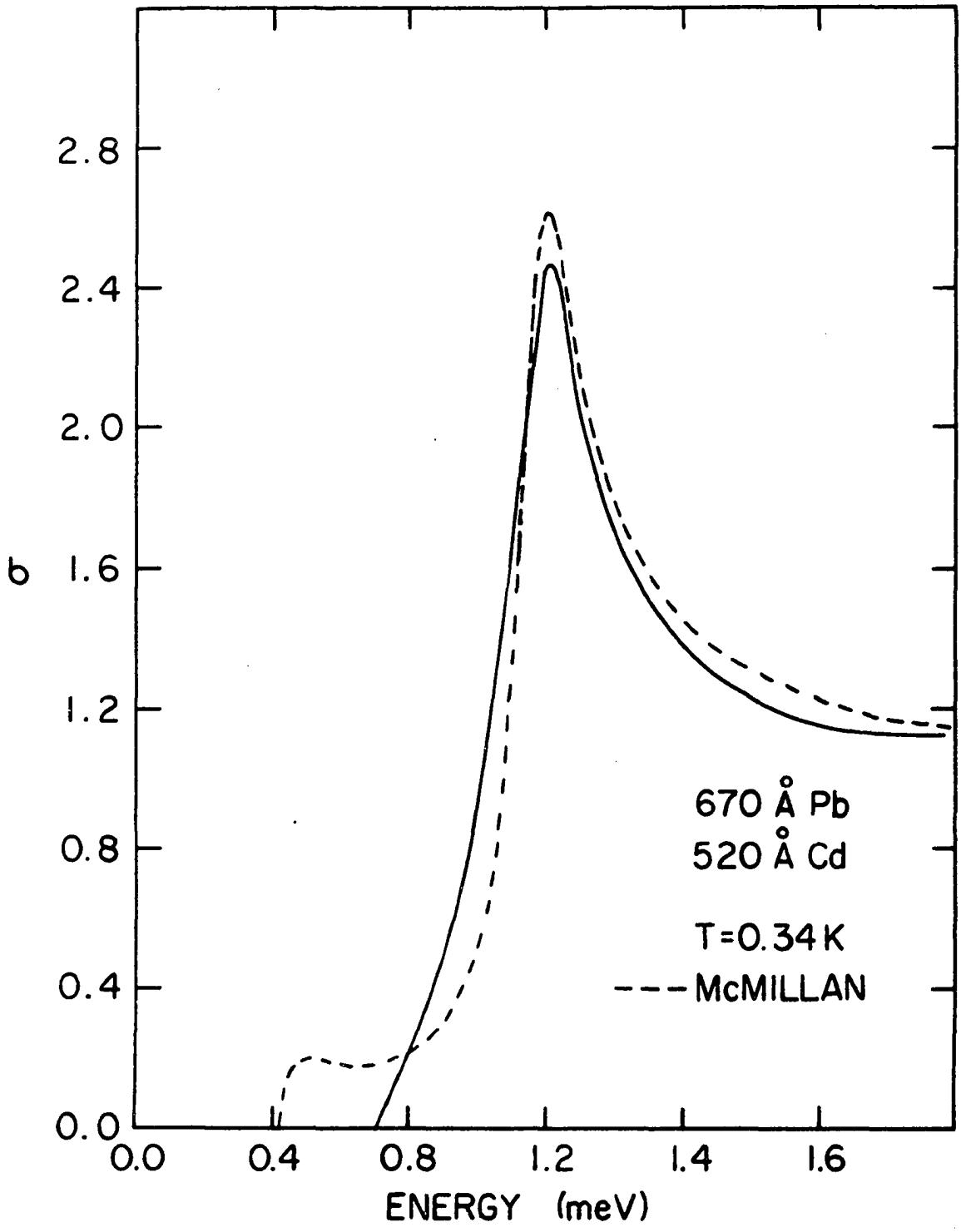
2.8
2.4
2.0
1.6
1.2
0.8
0.4
0.0
b
0.0
0.4
0.8
1.2
1.4
1.6
ENERGY (meV)
670 Å Pb
520 Å Cd
T=0.34 K
---McMILLAN

Figure 20. Tunneling conductance near the gap edge and the prediction of the McMillan model for the 330Å Pb-Cd proximity sandwich

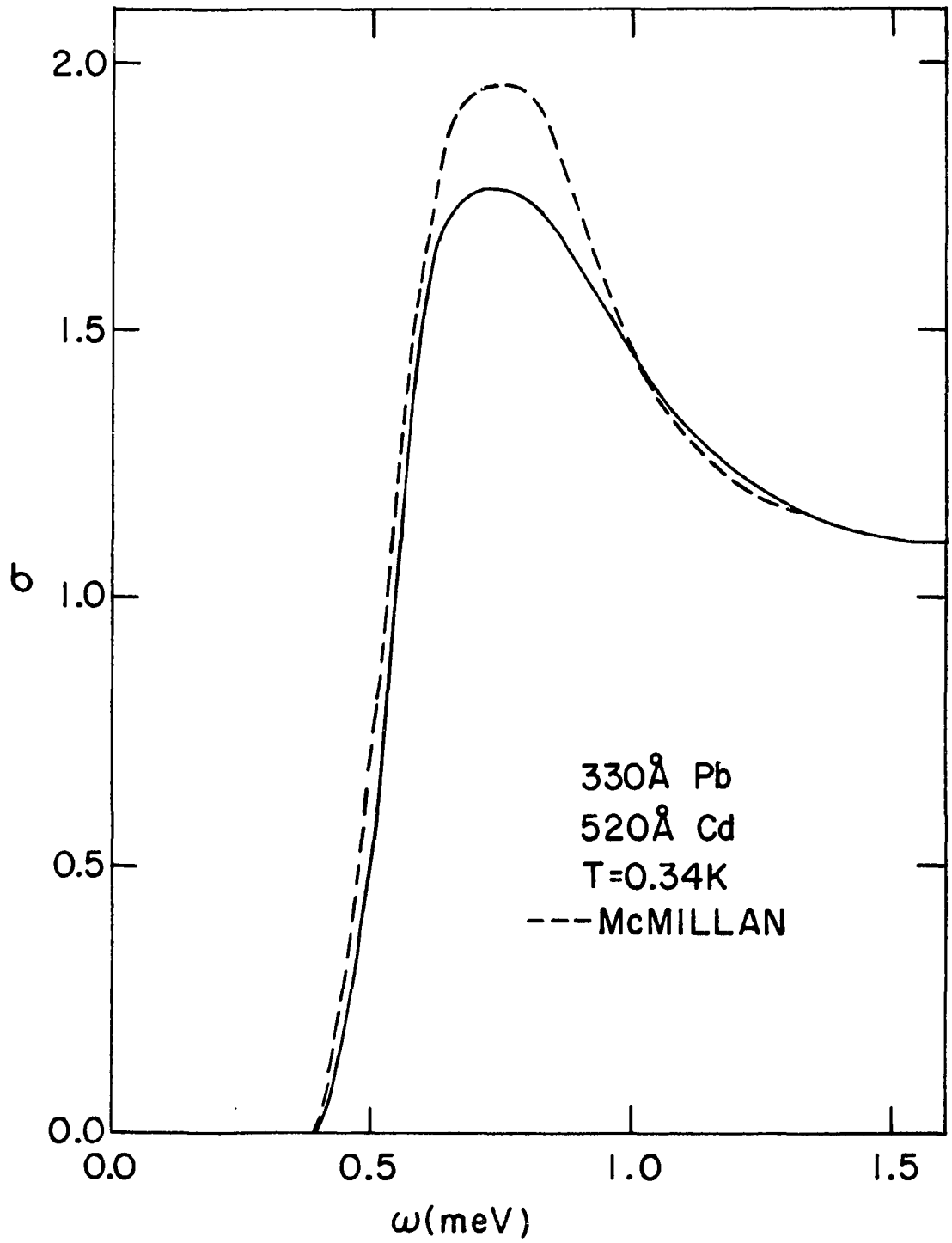
2.0
1.5
1.0
0.5
0.0
b
0.0
0.5
1.0
1.5
ω(meV)
330Å Pb
520Å Cd
T=0.34K
---McMILLAN

Figure 21. The thermally smeared density of states (solid line) calculated from the McMillan model, $\Gamma_S = 0.079$, $\Gamma_N = 0.423$, $\Delta_S^{Ph} = 1.23$, $\Delta_N^{Ph} = 0.144$, and the experimental results (circles) for the 950Å proximity sandwich

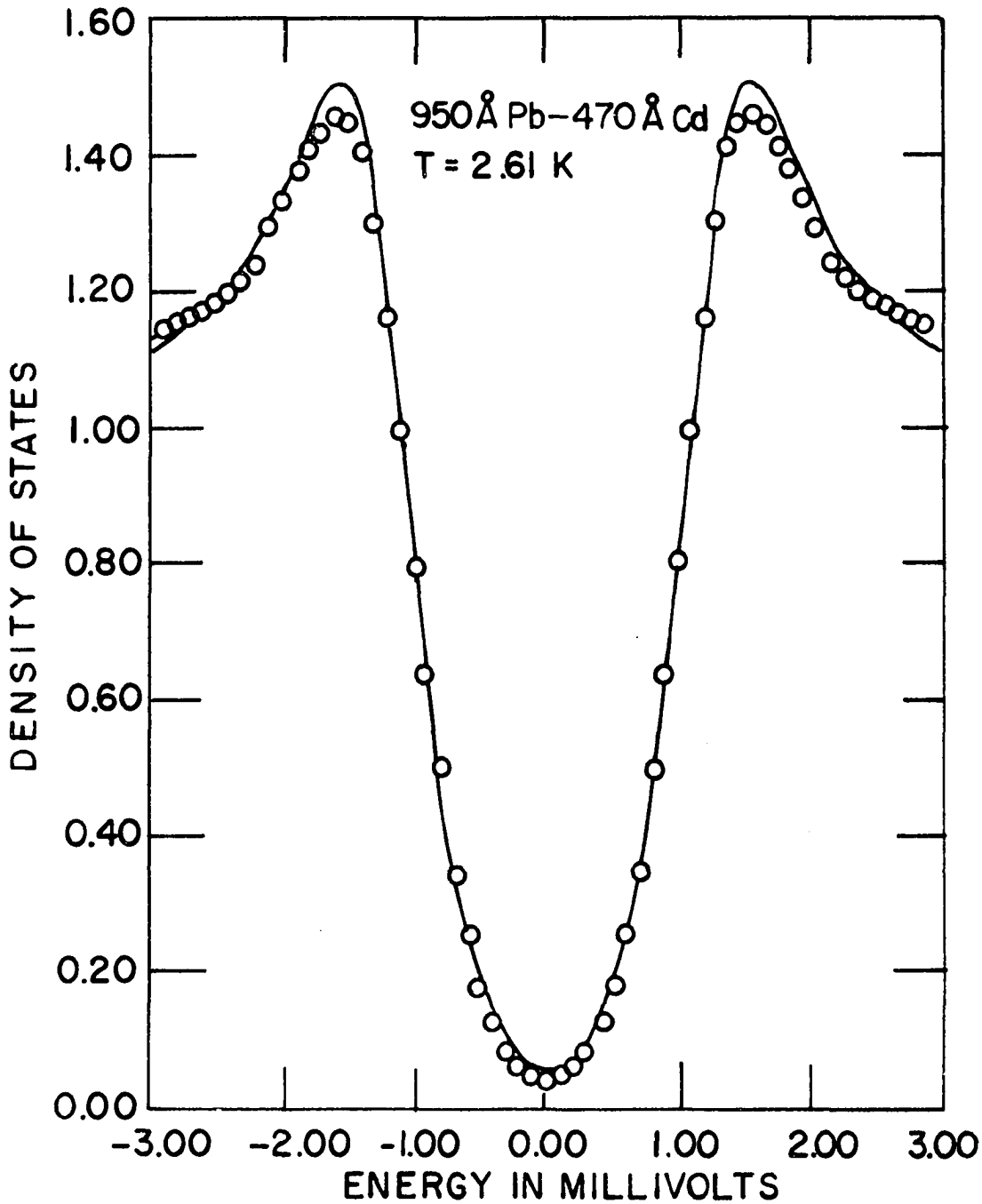
950Å Pb–470Å Cd
T = 2.61 K
DENSITY OF STATES
1.60
1.40
1.20
1.00
0.80
0.60
0.40
0.20
0.00
-3.00
-2.00
-1.00
0.00
1.00
2.00
3.00
ENERGY IN MILLIVOLTS

Figure 22. The thermally smeared density of states (solid line) calculated from the McMillan model, $\Gamma_S = 0.132$, $\Gamma_N = 0.492$, $\Delta_S^{Ph} = 1.15$, $\Delta_N^{Ph} = 0.181$ and the experimental results (circles) for the 670Å proximity sandwich

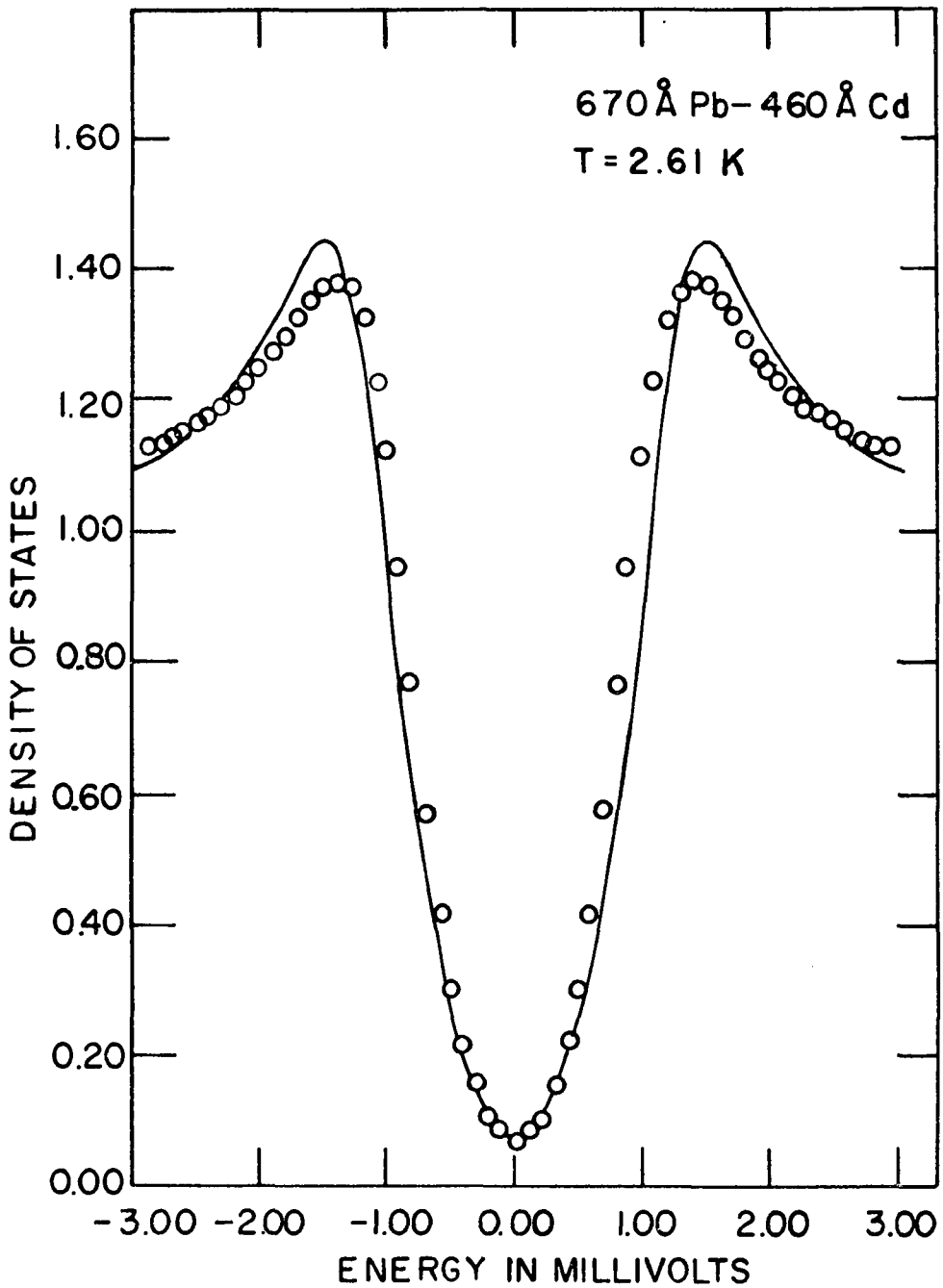
670 Å Pb–460 Å Cd
T = 2.61 K
DENSITY OF STATES
1.60
1.40
1.20
1.00
0.80
0.60
0.40
0.20
0.00
-3.00
-2.00
-1.00
0.00
1.00
2.00
3.00
ENERGY IN MILLIVOLTS

Figure 23. The thermally smeared density of states (solid line) calculated from the McMillan model, $\Gamma_S = 0.183$, $\Gamma_N = 0.517$, $\Delta_S^{Ph} = 1.04$, $\Delta_N^{Ph} = 0.237$, and the experimental results (circles) for the 500Å proximity sandwich

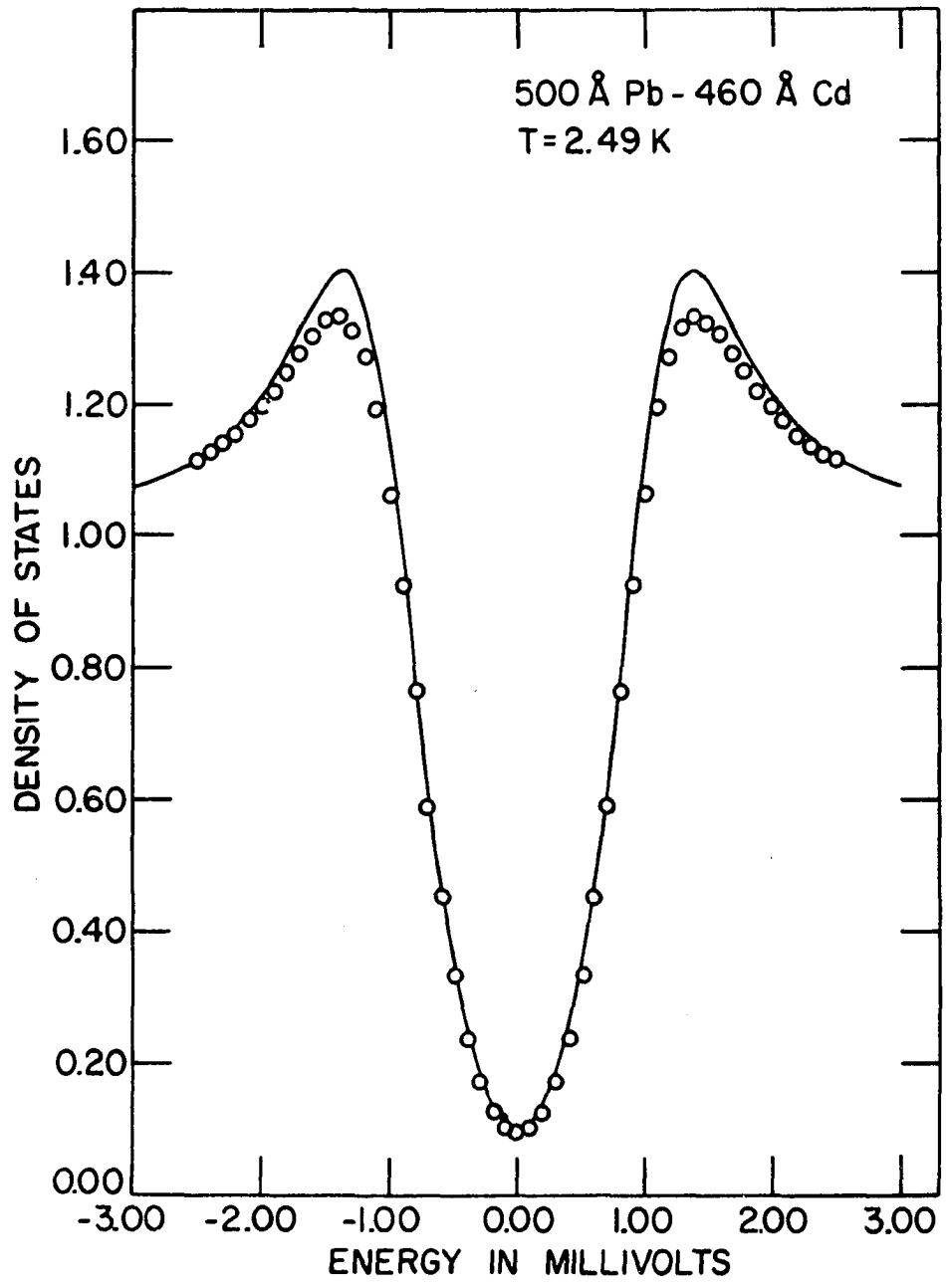
500 Å Pb - 460 Å Cd
T = 2.49 K
DENSITY OF STATES
1.60
1.40
1.20
1.00
0.80
0.60
0.40
0.20
0.00
-3.00
-2.00
-1.00
0.00
1.00
2.00
3.00
ENERGY IN MILLIVOLTS

Figure 24. The thermally smeared density of states (solid line) calculated from the McMillan model, $\Gamma_S = 0.321$, $\Gamma_N = 0.535$, $\Delta_S^{Ph} = 0.72$, $\Delta_N^{Ph} = 0.363$, and the experimental results (circles) for the 330Å proximity sandwich

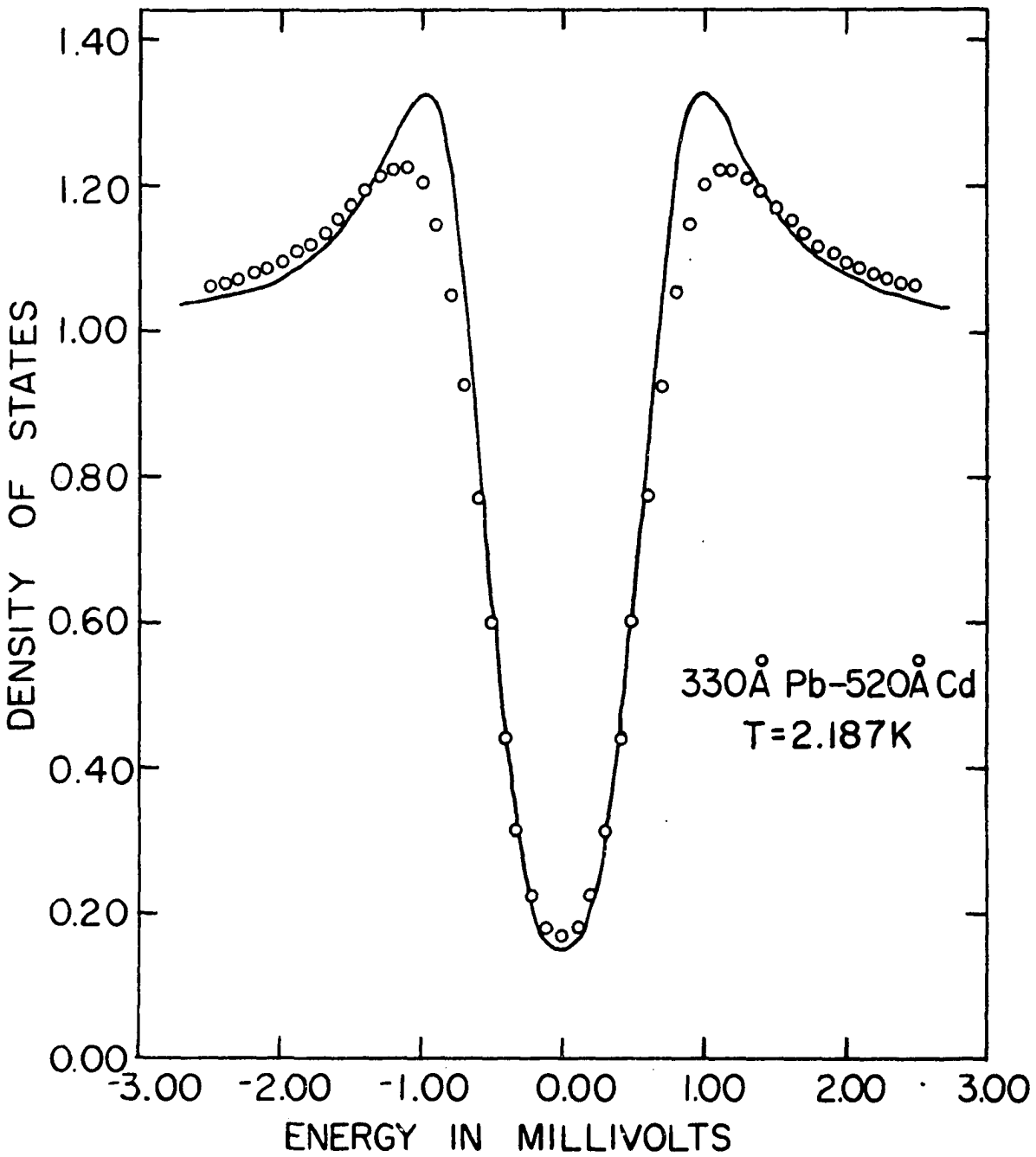
1.40
1.20
1.00
0.80
0.60
0.40
0.20
0.00
DENSITY OF STATES
-3.00
-2.00
-1.00
0.00
1.00
2.00
3.00
ENERGY IN MILLIVOLTS
330Å Pb-520Å Cd
T=2.187K

Figure 25. Structure in the electron density of states caused by phonon coupling

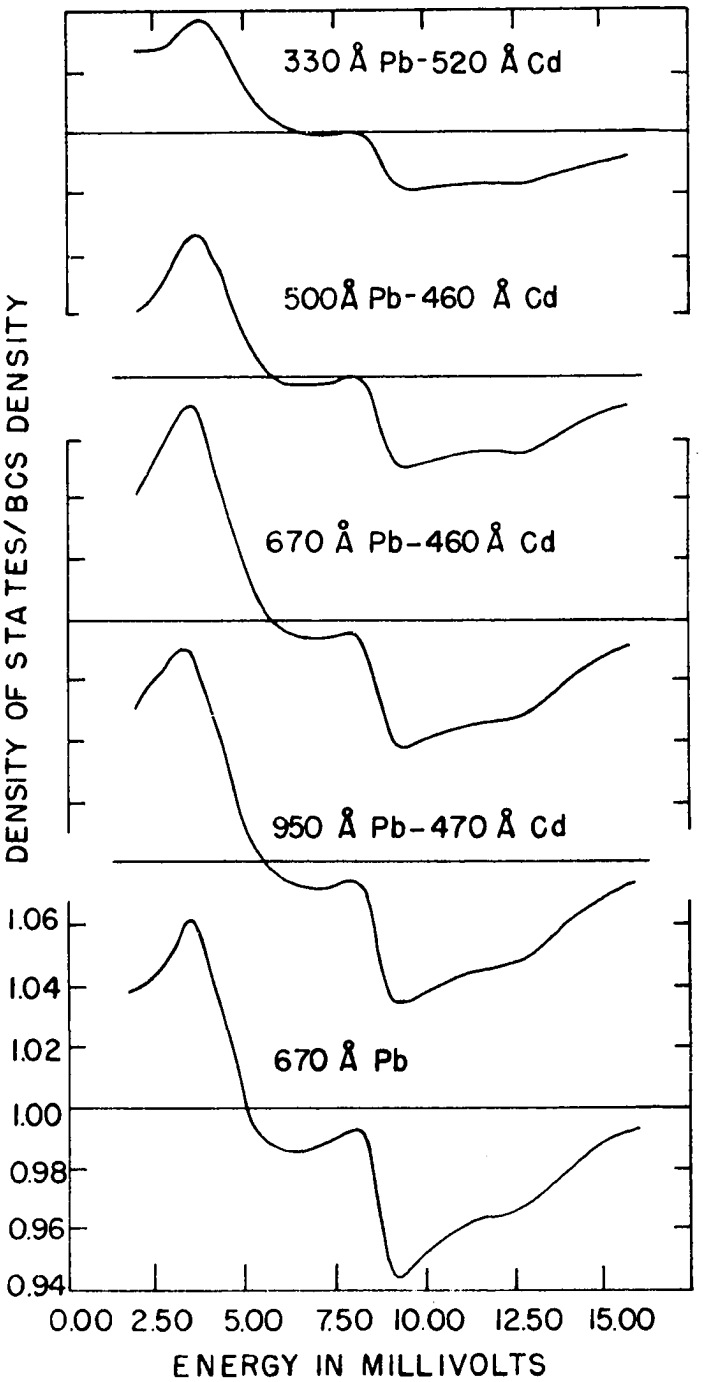
330 Å Pb-520 Å Cd
500Å Pb-460 Å Cd
670 Å Pb-460 Å Cd
950 Å Pb-470 Å Cd
670 Å Pb
DENSITY OF STATES/BCS DENSITY
1.06
1.04
1.02
1.00
0.98
0.96
0.94
0.00 2.50 5.00 7.50 10.00 12.50 15.00
ENERGY IN MILLIVOLTS

Figure 26. Phonon spectral function, derived assuming $\mu^* = 0.13$

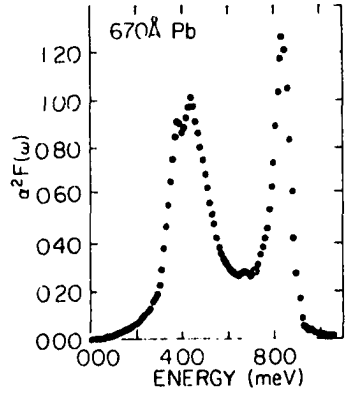

Al-Al_2O_3-Pb-Cd
TUNNEL
JUNCTIONS

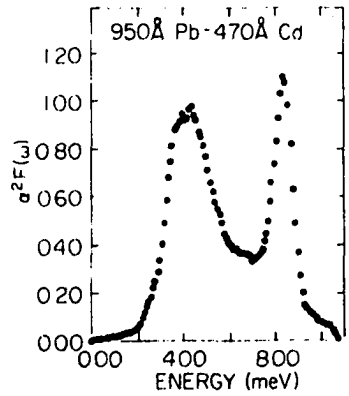

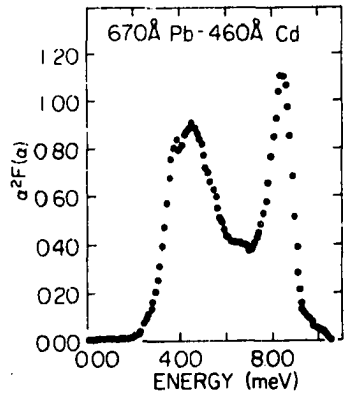

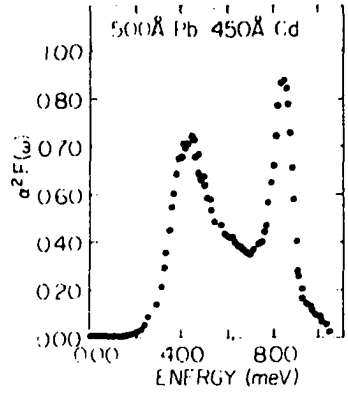

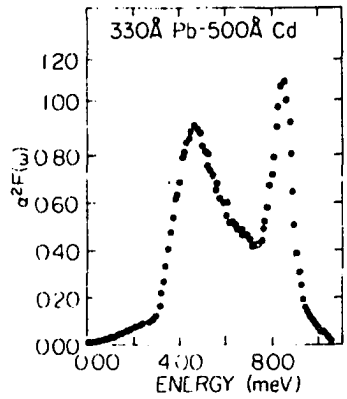

Figure 27. Effect of the lifetime modification on the calculated phonon spectral function

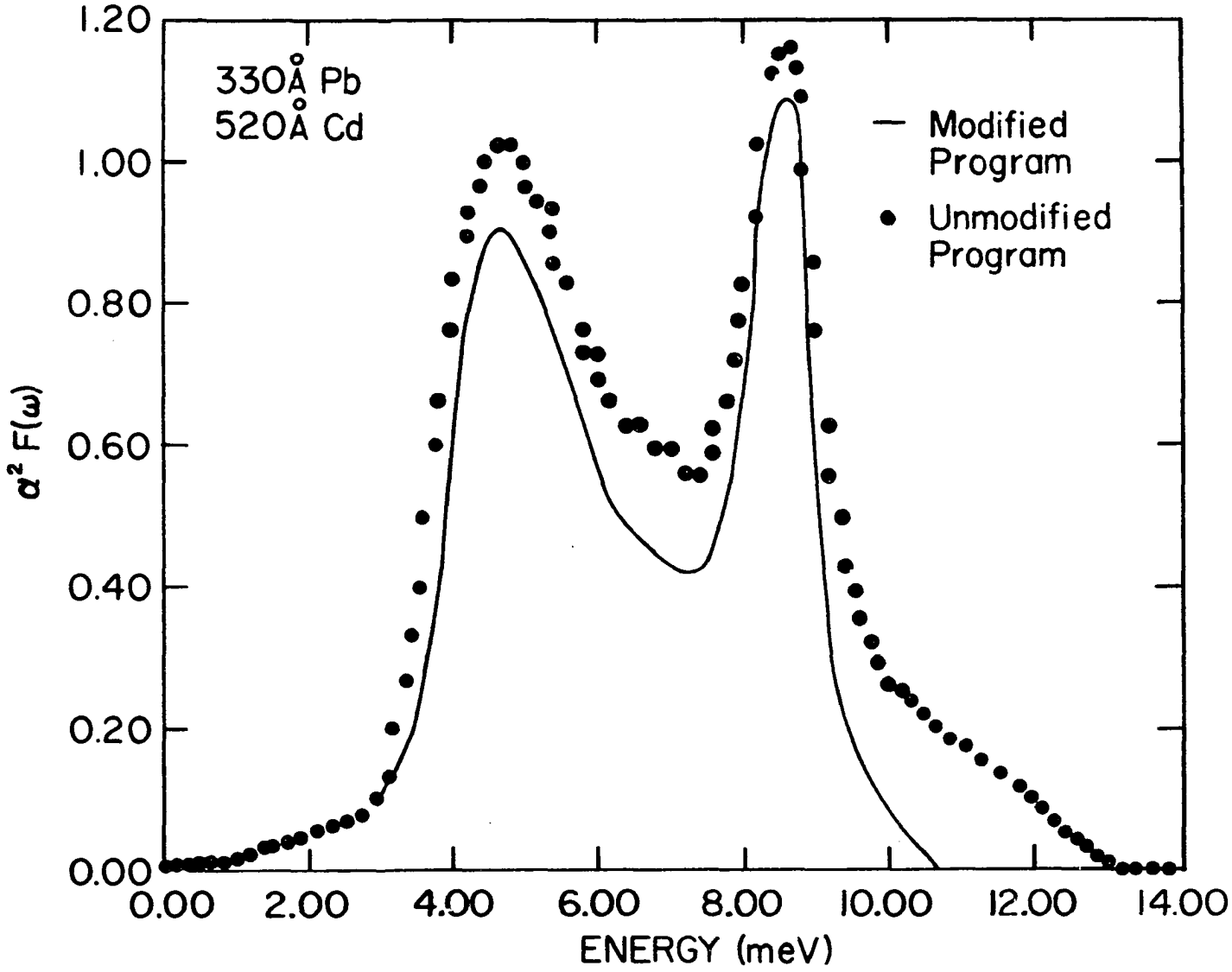
330Å Pb
520Å Cd
Modified Program
Unmodified Program
$\alpha^2 F(\omega)$
1.20
1.00
0.80
0.60
0.40
0.20
0.00
0.00
2.00
4.00
6.00
8.00
10.00
12.00
14.00
ENERGY (meV)

Figure 28. The real and imaginary parts of the pair potential calculated for the 500Å Pb-Cd proximity sandwich

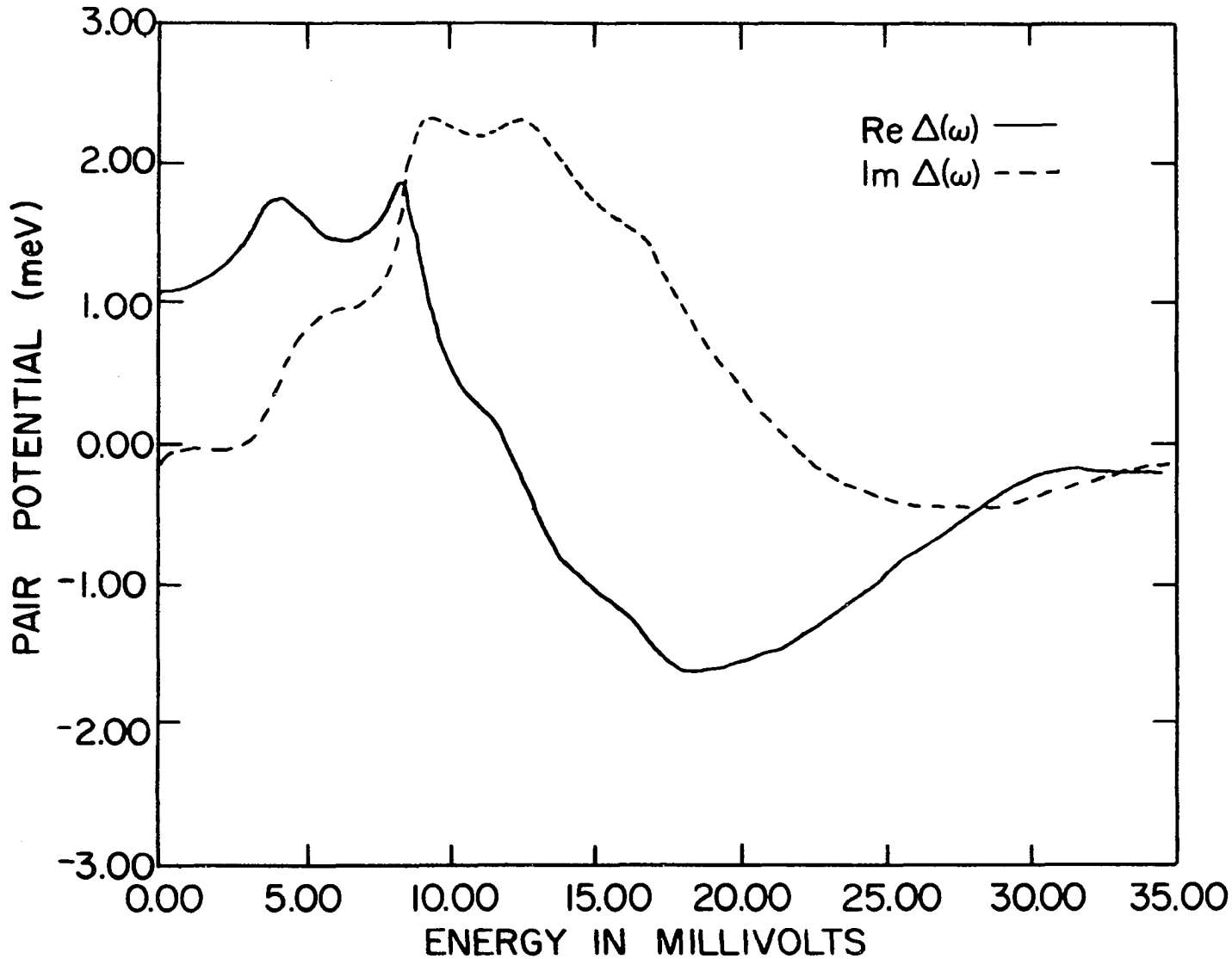
3.00
2.00
1.00
0.00
-1.00
-2.00
-3.00
PAIR POTENTIAL (meV)
Re Δ(ω)
Im Δ(ω)
0.00
5.00
10.00
15.00
20.00
25.00
30.00
35.00
ENERGY IN MILLIVOLTS

BIBLIOGRAPHY

1. I. Giaever and K. Megerle, Phys. Rev. 4, 1101 (1961).

2. J. Bardeen, L. N. Cooper, and J. R. Schrieffer, Phys. Rev. 106, 162 (1957).

3. R. Meservey and B. B. Schwartz, in Superconductivity, edited by R. D. Parks (Marcel Dekker, New York, 1969) Vol. 1, p. 117.

4. N. V. Zavaritskii, Soviet Phys. JETP 18, 1839 (1963).

5. J. D. Leslie, J. T. Chen, and T. T. Chen, Can. J. Phys. 48, 2783 (1970).

6. C. G. Gianquist and T. Claeson, J. Phys. Chem. Solids 27, 705, 719 (1966).

7. N. R. Werthammer, Phys. Rev. 132, 2440 (1963).

8. P. G. de Gennes and E. Guyon, Phys. Lett. 3, 168 (1963).

9. P. Fulde and K. Maki, Phys. Rev. Lett. 18, 675 (1965).

10. J. C. Fisher and I. Giaever, J. Appl. Phys. 32, 172 (1961).

11. L. I. Schiff, Quantum Mechanics (McGraw-Hill Book Company, New York, 1955), p. 92.

12. C. Kittel, Thermal Physics (John Wiley & Sons Inc., New York, 1969), p. 137.

13. J. Bardeen, Phys. Rev. Lett. 6, 57 (1961).

14. J. R. Schrieffer, Theory of Superconductivity (W. A. Benjamin, Inc., New York, 1964).

15. M. H. Cohen, L. M. Falicov, and J. C. Phillips, Phys. Rev. Lett. 8, 316 (1962).

16. J. W. Wilkins, Ph.D. thesis, University of Illinois, 1963 (unpublished).

17. P. H. Smith, S. Shapiro, J. L. Miles, and J. Nicol, Phys. Rev. Lett. 6, 686 (1961).

18. J. M. Ziman, Principles of the Theory of Solids (Cambridge University Press, Cambridge, 1964), p. 324.

19. A. A. Abrikosov and L. P. Gorkov, Zh. Eksp. Teor. Fiz. 39, 1781 (1960).

20. P. J. Davis, in Handbook of Mathematical Functions, edited by M. Abramowitz and I. A. Stegun (U. S. Government Printing Office, Washington, D. C., 1964), p. 253.

21. S. Skalski, O. Betbider-Matibet, and P. R. Mould, Phys. Rev. 136, A1500 (1964).

22. T. Claeson and S. Gygax, Solid State Commun. 4, 385 (1965).

23. J. J. Hauser, Phys. Rev. 164, 558 (1967).

24. E. Guyon, A. Martinet, S. Mauro, and F. Meunier, Physik Kondensierten Materie 5, 123 (1966).

25. W. L. McMillan, Phys. Rev. 175, 2, 537 (1968).

26. Y. Nambu, Phys. Rev. 117, 648 (1960).

27. L. Y. L. Shen, Phys. Rev. Lett. 24, 1104 (1970).

28. C. J. Adkins and B. W. Kington, Phys. Rev. 177, 777 (1969).

29. S. M. Freake and C. J. Adkins, Phys. Lett. 29A, 382 (1969).

30. J. Vrba and S. B. Woods, Phys. Rev. B 3, 2243 (1971).

31. D. K. Finnemore, D. E. Mapother, and R. W. Shaw, Phys. Rev. 118, 127 (1960).

32. J. M. Rowell and L. Kopf, Phys. Rev. 137, A907 (1965).

33. S. Bermon and D. M. Ginsberg, Phys. Rev. 135, A306 (1964).

34. P. W. Anderson, in Proc. of the Seventh Intern. Conf. on Low Temp. Physics, edited by G. M. Graham and A. C. Hollis-Hallet (University of Toronto Press, Toronto, 1961).

35. G. M. Eliashberg, Zh. Eksp. Teor. Fiz. 38, 966 (1960).

36. A. B. Migdal, Zh. Eksp. Teor. Fiz. 34, 1436 (1958).

37. P. Morel and P. W. Anderson, Phys. Rev. 125, 1263 (1962).

38. W. L. McMillan, Phys. Rev. 167, 331 (1968).

39. G. J. Culler, B. D. Fried, R. W. Huff, and J. R. Schrieffer, Phys. Rev. Lett. 8, 399 (1962).

40. J. R. Schrieffer, D.J. Scalapino, and J. W. Wilkins, Phys. Rev. Lett. 10, 336 (1963).

41. J. M. Rowell, P. W. Anderson, and D. E. Thomas, Phys. Rev. Lett. 10, 334 (1963).

42. B. N. Brockhouse, T. Arase, G. Caglioti, K. R. Rao, and A. D. B. Woods, Phys. Rev. 128, 1099 (1962).

43. D. J. Scalapino, in Superconductivity, edited by R. D. Parks, (Marcel Dekker, New York, 1969) Vol. 1, p. 449.

44. W. L. McMillan and J. M. Rowell, Phys. Rev. Lett. 4, 108 (1965).

45. L. F. Lou and W. J. Tomash, Phys. Rev. Lett. 29, 858 (1972).

46. W. L. McMillan and J. M. Rowell, in Superconductivity, edited by R. D. Parks, (Marcel Dekker, New York, 1969) Vol. 1, p. 561.

47. L. Y. L. Shen, Phys. Rev. Lett. 29, 1082 (1972).

48. R. C. Dynes and J. M. Rowell, Phys. Rev. B 11, 1884 (1975).

49. R. Glang, in Handbook of Thin Film Technology, edited by L. I. Maissel and R. Glang (McGraw-Hill, Inc., New York, 1970), pp. 1-16.

50. R. J. Delfs, Ph.D. thesis, Iowa State University, 1975 (unpublished).

51. W. R. Decker, Ph.D. thesis, Iowa State University, 1971 (unpublished).

52. K. W. Taconis, in Progress in Low Temperature Physics, edited by C. J. Gorter (North-Holland Publishing Co., Amsterdam, 1961), Vol. III.

53. B. A. Haskell, Ph.D. thesis, Iowa State University, 1971 (unpublished).

54. D. K. Finnemore, Ames Laboratory of the United States Atomic Energy Commission Data Book DFK-9, 1968 (unpublished).

55. A. C. Rose-Innes, Low Temperature Techniques, (English Universities Press Ltd., London, 1964).

56. J. S. Rogers, Rev. Sci. Instrum. 41, 1184 (1970).

57. J. S. Rogers, J. G. Adler, and S. B. Woods, Rev. Sci. Instrum. 35, 208 (1964).

58. M. Hansen, Constitution of Binary Alloys (McGraw-Hill, New York, 1958).

59. I. Giaever, Phys. Rev. Lett. 5, 464 (1960).

60. J. L. Miles and P. Smith, J. Electrochem. Soc. 110, 1240 (1963).

61. R. C. Jaklevic and J. Lambe, Phys. Rev. Lett. 17, 1739 (1966).

62. S. Bermon, National Science Foundation Grant No. NSF-GP110, Technical Report No. 1, 1964.

63. J. M. Rowell and W. L. McMillan, Phys. Rev. Lett. 16, 453 (1966).

64. L. P. Gor'kov, Soviet Phys. JETP 7, 505 (1958).

65. Sam Liu, Private Communication.

ACKNOWLEDGEMENTS

The author wishes to thank Dr. D. K. Finnemore for his valuable advice and guidance throughout the course of this work and especially for his continuing interest and encouragement while this manuscript was being prepared in absentia. The author also wishes to thank Dr. Sam Liu for his suggestions for modifying the unfolding program.

Thanks are also extended to the members of Dr. Finnemore's low temperature group for the many helpful discussions that contributed to this work. Special thanks are in order for Mr. J. E. Ostenson for his dependable good advice in so many areas.

Finally, the author wishes to extend his most sincere appreciation to his wife, Joan, for her continual support and understanding.